Design of an MRI Compatible Robot for Wrist Rehabilitation

by

Sarah E. Mendelowitz

S.B., Massachusetts Institute of Technology (2003)

Submitted to the Department of Mechanical Engineering
in Partial Fulfillment of the Requirements for the degree of

Master of Science in Mechanical Engineering

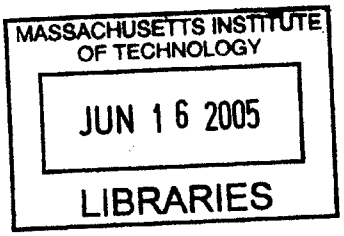

at the

MASSACHUSETTS INSTITUTE OF TECHNOLOGY

June 2005

Signature of Author .....
Department of Mechanical Engineering
May 6, 2005

Certified by .....
Hermano Igo Krebs
Principal Research Scientist
Thesis Supervisor

Accepted by .....
Lallit Anand
Chairperson, Department Committee on Graduate Students

Design of an MRI Compatible Robot for Wrist Rehabilitation

by

Sarah E. Mendelowitz

Master of Science in Mechanical Engineering

Abstract

Magnetic Resonance Imaging (MRI) can be used to study the effects of robotic therapy on stroke patients. This thesis focuses on the design of an MRI compatible wrist robot to be used as a clinical tool for studying the stroke recovery process and the effectiveness of robotic therapy. The robot must comply with strict MRI compatibility requirements, which require careful selection of materials and components. The actuation approach consists of a non-MRI compatible electric motor placed outside the MR room, which is used to drive an MRI compatible hydraulic system. A novel, low friction, MRI compatible hydraulic vane motor was designed for use in the hydraulic system. The robot was designed for use with two interchangeable transmission alternatives: differential gears or friction drive. A stand was designed to allow the wrist robot and patient to fit comfortably within the MRI machine. The MRI compatible wrist robot was assembled and qualitatively tested.

Thesis Supervisor: Hermano Igo Krebs
Title: Principal Research Scientist

Contents

List of Figures

List of Tables

Chapter 1

Introduction

1.1 Motivation

The objective of this research is to develop a wrist robot for stroke rehabilitation that can be safely and effectively used in a Magnetic Resonance Imaging (MRI) machine. Several rehabilitation robots have been developed by previous members of the Newman Laboratory for Biomechanics and Human Rehabilitation. The approach for this research project is to redesign one of the existing robots so that it can function in the MRI machine. Placing a robot inside the MRI machine will enable the study of the brain while robotic therapy is taking place.

The wrist robot was chosen for redesign based on several reasons. First, the wrist robot is relatively small and compact. This makes it easier to fit into the confined space of an MRI machine. Secondly, experience with the existing wrist robot has shown that a patient is likely to keep the rest of the body stationary during exercise. Because the patient's brain will be scanned by the MRI machine during therapy, it is important that the head be kept extremely still. For comparison, patients using the MIT MANUS, which exercises the muscles in the arm and shoulder, induce movement in their head when they move the shoulder. Thus, the wrist robot seemed to be the most appropriate of the existing rehabilitation robots to adapt for use in the MRI machine.

The design of an MRI compatible wrist robot requires several steps. A thorough investigation of the background material is conducted. Preliminary design work is used to evaluate the advantages and disadvantages of the various design options. Proof of concept testing is

performed on key design elements. Extensive analysis is required to evaluate and guide design decisions. Finally, a detailed design of the robot is created. This thesis describes the process used to design the MRI compatible wrist robot.

1.2 Chapter Overview

This thesis consists of seven chapters. Following this introductory chapter, Chapter 2 describes the necessary background information, which will lay the groundwork for the project. The third chapter is devoted to actuator design. Chapter 3 describes the actuator selection process and the design, analysis, and testing of a hydraulic vane motor. In Chapter 4 the selection of the transmission for the MRI compatible wrist robot is discussed. Chapter 5 describes the selection process for the remaining robot elements, which includes the materials, bearings, hoses and fittings, seals, and electric motor. The sixth chapter will include the detailed design for all elements of the robot. This will include all calculations and final design decisions. Chapter 7 comments on the assembly and debugging process required for the completed design. Finally, Chapter 8 will conclude this thesis and comment on the future work that must be done for the MRI compatible wrist robot.

Chapter 2

Background

The information presented in this chapter provides the necessary background for this project. Seven topics are discussed, which include stroke, human anatomy relevant to the project, the original wrist robot, how MRI works, MRI compatibility, prior art for MRI compatible robotics, and the functional requirements for the MRI compatible wrist robot.

2.1 Stroke

A stroke occurs when blood flow to a particular region of the brain is interrupted by a blockage or hemorrhage[1]. Without blood flowing to the brain the affected tissue will become damaged. This damage, referred to as a lesion, often results in the loss of a particular body function, such as motor, sensory, visual, or auditory functions. Approximately fifty percent of stroke patients will lose their motor skills after a stroke. As a result, a patient will have limited or no ability to use their arm, hand, or leg. To regain use of their motor skills most patients undergo extensive therapy.

Robotic rehabilitation has been successfully used as stroke therapy[2]. A variety of stroke rehabilitation robotics exist for the arm, wrist, and legs. Robotic therapy gives a patient more repetition and control than conventional therapy in which a physical therapist manually moves a patient's limb. The stroke rehabilitation robots developed at the Newman Laboratory for Biomechanics and Human Rehabilitation use a computer prompt to signal a patient to move to a particular point. If the patient is able to move the robot allows the patient to move freely.

However, if the patient is unable to move or moves in the wrong direction the robot will assist the patient in reaching the target.

The process that the brain uses to repair itself is very much unknown. It is believed that some reorganization of the brain takes place. The location in the brain that this reorganization occurs is a topic of many motor recovery studies. Studying the brain during therapy will help researchers understand the process by which motor skills are relearned.

2.2 Anatomy

To properly design a wrist robot for use inside an MRI machine it is important to understand certain aspects of human anatomy. First, it is necessary to know how the wrist moves. This will allow the robot to provide the necessary degrees of freedom and ranges of motion to be exercised. Second, it is important to determine the average size of the human wrist, hand, and arm. This is important so the robot can be properly sized. Finally, it is important to determine the dimensions of the human body that are important for fitting inside the MRI machine. The robot must be able to fit inside the MRI machine with a patient. Therefore, determining the space the patient will need is important so that the robot can be sized appropriately.

2.2.1 Wrist Motions

The wrist has three degrees of rotational freedom. Each of these degrees of freedom has a corresponding range of motion. This section outlines the values and terminology required to understand the motion of the wrist.

The flexion and extension motions are shown in Figure 2-1. The range of motion for most people is 70 degrees of extension and 65 degrees of flexion[3].The abduction and adduction motions are shown in Figure 2-2. The range of motion for adduction is 30 degrees and that of abduction is 15 degrees. The final degree of freedom is pronation and supination as shown in Figure 2-3. The range of motion is 90 degrees for both pronation and supination. The MRI compatible wrist robot is designed to exercise only the flexion/extension and abduction/adduction degrees of freedom. The reason for eliminating the pronation/supination actuation is discussed in Section 2.7.

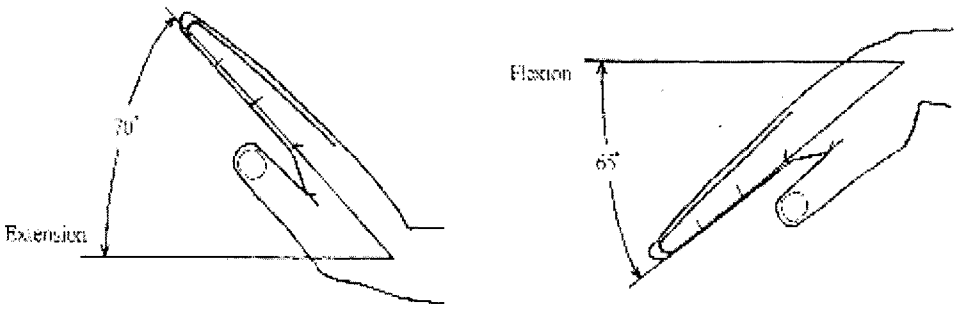

Figure 2-1: The range of motion for flexion and extension of the wrist[3]

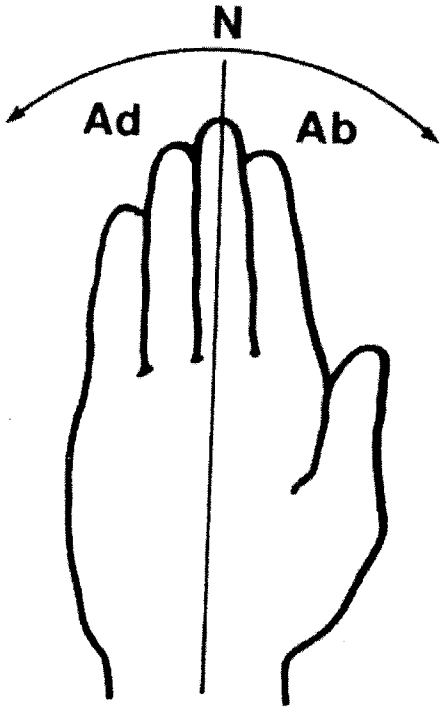

Figure 2-2: Abduction/adduction of the wrist[5]

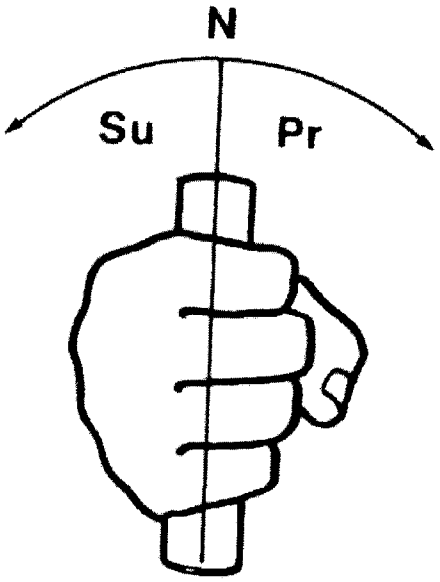

Figure 2-3: Pronation/supination of the wrist[5]

2.2.2 Body Dimensions

There are two types of body dimensions that are important in the design of an MRI compatible wrist robot. First, various dimensions of the wrist and arm are required so that the robot can be properly sized. Second, dimensions of the torso are important to ensure that the robot and a human can both fit within the MRI machine. Two dimensions were deemed critical in regards to the design of the robot. First, the distance from the wrist to the center of the hand as it grips a handle is shown in Figure 2-4 as dimension H [3]. This dimension is 3.0 inches for the 50 percentile male. The second important dimension is the distance from the elbow to the wrist, which is labeled as dimension L in Figure 2-5. This dimension is 10.1 inches for the 50 percentile male.

The maximum body width and thickness are important to determine how much space a patient uses in the MRI machine. Thus, the amount of space remaining can be estimated and occupied by the robot. The width of the hips, shown in Figure 2-6 as dimension 19, of the 50

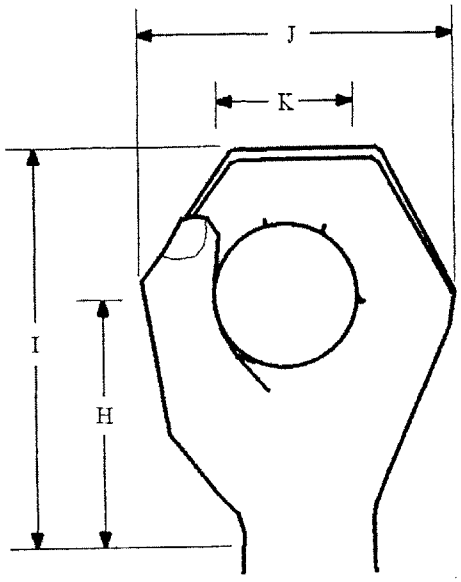

Figure 2-4: The dimensions of the hand[3]

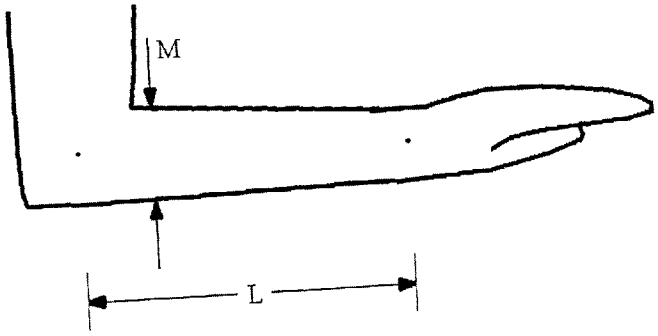

Figure 2-5: The dimensions of the forearm[3]

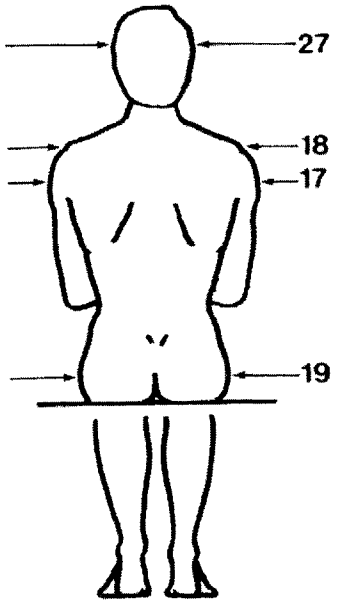

Figure 2-6: Width of the hips[5]

percentile male is 14.2 inches[4]. The thickness across the abdomen, illustrated in Figure 2-7 as dimension 21, is 10.5 inches for the 50 percentile male.

2.3 Wrist Robot

The original wrist robot was designed by Dustin Williams. The details of the design can be found in Williams' Master's thesis and the characterization of the design can be found in the Master's thesis of James Celestino[3] [6]. However, a brief overview of the design is included here. It is important to note that the original wrist robot was not designed to be MRI compatible. As a result, most of the robot must be altered to comply with the constraint that it will be used inside an MRI machine. Nonetheless, the original design of the wrist robot is a valuable starting point for designing an MRI compatible counterpart.

The design of the original wrist robot is shown in Figure 2-8. The design is capable of actuating all three degrees of freedom of the wrist: flexion/extension, abduction/adduction,

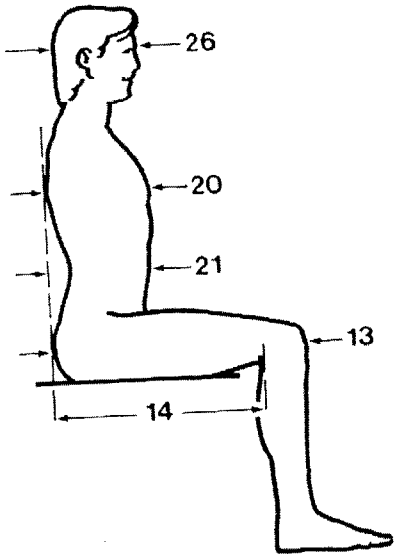

Figure 2-7: Thickness of the abdomen[5]

and pronation/supination. Electric motors are used as actuators for all degrees of freedom. The transmission for the flexion/extension and abduction/adduction movements is a differential gear. A differential gear transmission allows both actuators to remain stationary while providing two degrees of rotational freedom. Each degree of freedom is controlled by the relative rotation of the two actuators. The details of the differential gear transmission that Williams designed can be seen in Figure 2-9.

The pronation/supination motion utilizes curved slide rings as its transmission. The slide rings act as an open gear with a large diameter. When the pronation/supination actuator is enabled the curved slide rings will rotate, moving with it the other two actuators, the differential transmission, and the handle mechanism. A picture of the curved slide rings can be seen in Figure 2-10.

The linear slider provides an additional unactuated degree of freedom. This is required because the wrist axes and the robot axes are not coincident. The slider therefore accommodates for the misalignment of the two sets of axes. Additional parts, such as the forearm support, handle connection, and distal wrist connection, were designed to assist attaching the patient to

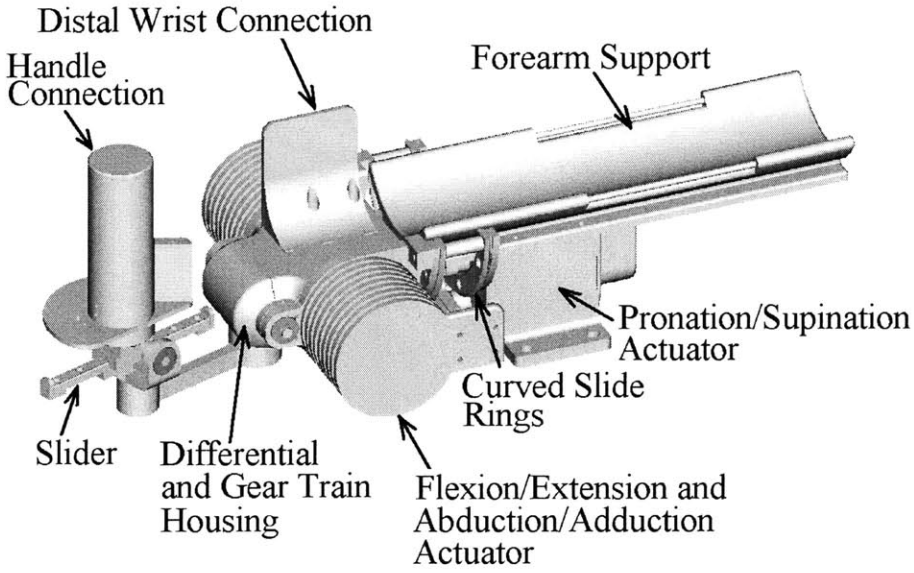

Figure 2-8: Solid model of original wrist robot[3]

the robot.

Several changes have been made to the original design of the wrist robot. The current configuration of the wrist robot is pictured in Figure 2-11. Some of the design changes include adjustments in the transmission, handle mechanism, and patient connection. Overall, the methodology of the design has been unaltered.

2.4 MRI

To understand the important aspects in designing an MRI compatible robot, it is useful to understand MRI. This section explains what MRI is and how it works. This will give insight into why designing a machine for the MRI environment is drastically different and has strict requirements.

Magnetic Resonance Imaging (MRI) is a noninvasive procedure that allows the internal parts of the body to the imaged. This procedure is carried out by an MRI machine. MRI is used as a medical tool to assist in the diagnosis of illnesses and injuries and to allow the study of various parts of the body. The technology behind MRI is somewhat complex. However, a

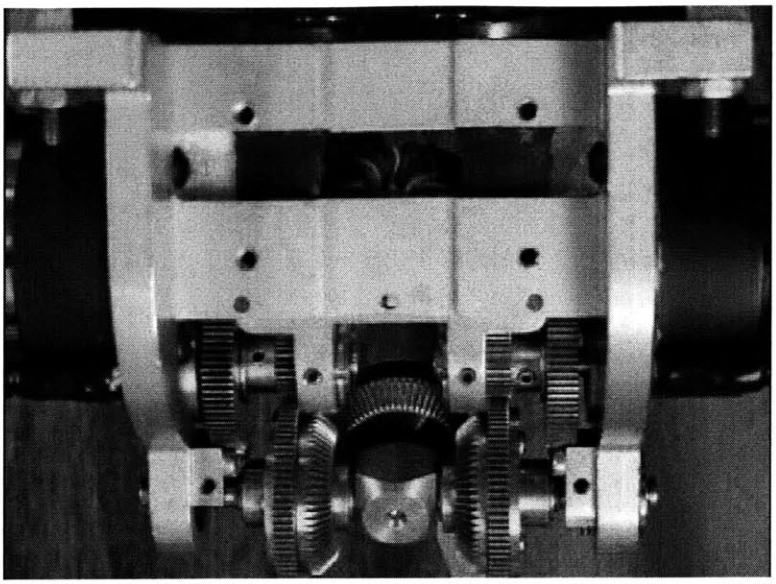

Figure 2-9: Differential gear transmission in the original wrist robot design[6]

brief explanation of how MRI works has been included.

MRI is based on altering the spin and orientation of an atom's nucleus and measuring the affects of this alteration[7] [8]. For the purpose of MRI, hydrogen is the atom of interest. This is because hydrogen is sensitive to magnetic fields and present in both water and fat. The body is primarily composed of water and fat, making the measurement of these two materials particularly important. For simplicity, the process of MRI is typically described referring to the nucleus as a proton. This is because the hydrogen atom has only one proton in its nucleus. Therefore, in this thesis, one proton will refer to one nucleus and several protons will refer to several nuclei.

The proton of an atom naturally has a spin and angular momentum which creates a magnetic field. Figure 2-12 illustrates a spinning proton and its corresponding magnetic field B. In a normal environment the protons are randomly oriented and in turn their magnetic fields are also randomly oriented. This means that the magnetic field vectors of a group of protons sum to zero leaving no net magnetization.

When a proton is placed in a magnetic field, B_o, it will begin to process about that magnetic field vector at a particular frequency, ϖ_o, as shown in Figure 2-13. The frequency of this motion

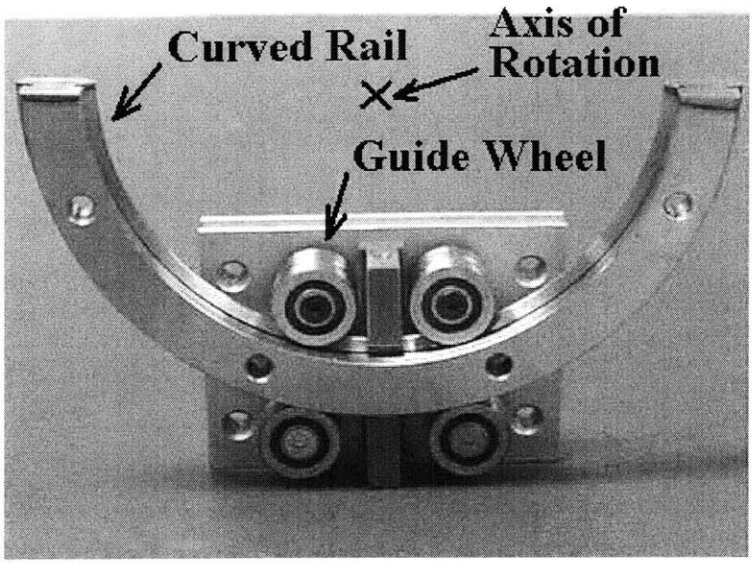

Figure 2-10: Curved slide rings in the original wrist robot design[6]

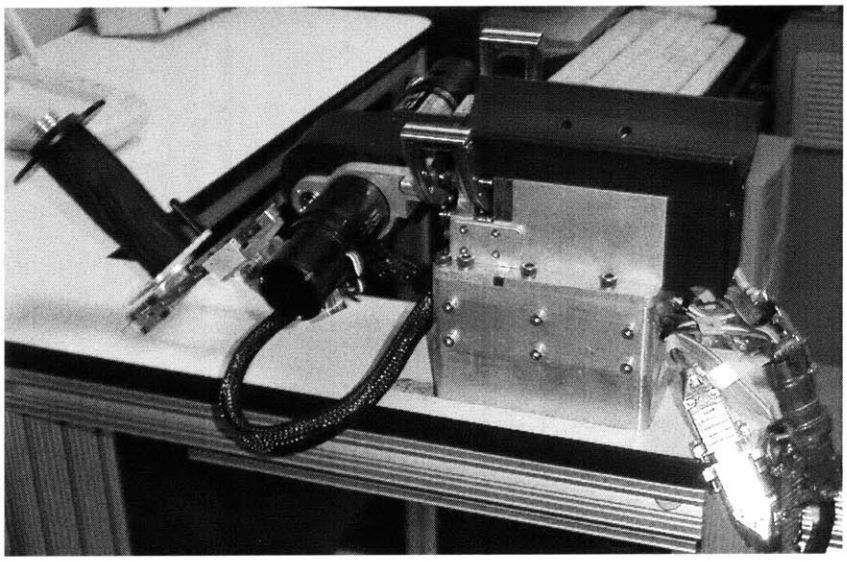

Figure 2-11: Current wrist robot

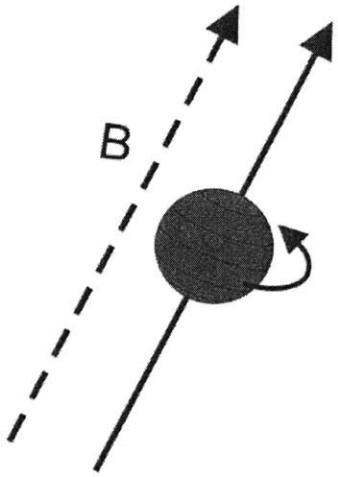

Figure 2-12: Spin and magnetic field of an atom [8]

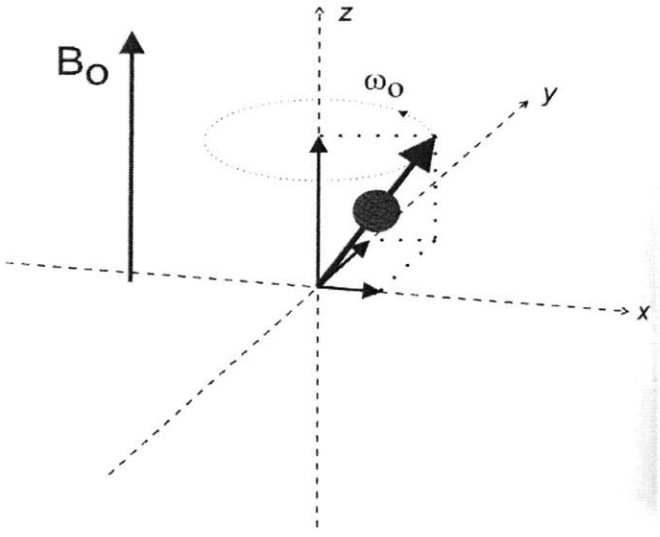

Figure 2-13: Atom procession due to applied magnetic field [8]

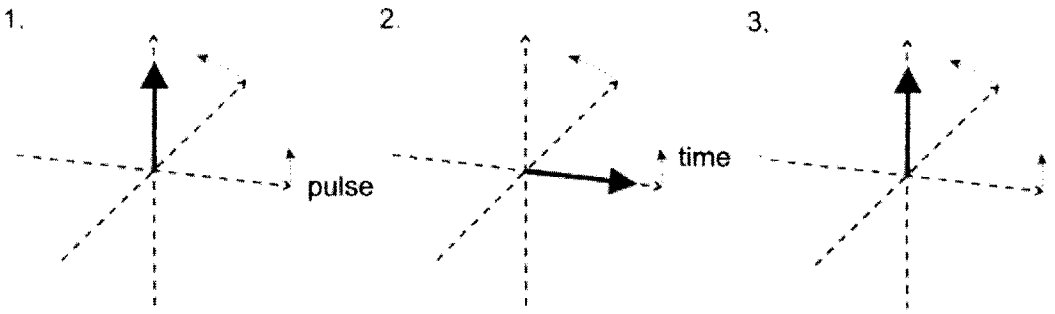

Figure 2-14: The changes in state exhibited by a proton [8]

is determined by the following equation and referred to as the Larmor Frequency,

$$\omega_o = \frac{\gamma B_o}{2\pi} \tag{2.1}$$

where γ is the gyromagnetic ratio, a constant unique to the nucleus of each element. The alignment of the proton creates a constant, non-zero magnetic field parallel to B_o. This vector is depicted in Figure 2-13 pointing in the z direction. However, the vectors in the x and y directions are varying with time. Therefore, when many protons are considered there will be a net magnetization in the z direction, but zero net magnetization in the x and y directions.

The next step in the process is to expose the protons to a radio frequency (RF) pulse. The protons will absorb the energy of the RF pulse at the Larmor Frequency. This energy absorption will cause the proton to change state and thus orientation in the magnetic field. Originally, the proton is said to be in the low energy "spin up" state. With the addition of energy the proton is excited into the high energy "spin down" state. This process is illustrated in Figure 2-14, where step one is "spin up" and step two is "spin down". When the RF pulse is turned off, the protons will return to their original state emitting energy at the Larmor Frequency. This step is illustrated in step three of Figure 2-14.

The MRI process will produce a voltage in a properly placed loop of wire. This signal will contain information related to the frequency of the protons and the magnitude of their

magnetization. The frequency information is used to determine the material being imaged and the location of each proton. The material is determined based on the varying natural magnetic field of different molecular structures. Basically, water will have a different natural magnetic field than fat. The location of a particular proton is determined by magnetic field gradients. These gradients are small perturbations in the applied magnetic field, B_o, that vary linearly with position. This causes each proton to resonate at a unique frequency that depends on its position as shown in the following equation,

$$\omega_i = \gamma (B_o + G \cdot r_i) \tag{2.2}$$

where G is the gradient, and r_i is the position.

Thus images can be produced that are spatially accurate and also provide information about the material being imaged. MRI takes advantage of a material's ability to magnetize in the presence of a magnetic field. This proves to be extremely valuable in imaging the body; however, it can produce negative effects when other materials, such as those used to build a robot, are present. The next section will explore these negative effects and describe the care that must be taken to avoid them.

2.5 MRI Compatibility

MRI compatibility will be a key issue in the design of this robot. MRI compatibility is a qualitative description of how obtrusive a particular material is when placed in the MRI machine[9]. There are two degrees of magnetic compatibility. The first kind of magnetic compatibility exists when there are no forces or torques exerted on the object when it is inside the MRI machine. The second kind of magnetic compatibility occurs when the object produces negligible effects on the MR image. It is important that the materials used in this robot have magnetic compatibility of both kinds.

It is extremely dangerous to place materials within the MR room that experience forces or torques due to the magnet. This can cause the materials to fly toward the magnet, which can cause serious injury to the patient. The second kind of magnetic compatibility is important so that the MR images are clear and reliable. The following figures illustrate the effects of having

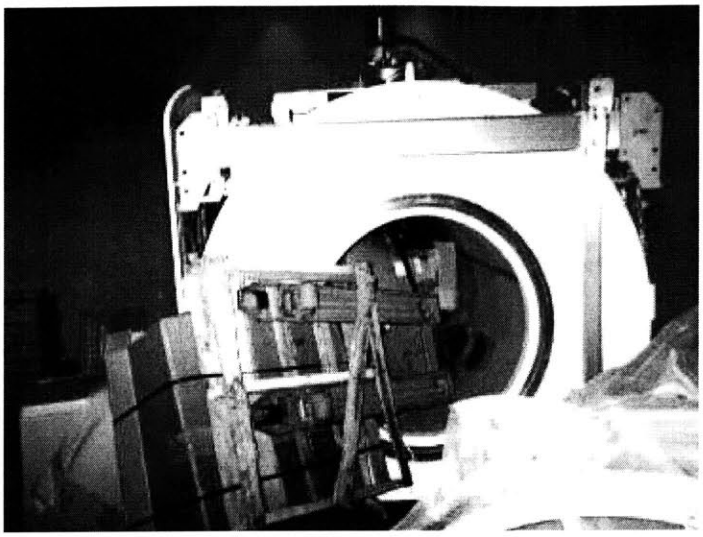

Figure 2-15: Pallet jack attracted to the magnet of an MRI machine[10]

materials within the MR room that are not compatible. An example of failure to comply with MRI compatibility of the first kind is illustrated in Figure 2-15. Here a pallet jack has been pulled into the MRI machine. Clearly this is a dangerous situation that could seriously injure a patient in the MRI machine. In Figure 2-16, the MR image is distorted due to a patient's dental fillings, which were not MRI compatible. This is an example of failure to comply with MRI compatibility of the second kind.

Magnetic susceptibility is a quantitative measure of magnetic compatibility. The magnetization of a material is the quantity that affects a material's compatibility. There are two types of magnetization: inherent and induced. The total magnetization of a material is the sum of the induced magnetization and the inherent magnetization as shown in Equation 2.3, where M_t is the total magnetization, M_i is the induced magnetization, and M_o is the inherent magnetization[9].

$$M_t = M_o + M_i \tag{2.3}$$

Inherent magnetization is the magnetization that a material possesses even in the absence of a magnetic field. It is important that the materials used in a MRI compatible robot have

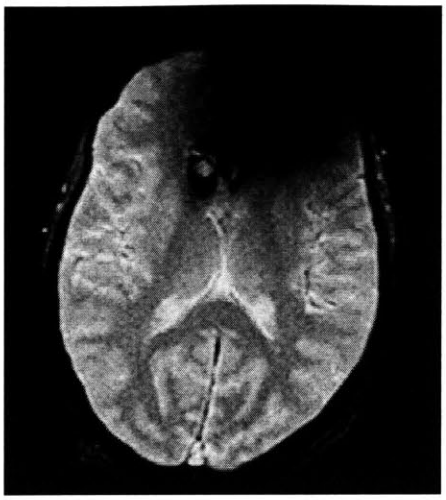

Figure 2-16: MRI image degraded by a patient's dental fillings [11]

zero inherent magnetization. This will ensure that the material will not experience forces and torques due to the magnetic field and will thus have magnetic compatibility of the first kind. When a material is placed in a strong magnetic field an additional magnetization can be induced in the material. The induced magnetization is equal to the magnetic susceptibility multiplied by the field strength as shown in Equation 2.4, where X is the susceptibility and H is the field strength.

$$M_i = \mathrm{X}H \tag{2.4}$$

The induced magnetization is responsible for degrading the MR image making a material fail the requirements for MRI compatibility of the second kind. Thus, materials should have a low induced magnetization. This in turn means that the magnetic susceptibility must be low. Ideally, the magnetic susceptibility should be near that of water which is -9.05 x 10^{-5}. This is because the human body is composed primarily of water. Therefore, materials with susceptibilities close to water will have minimal effects on the MR images. A chart illustrating the range of materials and their susceptibilities is shown in Figure 2-17.

Most of the materials that are commonly used in the MRI machine have a maximum susceptibility value on the order of $\pm 10^{-5}$. A negative susceptibility means that the material is

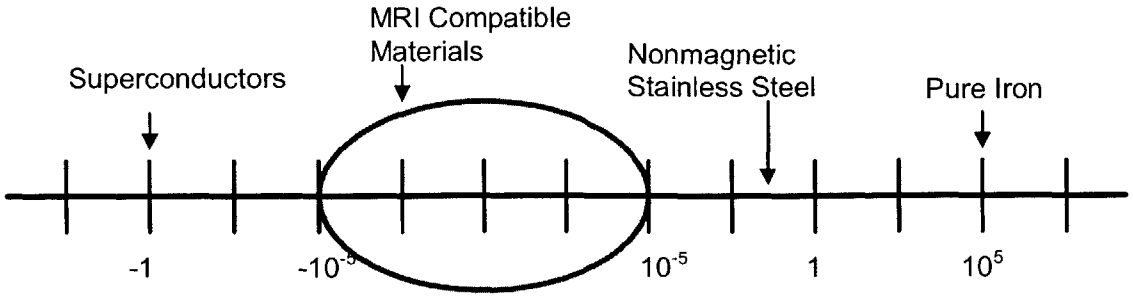

Figure 2-17: Range of materials and their susceptibilities.

Material	Susceptibility
Water	-9.05×10^{-6}
Copper	-9.63×10^{-6}
Glass	-13.88×10^{-6}
Graphite	-8.5×10^{-6}
Aluminum	20.7×10^{-6}

Table 2.1: Susceptibility of various materials.

diamagnetic. A diamagnetic material will align perpendicular to the applied magnetic field because it is repelled by the magnetic poles. A positive susceptibility means that the material is paramagnetic. When a paramagnetic material becomes magnetized due to an applied magnetic field it will align parallel to the magnetic field. Table 2.1 compares the susceptibility of some MRI compatible materials with that of water. The materials listed in Table 2.1 are possible materials for use in this application however many others do exist.

Another consideration regarding MRI compatibility is electrical compatibility. The RF pulse can induce eddy currents into a conductive material. An eddy current can degrade the image quality and even generate heat. To avoid eddy currents the design should avoid consisting of loops of conductive materials. The human body can conduct electricity so loops that are completed by a patient's body should especially be avoided.

Overall, MRI compatibility places a number of strict constraints on the design of an MRI compatible robot. However, these constraints can be overcome. This has been demonstrated by the numerous MRI compatible robots that exist with a variety of uses and constructions.

2.6 Prior Art

Several machines have been designed for use in the MRI machine. They are used for a variety of applications; however, the majority of the designs are aids in performing surgical procedures. These MRI compatible devices are useful in examining the types of materials, actuators, and sensors that have been useful in the past.

For example, one MRI compatible robot is designed to perform breast interventions[12]. This particular robot made use of ultrasonic motors, optical encoders, and a variety of polymers including polyethylene, acrylic, delrin, fiberglass, and nylon. The motor was housed in a conductive material that could distort the MR images. Therefore, the design placed the actuators near the patients feet, approximately one meter from the image center. This particular robot reported no image distortion and no noise due to the operation of the ultrasonic motors

A robot designed for trans-nasal neurosurgery, used a design technique in which materials that were not ideal in terms of MRI compatibility could be used according to their distance from the imaging area[13]. The idea of the research was that a material's effect on the MR image was inversely proportional to the distance from the image location and proportional to the volume of the material. Thus, non-ideal materials could be used if they are small and far from the imaging center. The authors used only nonmagnetic materials within 0.3m of the image location. They used "low magnetic" materials between 0.3m and 0.7m and used a small amount of ferromagnetic material beyond 0.7m. The robot was driven by non-magnetic ultrasonic motors, rotary encoders, and potentiometers. The robot functioned without problems within the MRI machine. However, the authors reported that the ultrasonic motors generated a large amount of noise when they were active.

A limited amount of research has been done on MRI compatible robots for brain studies related to human motor function. For example, one design uses a hydraulic system of MRI compatible linear cylinders driven by an electric motor placed outside the MR room[14]. The linear cylinders are equipped with a belt drive to convert between linear and rotary motions. This simple actuator idea was successfully tested in the MRI machine with a human subject. Additionally, they conducted a study of the system dynamics[15]. The natural frequency of the hydraulic system was about 7 Hz with a bandwidth of 20 Hz. These numbers could be significantly improved by using shorter hose lengths.

Finally, this lab has received a patent which outlines the concept for producing an MRI compatible robot[16]. This patent suggests the use of a robot to interact with a human subject inside an MRI machine. This robot could contain some sort of actuators, such as cables or hydraulics, and sensors, possibly utilizing optics. The robot would comply with requirements for MRI compatibility. This thesis will be an attempt to create a robot based on the patented idea.

2.7 Functional Requirements

A set of functional requirements were developed as guidelines and goals for this design. The functional requirements for this robot are largely based on the requirements for the original wrist robot. However, some additional constraints were added so that the robot will be compatible within an MRI machine.

2.7.1 Degrees of Freedom

The original wrist robot is capable of providing three degrees of freedom, which allows the wrist to move in flexion/extension, abduction/adduction, and pronation/supination. However, the design of this MRI compatible robot will have two degrees of freedom thus capable of actuating the flexion/extension and abduction/adduction motions of the wrist. Excluding the third degree of freedom reduces the size and complexity of the design significantly. The size is reduced because the actuator and mechanism for the additional degree of freedom can be eliminated. In the original wrist robot, the pronation/supination actuator was designed to lift the actuators for the other two degrees of freedom. This increased the force requirements for the pronation/supination actuator and adds requirements that the other actuators be small and light. Eliminating this degree of freedom also eliminates these concerns. This is particularly important because the actuators must be specially designed. Therefore, optimizing the design for weight will add unnecessary complexity.

2.7.2 Endpoint Torque

This robot must be capable of providing sufficient force to move the wrist of a patient. This means that the weight of the wrist must be moved against gravity and that any natural spasticity in the muscles must be overcome. According to experimentation done during the development of the original wrist robot, 1.2 Nm are required to move the wrist in flexion, extension, abduction, and adduction[3].

2.7.3 Endpoint Impedance

Impedance describes the ability of the robot to be backdriven by a patient. Impedance can be affected by the friction and inertia of the system. Qualitatively, impedance what a patient feels as he or she moves the robot while it is not active. The friction and inertia should be low, such that, the patient feels as if he or she is moving without a robot. The quantitative values set for the friction and inertia in the original wrist robot will also be used as goals in this application. The endpoint inertia should therefore be limited to 29-44 kg-cm^2 and the endpoint friction should be kept less than .21 Nm[3].

2.7.4 MRI Compatibility

All of the materials used in the robot must be MRI compatible if they are to be placed in the MR room. This includes all actuators, fasteners, transmission components, and structural materials. In short, this means that all materials must have zero inherent magnetization. Additionally, each material should have a small magnetic susceptibility. Ideally the susceptibility should be kept near -9.05 $\times$ 10^{-6}, which is that of water. When these two criteria are met the machine will have negligible effects on the quality of the MR image and will not be affected by the magnetic forces making it safe for use in an MRI machine. A more detailed description and definition of MRI compatibility can be found in Section 2.5.

2.7.5 Size

The robot must be designed to fit inside the MRI machine with a patient. The typical MRI machine has a closed bore so that the patient's entire body is enclosed as seen in Figure

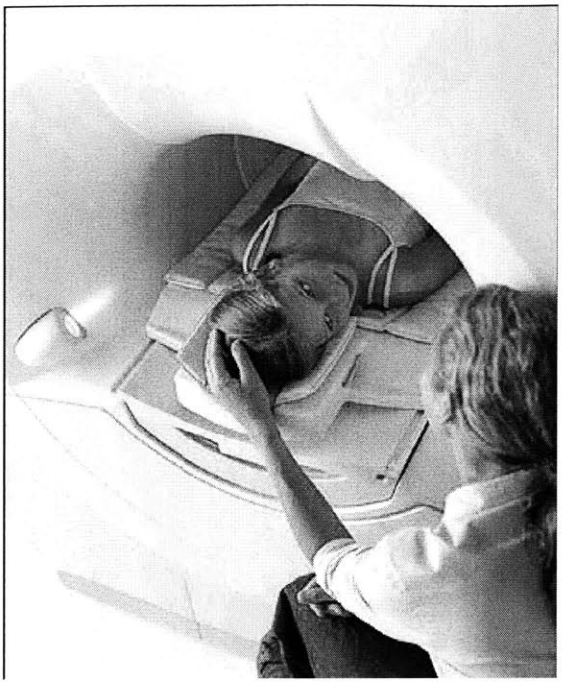

Figure 2-18: A patient inside a closed bore MRI machine[17]

2-18. The bore of the standard closed bore MRI machine is 60cm in diameter.

However, there are several other varieties of MRI machines where space is not as strict of a criterion. For example, there are MRI machines that are designed for only imaging the head as shown in Figure 2-19. In this case only the head is enclosed in the MRI machine. The robot can then be placed outside the bore of the MRI machine where space is less of an issue.

Additionally, open MRI machines provide more space than the traditional closed bore machines as shown in Figure 2-20. However, this design produces images that have a poorer quality. Therefore, they are not normally used for functional MRI (fMRI), the MRI process required for studying brain activity.

To reach the largest number of users, it was decided that the robot would be designed for the strictest size constraint, namely the closed bore MRI machine. Therefore, the patient and robot must fit within a 60cm diameter. Figure 2-21 illustrates the space remaining in a closed bore MRI machine when a patient is inside the machine. The remaining space can be filled with the MRI compatible wrist robot. The maximum dimensions of the unfilled space inside

Figure 2-19: Siemens Allegra MRI machine for imaging the head[18]

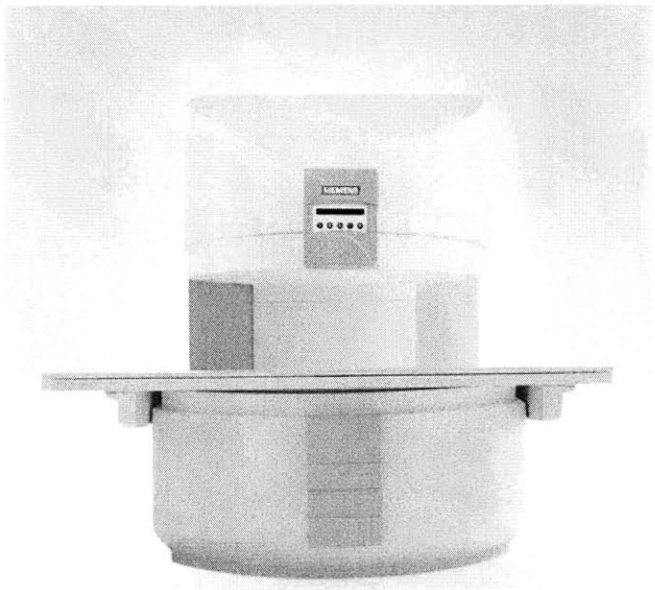

Figure 2-20: Siemens C!, an open MRI machine[19]

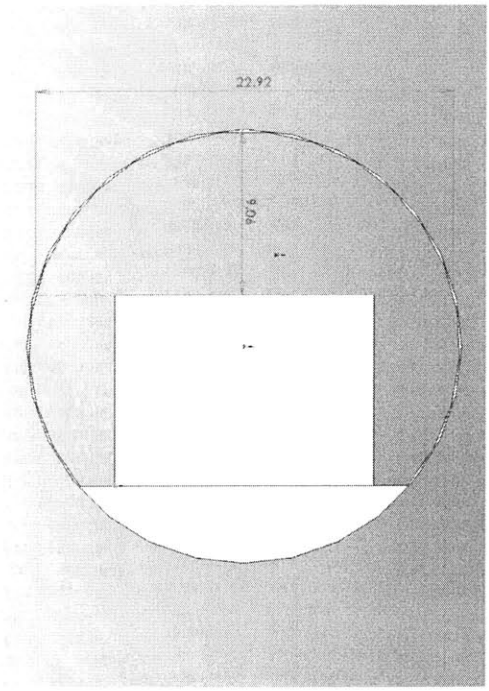

Figure 2-21: Diagram of the space remaining in a 60 cm closed bore MRI machine, where the solid section represents the dimensions of the human body

the MRI machine are 22.92 inches and 9.06 inches, as indicated on the drawing. The robot must not exceed these maximum dimensions.

Chapter 3

Actuator Design

3.1 Actuator selection

The actuators used in the original wrist robot are electromagnetic motors, which are not MRI compatible. Therefore, several alternative actuators were considered for this robot. These actuators include ultrasonic motors, pneumatics, and hydraulics. These actuators were considered because they are not electromagnetic and they produce forces and displacements within the order of magnitude required for this application. The actuators were then compared using the functional requirements as a guide.

3.1.1 Ultrasonic motor

An ultrasonic motor is a technology that used piezoelectric actuators to produce large rotary or linear motions. Ultrasonic motors are actuated using a ceramic piezoelectric strip as a stator which is in contact with a metal or ceramic rotor[20]. A high frequency wave is then induced into the stator. The nature of the wave causes the rotor to translate. Because there are no magnetic parts, the ultrasonic motor can be constructed of magnetically compatible materials and produce the same general effect as an electromagnetic motor. Figure 3-1 illustrates a linear ultrasonic motor.

Two companies were identified that produce ultrasonic motors that are feasible for this application. Adaptronics offers a rotary ultrasonic motor USR60 that produces 1 Nm of torque. This torque would have to be amplified with a mechanical gear ratio of 1.2:1. The size of the

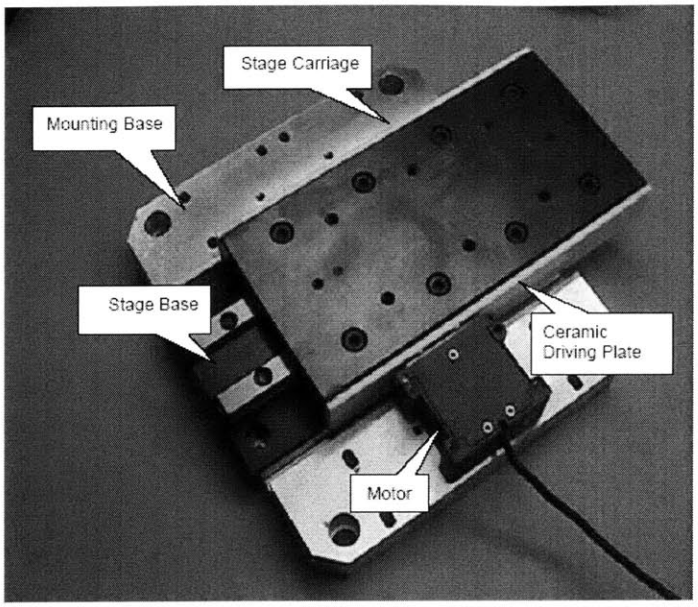

Figure 3-1: Nanomotion HR8 ultrasonic motor[20]

USR60 is approximately 6x5x5cm. Nanomotion manufactures a linear ultrasonic motor HR8 that provides 35 N of force. The linear motion can be easily converted to rotary motion by using a ring shaped stator rather than the linear stator shown in Figure 3-1. To provide the required torque for this application the HR8 would need a stator with a 6.9 cm diameter. The size of the HR8 is 4x5x3 cm.

Although the ultrasonic motor seems like a viable option in terms of size and torque, the inherent friction in an ultrasonic motor make this option inappropriate for this application. The principle behind the ultrasonic motor explains the source of this inherent friction. The rotor and stator are pressed together with a specific amount of preload force. This force multiplied by the coefficient of friction between the rotor and stator specifies the amount of friction that must be overcome to backdrive the unenergized motor. The ultrasonic motor also uses the friction force to produce a drive force. Therefore, the motor cannot produce a drive force that is greater than the friction force. If 1.2 Nm of drive torque are required for this application than a patient will likewise need to produce 1.2 Nm of torque to backdrive an ultrasonic motor. The ultrasonic motor is therefore inherently non-backdrivable. Backdrivability is a key requirement

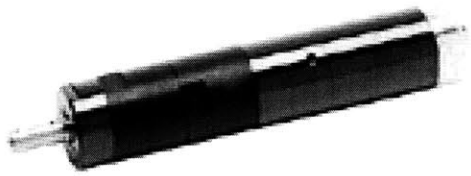

Figure 3-2: Air motor from Atlas-Copco[21]

for this application therefore ultrasonic motors are not a feasible alternative for the actuator in this design.

3.1.2 Pneumatics

Pneumatic actuators use air to produce forces or torques. There are linear pneumatic actuators, referred to as pneumatic cylinders, and there are rotary pneumatic actuators, referred to as air motors. Both options will be discussed in this section.

An air motor is driven by a compressed air source that rotates either vanes or pistons located inside the motor housing. There are several companies that manufacture air motors examples of which can be seen in Figure 3-2 and Figure 3-3.Pneumatic cylinders are also manufactured by a variety of companies. The cylinders vary in size, material, and seal type. Both air motors and pneumatic cylinders can achieve forces that are of the right magnitude for this application. Additionally, they are manufactured in sizes that are reasonable for this application. However, pneumatic actuators have several disadvantages that are difficult to overcome. Air motors are typically made of materials that are not MRI compatible. Therefore, a custom designed motor would have to be developed. Cylinders, on the other hand, can be purchased in a variety of materials some of which are fully MRI compatible. For example, Beco Manufacturing Co. produces pneumatic cylinders composed entirely of plastic, as shown in Figure 3-4.

Pneumatic actuators are operated from a source of compressed air. The thesis of Justin

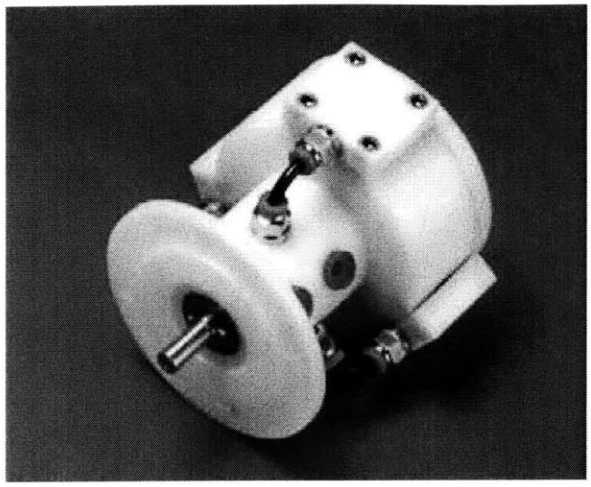

Figure 3-3: Air motor from Dynatork[22]

Figure 3-4: Plastic pneumatic cylinder manufactured by Beco[23]

Verdirame shows that regulating a fluid flow from a pressure source is a difficult task[27]. Verdirame was studying the effects of controlling a hydraulic motor with a pump and valve. He was unable to achieve the desired bandwidth with his design. Pneumatics function in a similar way to hydraulics. However, due to the compressibility of air the bandwidth could be worse than was seen using an incompressible fluid. Finally, pneumatic actuators include a significant amount of friction. For example, most air motors have gear ratios included in their design to amplify the torque output, which contributes friction to the system. Friction could also result from the use of seals to contain the air within the device.

3.1.3 Hydraulics

Two options for hydraulic actuation are available. Hydraulic cylinders provide linear motion and hydraulic motors provide rotary motion. Both hydraulic alternatives will be discussed in this section.

Hydraulic Cylinders

The idea for using hydraulic cylinders is to use them as part of a transmission system linking an electromechanical motor placed outside the MR room to magnetically compatible cylinders that are inside the MRI machine. Recall that this concept was used in an MRI compatible robot discussed in Section 2.6[14]. Additionally, a similar idea was developed within the Newman Laboratory for Biomechanics and Human Rehabilitation by PhD. student Steven Buerger[28]. Buerger's focus was on developing lightweight and low impedance actuators; therefore, his design is not MRI compatible. The prototype developed by Buerger consisted of a system of two hydraulic cylinders and a linear motor as shown in Figure 3-5.

The linear motor was used to drive one of the cylinders which would cause the remote cylinder to be actuated. The idea is particularly useful for an MRI application because it separates the endpoint from the electromagnetic actuator.

There are several advantages to using hydraulic cylinders in this application. First, the size of the electric motor and cylinders can be adjusted to achieve the desired forces. For example, having two cylinders with different cross sectional areas will make an effective gear ratio. The pressure in a closed system is constant which yields the following equation

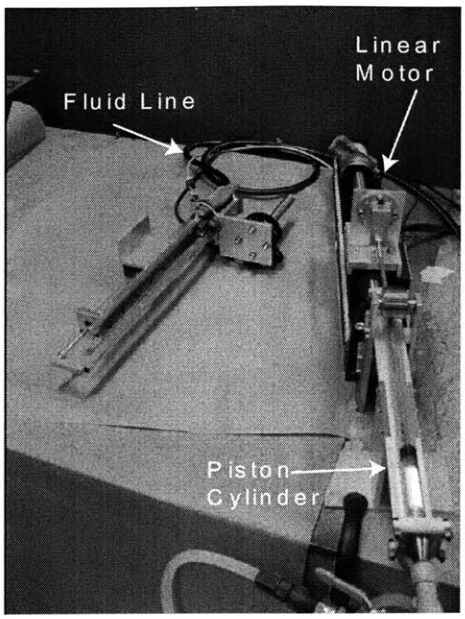

Figure 3-5: Prototype of lightweight, low impedance hydraulic actuator[28]

$$\frac{F_{in}}{A_{in}} = \frac{F_{out}}{A_{out}} \tag{3.1}$$

where F_{in} is the input force, F_{out} is the output force, A_{in} is the area of the input piston, and A_{out} is the area of the output piston. Therefore, if the area of the output piston is greater than the area of the input piston the output force will be amplified relative to the input force. The variety of options in pistons and electric motors makes the force requirement achievable with a multitude of different combinations. This effective gear ratio can be used to eliminate the need for gears or other mechanical advantages that can introduce negative effects such as friction.

With regards to size, only the actuators inside the MRI machine are of concern. This would be one cylinder for each degree of freedom. Hydraulic cylinders come in a variety of sizes in both stroke length and diameter. Therefore, one can be confident hydraulic cylinders that fit within the size envelop can be found. The friction of the system is dependent on several factors. The cylinders will have friction primarily due to the variety of seals that they employ. Airpot manufactures cylinders in which no seal is used between the cylinder and piston. Instead a tight tolerance is held between the two components to minimize leakage. According to the

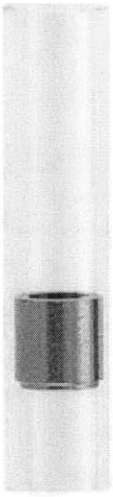

Figure 3-6: Airpot cylinder composed of glass and graphite[24]

Airpot catalog these cylinders have less than 1 N of static friction. The electric motor also contributes friction to the system. The linear motor used in Buerger's setup had a static friction level on the order of 3.5 N[28]. Finally, friction is introduced due to the effects of the fluid. There are several options for MRI compatible cylinders. For example, Airpot cylinders are composed of a glass cylinder and a graphite piston as shown in Figure 3-6. Both materials are MRI compatible.

There is one disadvantage to using hydraulic cylinders. A cylinder is a linear actuator and this application requires rotary motion. Therefore, a transmission system must be designed to convert the linear motion into rotary motion. Overall, hydraulic cylinders seem like a viable option for this application.

Hydraulic Motors

Hydraulic motors are commercially produced with a variety of different mechanisms. For example, the vane motor shown in Figure 3-7 uses spring loaded vanes to generate torque. An internal gear motor, or gerotor, uses two non-concentric gears to produce a torque as shown in Figure 3-8.

Figure 3-7: Vane motor from Rineer[25]

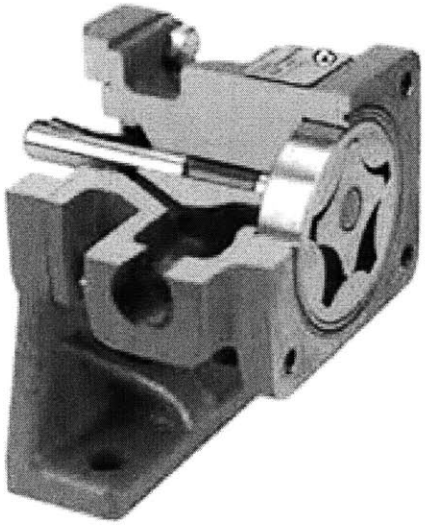

Figure 3-8: Gerotor pump from Viking Pump[26]

Unfortunately, there are several commonalities that make all commercially available hydraulic motors difficult to adapt to this application. First, hydraulic motors are generally used in high torque applications. This MRI compatible robot has relatively low torque requirements. Secondly, hydraulic motors have high friction. The friction is due to the seals that are used to isolate the motor chamber from the environment. Most hydraulic motor designs also require seals to isolate internal chambers. Because a hydraulic motor is used for high torque applications, the friction is comparatively small. However, the friction is far larger than the requirements set for this robot. For example, hydraulic actuators from Micromatic are designed to backdrive at a maximum pressure of 50 psi. That corresponds to approximately 22 Nm of torque which is extremely high for this application. Finally, hydraulic motors are generally made out of steel which is not an MRI compatible material. There are companies that are willing to customize their motors to make them MRI compatible. However, this is costly and does not eliminate the friction problem.

Although, commercially available hydraulic motors may not be feasible there are simple versions of hydraulic motors that could be custom designed to meet the needs of this application. For example, a single vane hydraulic motor, as shown in Figure 3-9, is composed of a single vane within a housing. As fluid is pumped into the housing the vane rotates. The design contains a barrier that separates the inlet and outlet sides of the motor. This barrier reduces the maximum allowable rotation to less than 360 degrees. However, this is not an issue because the motion of the wrist is also limited.

The single vane hydraulic motor functions much like a rotary hydraulic piston, where the motor housing is the cylinder and the vane is the piston. Because Airpot was successful in using no seal between the cylinder and piston, it was speculated that a similar approach could be used in the hydraulic vane motor such that no seal was used between the vane and motor housing. Thus, the hydraulic motor could be used in the same fashion as the hydraulic piston. A transmission system consisting of two hydraulic motors or a hydraulic motor and hydraulic piston can be driven by an electric motor placed outside the MR room as illustrated in Figure 3-10. Therefore, the hydraulic motor can take advantage of all the benefits of the hydraulic cylinders described in the previous section with the added benefit of naturally providing rotary motion. Theoretically, a custom designed single vane hydraulic motor could be designed for

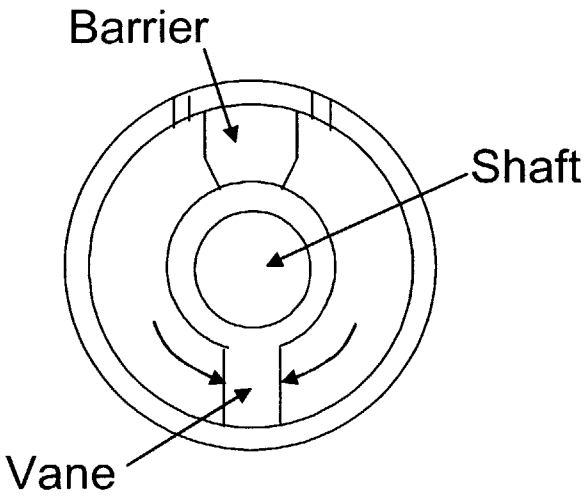

Figure 3-9: Single vane hydraulic motor

low friction, MRI compatibly, and small size.

The concept of a low friction hydraulic vane motor is novel and thus requires testing. The following section describes the design of an initial prototype and proof of concept testing for an MRI compatible, low friction hydraulic vane motor. Assuming the concept for this new hydraulic motor is successful it would be the most appropriate actuator for this application. It would meet all of the functional requirements and be the most convenient for adaptation into the design of an MRI compatible wrist robot.

3.2 Hydraulic Vane Motor

This section outlines the proof of concept design, analysis, and testing performed for the hydraulic vane motor. First, a fluid analysis of the vane motor was performed to explore the importance of various dimensions and attributes in the design. Next, a prototype of the hydraulic motor was designed and built. Analysis was performed on this design to ensure its structural strength. Finally, experimental testing was performed to determine the feasibility of the concept and to examine the effects of various design trade-offs.

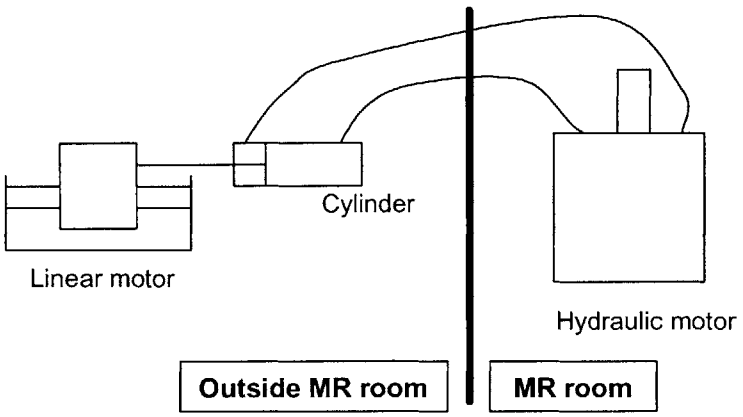

Figure 3-10: Concept for hydraulic vane motor actuation system

3.2.1 Analysis of Vane Motor

To better understand the physics behind the vane motor and actuator system a fluid analysis was performed. This analysis outlines the important parameters in the design of this system with particular attention to factors that can influence the functional requirements set for the MRI compatible robot. Additionally, a structural analysis was performed to ensure the safety and durability of the hydraulic motor design.

Fluid Analysis

The design of a hydraulic motor is based on two major parameters: the efficiency and the torque output. The torque output is based on the amount of friction in the system. Clearly more friction will result in less torque output. The actual torque, T_a, produced by the motor is the difference between the theoretical torque, T_t, and the torque lost to friction, T_f.

$$T_a = T_t - T_f \tag{3.2}$$

The theoretical torque is given by the following equation

$$T_t = \frac{V_D P}{2\pi} \tag{3.3}$$

where V_D is the volumetric displacement in m^3/rev, and P is the fluid pressure.

The total efficiency of the motor is based on two quantities, the volumetric efficiency, η_v, which accounts for fluid loss due to leakage, and the torque efficiency, η_t, which accounts for torque lost to friction. The volumetric and torque efficiencies are determined by the following equations

$$\eta_v = \frac{Q_a}{Q_t} \tag{3.4}$$

$$\eta_t = \frac{T_a}{T_t} \tag{3.5}$$

where Q_a is the actual volumetric flow rate and Q_t is the theoretical volumetric flow rate. The total efficiency, η_{total}, is therefore the product of the volumetric and torque efficiencies.

$$\eta_{total} = \eta_v \eta_t \tag{3.6}$$

Thus, to design an efficient motor it is important to keep the friction and fluid loss due to leakage as low as possible. Most of the friction in a hydraulic motor is a result of seals which are employed to eliminate sources of fluid loss. The seals are generally made from rubber which has a high coefficient of friction. Additionally, they are used on dynamic surfaces such as a rotating shaft. Therefore, seals can be an enormous source of friction. A difficult trade-off exists between friction and leakage. To eliminate fluid loss one must be willing to increase the friction in the motor and vice versa. This trade-off will be the focus of the experimental testing discussed in a later section.

Friction Seals are not the only source of friction in a hydraulic system. The fluid itself introduces friction into the system. The system of hydraulic cylinder, hydraulic motor, and fluid lines was modeled to predict the friction. The friction model was then used to evaluate how changing the geometry of the various components would affect the friction in the system. The model consists of one cylinder, two lines, and a hydraulic motor. For simplicity the hydraulic

motor was modeled as a straight cylinder. However, losses due to the curvature of the motor were accounted for. There are two ways in which pressure is lost due to friction. The first is due to laminar head loss, assuming the flow inside the system is laminar. The following equation describes the head loss

$$h_l = \frac{32\mu LV}{\rho g d^2} \tag{3.7}$$

where h_l is the head loss, L is the length of the line or cylinder, V is the velocity of the fluid, g is acceleration due to gravity, d is the diameter of the line or cylinder, ρ is the density of the fluid, and μ is the viscosity of the fluid[29].

The second source of pressure loss is minor losses due to features in the system such as valves, bends, or junctions. This model includes three sources of minor losses sudden contractions, sudden expansion, and the curvature of the hydraulic motor. There are certainly many other features that could generate friction in the system. Minor losses are evaluated as proportional to a factor K. The K values for a sudden expansion and a sudden contraction are

$$K_{se} = (1 - \frac{d^2}{D^2})^2 \tag{3.8}$$

$$K_{sc} = .42(1 - \frac{d^2}{D^2}) \tag{3.9}$$

where D is the diameter of either the hydraulic cylinder or hydraulic motor. The K values for other minor losses are determined experimentally and must be looked up in a fluids text book. For a bend such as the one in a hydraulic motor K is equal to 0.3. The total head loss for a system is equal to the sum of the laminar head loss and the minor head loss.

$$h = h_l + \frac{V^2}{2g}\sum K \tag{3.10}$$

Because this system consists of three elements with different diameters, it was modeled as a

multi-pipe system. There are two general rules for dealing with multi-pipe systems. First, the flow rate is the same through each pipe.

$$Q_1 = Q_2 = Q_3 \tag{3.11}$$

therefore

$$V_1 d_1^{\,2} = V_2 d_2^{\,2} = V_3 d_3^{\,2} \tag{3.12}$$

The second rule for multi-pipe systems is that the head loss through the entire system is equal to the sum of the head loss through each individual pipe.

$$h_{total} = h_1 + h_2 + h_3 \tag{3.13}$$

Plugging Equation 3.10 into the Equation 3.13 gives the equation

$$h_{total} = \frac{32\mu}{\rho g}\left(\frac{l_1 V_1}{d_1^{\,2}} + \frac{l_2 V_2}{d_2^{\,2}} + \frac{l_3 V_3}{d_3^{\,2}}\right) + \frac{V_1^{\,2}}{2g} K_{sc} + \frac{V_2^{\,2}}{2g} K_{se} \tag{3.14}$$

The conservation of flow rate concept can be used to eliminate V_2 and V_3 and have the entire expression in terms of V_1. The resulting expression is

$$h_{total} = \frac{32\mu}{\rho g}\left(\frac{l_1 V_1}{d_1^2} + \frac{l_2 d_1^2 V_1}{d_2^4} + \frac{l_3 d_1^2 V_1}{d_3^4}\right) + \frac{V_1^2}{2g}(K_{sc} + K_{other}) + \frac{V_1^2 d_1^4}{2g d_2^4} K_{se} \tag{3.15}$$

The expression for h_{total} gives a pressure loss due to friction. However, we are concerned with the force that is lost due to friction. Therefore, h_{total} must be divided by the area of the hydraulic motor.

$$F_{friction} = \frac{h_{total}}{A_{hm}} \tag{3.16}$$

For this application a low friction value is desired. Therefore, the ideal system in terms of friction would have a low viscosity, slow velocity, short length, and large diameter components. Additionally, nonlinear sources of friction should be especially avoided. These frictional sources

grow with the square of the fluid velocity rather than the linear sources of friction which grow proportional to the velocity of the fluid.

Inertia The inertia in the fluid system is also of importance. The inertia has a contribution from several sources the linear motor, hydraulic motor, hydraulic cylinder, and hoses. The inertia of the total system can be express with the following equation

$$I_{total} = I_{hm} + I_{cyl}\left(\frac{A_v r_v}{A_p}\right)^2 + I_l\left(\frac{A_v r_v}{A_l}\right)^2 \tag{3.17}$$

where I is the inertia, A is the area, and r is the radius. The subscript hm refers to the hydraulic motor, cyl refers to the hydraulic cylinder, and l refers to the fluid lines. The inertia of a rotary element such as the hydraulic motor is given by the following equation

$$I_{rotary} = \frac{1}{2}mr^2 \tag{3.18}$$

The inertia of a linear element, such as the fluid lines, is given by

$$I_{linear} = \rho l A \tag{3.19}$$

or the mass of the fluid in the component.

The inertia of this system ideally should be kept as low as possible. Therefore, it is desirable to use a hydraulic motor with a small radius, for the inertia of a rotary element is proportional to the square of the radius. The inertia of the entire system is proportional to the radius to the fourth power. Additionally, the length of the linear elements should be kept short. The inertia is proportional to the length a linear element. Although the inertia of a linear element increases with a large diameter, the overall inertia of the system actually benefits from large diameter linear elements. Therefore, the fluid lines and piston should have large diameters. Finally, the overall apparent inertia can be reduced if the area of the element at the endpoint is made smaller than the area of the elements preceding it. In this case, the area of the hydraulic vane motor should be made large relative to the area of the hydraulic cylinder and fluid lines.

Compliance The final aspect of the fluid system that will be examined is the compliance. There are two sources of compliance in this system. The first is given by the hydraulic fluid. Although water is an incompressible fluid it still has a slight compliance, C_f, given by the following equation

$$C_f = \frac{V}{\beta} \tag{3.20}$$

where V is the volume of fluid and β is a constant equal to 2.1 GPa for water. The second source of compliance in the system is from the fluid lines that are capable of expanding due to the pressure of the fluid. The equation that determines the compliance in the fluid lines is

$$C_h = \left(\frac{\pi d_i^{\,2}}{4E}\right)\left(\frac{(1+\nu)d_o^{\,2} + (1-\nu)d_i^{\,2}}{t(d_o + d_i)}\right) \tag{3.21}$$

where d_i is the internal diameter of the hose, d_o is the outside diameter of the hose, t is the thickness of the hose wall, ν is the Poisson's ratio of the material, and E is the elastic modulus of the material[27]. According to this equation the ideal fluid line will have a small diameter, large wall thickness, and large elastic modulus.

It should be noted that the compliance is related differently to the line diameter compared to friction and inertia. Friction and inertia are improved with large line diameters. However, compliance is improved with a small line diameter. This is a trade off that should be explored further. For now, large line diameters will be used when possible because friction and inertia are important functional requirements of the system.

Structural Analysis

To understand and evaluate the structural validity of the design an analysis was performed. Three aspects of the motor were analyzed: shaft strength, vane strength, and motor housing strength. The dimensions in the design of this first prototype were made some what arbitrarily. They were based on the size of readily available materials and made large enough to facilitate machining, assembly, and testing. Critical components of the motor were evaluated to verify that they were properly sized to avoid structural failure.

Shaft The necessary shaft size for the motor was estimated based on the applied loads. The testing anticipated for this motor will only apply a torsional moment to the shaft. To avoid failure, the diameter of the shaft must satisfy the following relationship

$$d \geq \left(\frac{16M}{\pi\sigma}\right)^{1/3} \tag{3.22}$$

where M is the maximum torsional moment acting on the shaft and σ is the yield strength of the material[30]. In this prototype the shaft material will be aluminum which has a yield strength of 275 MPa. The torsional moment acting on the shaft must be at least 1.2 Nm, which is the required torque of the MRI compatible wrist robot. However, during testing a much higher torque could be encountered. Therefore, a safety factor should be added to the result of this equation. Solving Equation 3.22 results in a minimum shaft diameter of 0.11 inches. In fact, the shaft was designed with 0.75 inch diameter.

Vane The vane of the hydraulic motor was then evaluated to determine that it could withstand the fluid pressure present inside the hydraulic motor. The pressure of the fluid inside the motor was calculated based on the following equation

$$P = \frac{2\pi T}{V_d} \tag{3.23}$$

where T is the torque acting on the vane and V_d is the volumetric displacement. The expression for volumetric displacement is

$$V_d = \pi L(R^2 - r^2) \tag{3.24}$$

where L is the height of the vane, R is the inner radius of the motor housing, and r is the radius of the motor shaft. In this case, L is 4.0 inches, R is 2.0 inches, and r is 0.375 inches. Substituting Equation 3.24 into Equation 3.23 yields

$$P = \frac{2T}{L(R^2 - r^2)} \tag{3.25}$$

Solving Equation 3.25, the pressure inside the motor is found to be 9.5 kPa. This pressure is acting over the area of the vane

$$A_v = L(R - r) \tag{3.26}$$

Therefore, the force acting on the vane is 40 N. From the force the vane thickness, y, can be determined from the following equation

$$y \geq 2\sqrt{\frac{6F(R-r)}{L\sigma}} \tag{3.27}$$

where F is the force, and σ is the yield strength of aluminum. The result of Equation 3.27 yields a vane thickness of at least 0.05 inches. The vane thickness was made 0.25 inches which can safely accommodate any uncertainties in testing.

Motor Housing The motor housing was next analyzed to ensure that it could withstand the fluid pressure within the motor. There are two types of stresses that can develop in a cylindrical pressure vessel such as a hydraulic motor. The thickness of the vessel must be able to withstand these stresses as indicated by the following equation

$$t = \frac{\mathrm{Pr}}{\sigma_h} \tag{3.28}$$

where P is pressure, r is the inner radius of the motor housing, and σ_h is the hoop stress, which acts circumferentially on a cylindrical motor housing. Solving Equation 3.28 the thickness of the vessel constructed out of aluminum must be at least 6.90×10^{-5} inches.

The second stress equation is based on the longitudinal stress acting on a cylindrical pressure vessel. The thickness of the motor housing subject to a longitudinal stress, σ_l, is

$$t = \frac{\mathrm{Pr}}{2\sigma_l} \tag{3.29}$$

Solving Equation 3.29, the thickness of the vessel must be at least 3.45×10^{-5} inches for an aluminum construction. Both equations yield required thicknesses that are well below the standard dimensions in which aluminum stock is available. In fact, the thickness of the material

used in the design of the prototype was 0.25 inches.

The structural analysis has shown that the prototype design for the hydraulic vane actuator is robust. There is no concern that the motor will fail due to the strength of the materials or the size of the components.

3.2.2 Design of the Hydraulic Vane Motor

A prototype hydraulic vane motor was designed and built to test the feasibility of eliminating seals from a hydraulic motor in an effort to reduce friction. A single vane hydraulic motor has a relatively simple design with a limited number of parts. Therefore, it could be built in house, which gives the designer the freedom to make changes and improvements quickly. In addition, the prototype hydraulic vane motor was designed to provide an opportunity to test the importance of certain factors in the design. One important factor is the trade off between fluid loss and friction. Minimizing fluid loss due to leakage requires good seals which are generally high in friction. Likewise, minimizing friction would lead to increased leakage. The prototype was designed so that both options could be tested to compare the effectiveness of each and thus determine the best design. Other factors of the design that could be altered were the variety of shaft seal and fluid type. The details of these test variables will be discussed in greater detail in a later section.

The completed prototype can be seen in Figure 3-12 and Figure 3-14. A solid model of the prototype is shown in Figure 3-11 and Figure 3-13. The prototype was constructed out of aluminum stock for the majority of the parts. Aluminum is not the ideal material in terms of MRI compatibility, however it is readily available and easy to machine. For proof of concept testing, aluminum was the most convenient material. Thus, the motor housing was machined out of an aluminum pipe with and inner diameter of 4 inches. The top and bottom of the motor were also machined out of aluminum. Both pieces contained a groove for an o-ring made of Buna-N. These o-rings provided a static seal that contained the fluid within the motor housing. Four bronze screws were used to tighten the top and bottom of the motor together. The stop was machined out of aluminum and bolted inside the motor housing. Because of the stop's unusual size and shape, it was machined with wire EDM. Due to the presence of the stop the hydraulic motor can only achieve approximately 270 degrees of rotation. The aluminum

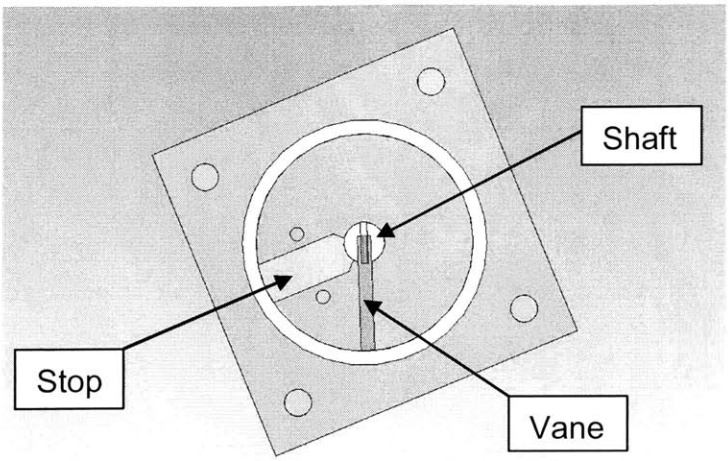

Figure 3-11: Section view of the initial prototype for the hydraulic vane motor

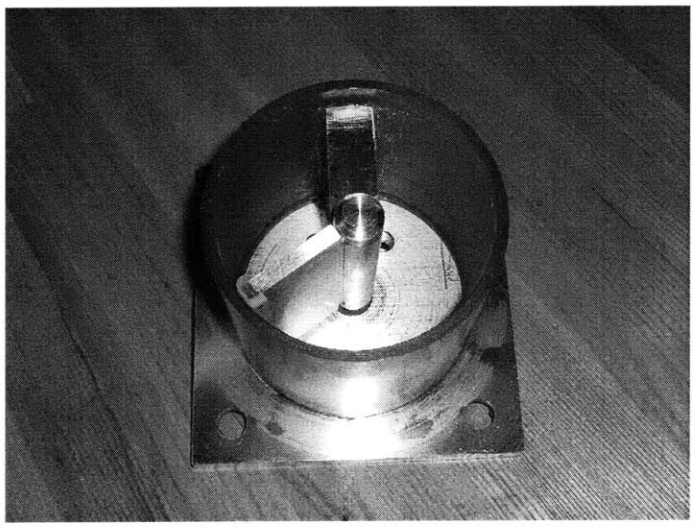

Figure 3-12: Inside view of the hydraulic vane motor prototype

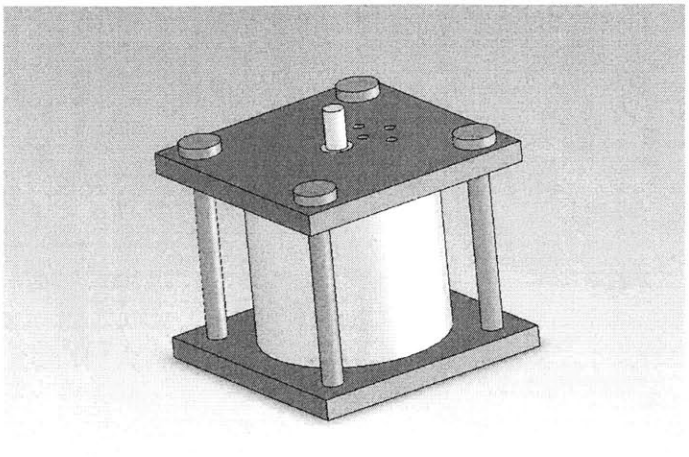

Figure 3-13: Solid model of the initial prototype for the hydraulic vane motor

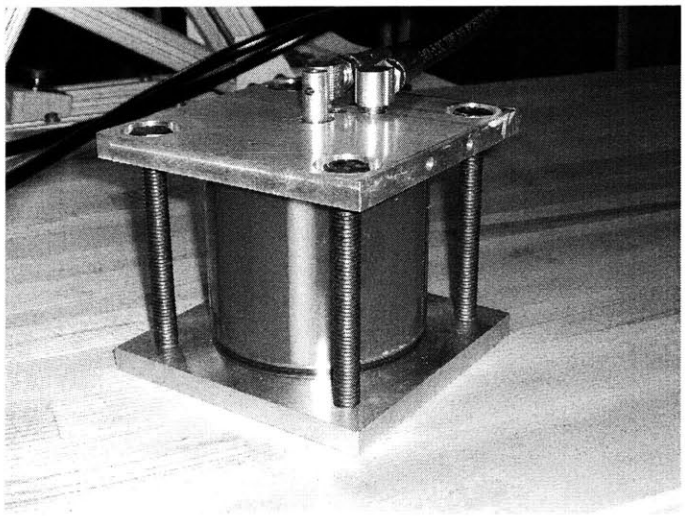

Figure 3-14: Assembled prototype of the hydraulic vane motor

shaft of the motor was machined with a groove to accommodate the vane. The vane could be bolted into the groove so that it would not be touching the motor wall or it could be placed in the shaft groove with a spring behind it so that it would be spring loaded against the motor wall. The vane was manufactured out of aluminum; however, a plastic tip was attached to the vane so that it would slide smoothly along the aluminum motor housing. Plain bearings made of Rulon J were used to provide low friction support between the shaft and the end caps of the motor.

Finding a proper spring to preload the motor vane against the motor wall required some trial and error. Conventional compression springs are made of steel which is not a magnetically compatible material. Additionally, compression springs tend to be long, which would be difficult to accommodate in this design. Other spring options include a leaf spring, or a springy material such as rubber. Leaf springs are not generally sold as off the shelf items. They are custom designed for the specific application. This is not a feasible option in terms of time, flexibility, and cost for a first prototype. Therefore, it was decided that rubber would be the simplest and most likely successful option to pursue. However, using rubber as a spring had its difficulties as well. There are two important considerations when using rubber. Rubber comes in a variety of thicknesses and durometers. To determine the most appropriate rubber to use in this application, an assortment of rubber sheets were purchased each sheet having a different durometer or thickness. Through testing, it was determined that rubber with a 1/32 inch thickness and 60 durometer hardness provided the most appropriate amount of preload.

Building this prototype in house helped iron out some design issues that will be useful in the final design. One important discovery was that aluminum pipe does not have a smooth or precise inside surface. Therefore, if pipe is used it must be bored out to make the inner diameter the exact desired dimension and to make the surface smooth so that the o-ring will seal properly. A second issue that could be improved upon is the visibility into the motor. When the motor is assembled it is not possible to see how well the parts fit together. For instance it would be nice to be able to see the gap between the vane and the motor wall and see of any gaps that may be larger than intended. This may be an issue for this initial prototype however it may not be important for the final design.

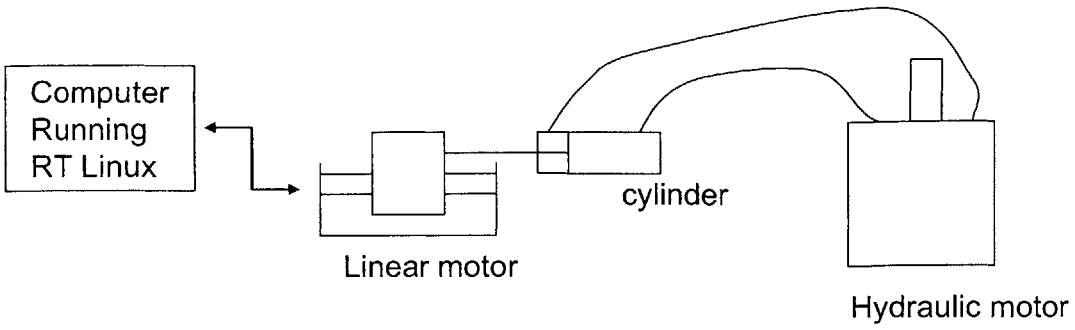

Figure 3-15: Experimental setup used to test the hydraulic vane motor

3.3 Testing of the Hydraulic Vane Motor

Proof of concept testing was performed on the hydraulic motor. The tests were primarily designed to determine the feasibility of eliminating seals from the typical hydraulic motor design. The hope was that eliminating the seals would reduce the friction.

3.3.1 Experimental Setup

The experimental setup consists of a linear motor, hydraulic cylinder, and the custom designed hydraulic vane motor. The components were arranged as shown in Figure 3-15. A picture of the system is shown in Figure 3-16.

It should be noted that all testing was done outside the MRI room. In the final design the hydraulic motor will need to be composed of MRI compatible materials because it will be located inside the MR room. For the testing of the prototype hydraulic vane motor MRI compatible materials were used as much as possible when convenient. However, MRI compatibility was not a testing requirement; therefore, it was not strictly enforced. For example, all sensors added to the basic setup did not comply with the MRI compatibility requirements.

Although the setup uses a linear motor and hydraulic cylinder, these components could be replaced with a rotary electric motor and hydraulic motor. The linear motor was used because it was readily available in the lab. Software to run the linear motor had been previously developed and only required modifications based on the specific experiments to be run. A real time control system, RT Linux, was used to run the linear motor and gather data from the

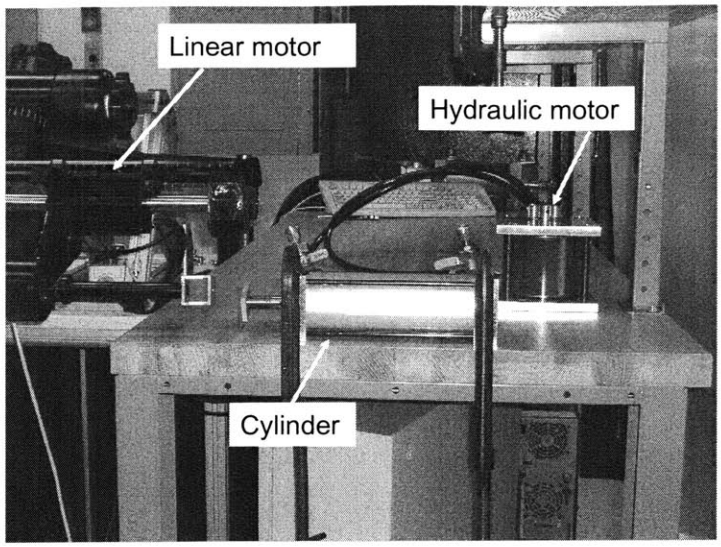

Figure 3-16: Picture of the test setup

sensors. The linear motor was already equipped with a force transducer and an encoder. A test jig was built for the hydraulic motor so that either an encoder or a force transducer could be attached. This test jig, shown in Figure 3-17, would lock the motor shaft to the motor housing when the force transducer was mounted. If the encoder was in place the shaft was free to rotate relative to the motor housing. The encoder used on the hydraulic motor was manufactured by Gurley Precision Instruments model R119, which has a maximum of 65,536 counts per revolution after quadrature decoding[31]. The force transducer purchased from ATI Industrial Automation was the Gamma model, which has a range of ± 100 lbf when used to measure torque and forces perpendicular to the sensor[32]. The hydraulic cylinder was connected to the hydraulic motor via two hoses. The hoses were reinforced Parker hoses with an inner diameter of 0.25 inches. Each hose was five feet in length. The system was connected by threaded fittings composed of brass.

The system was filled using the setup illustrated in Figure 3-18. A tank of fluid was placed above the system and gravity was used to draw the fluid into the various components. The fluid was pumped in by cycling the cylinder. The air was less dense than the fluid; therefore, the air would rise out of the system to be replaced by fluid. This method of filling the system

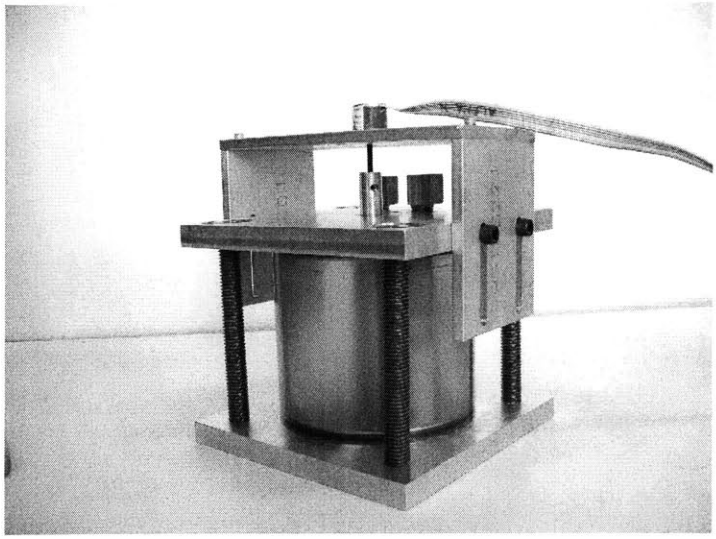

Figure 3-17: Picture illustrating the test jig holding the encoder

was slow; however, it proved to be suitable for testing purposes.

3.3.2 Experimental Procedures

The experiments were designed such that three values could be measured while three variables were changed. The three experiments performed on the experimental setup measured the relationship between the input force and output torque, the relationship between the input displacement and the output rotation, and the static friction in the system.

Several variables were designed into the system. First, the vane was designed such that it could touch the motor housing or not touch the motor housing. The first vane was designed to leave only a small clearance between the wall of the motor and the vane. This vane aimed to minimize the friction against the motor wall while allowing fluid leakage to occur. The second vane was designed so that the vane would rub against the motor wall. This design would minimize leakage but introduce friction.

Another variable was the type of seal for the shaft of the motor. Three different options for the seal were purchased. First, a plain bearing with a close tolerance would provide a low friction interface but possibly result in severe leakage. The second option was a rubber seal

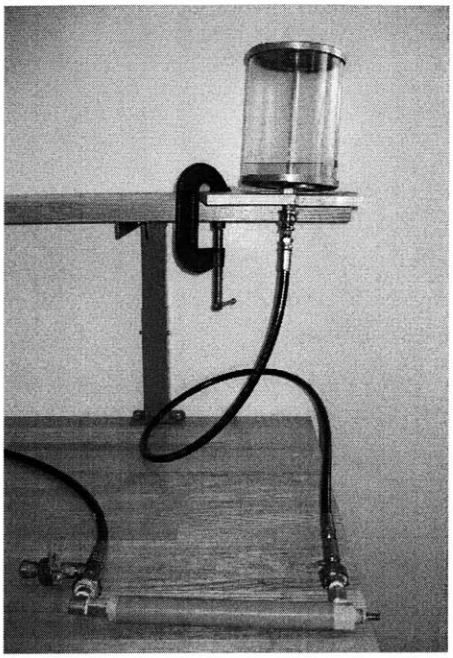

Figure 3-18: Setup used to fill the hydraulic system

which would eliminate all leakage but create high friction. The final option was a spring loaded Teflon seal, which has lower friction than the rubber seal but still maintains little to no leakage. The spring seal is not MRI compatible because the spring is composed of steel. However, it provides a good comparison until an MRI compatible version can be found.

The type of fluid used in the system was an additional variable that could be altered. Oil and water were the two fluid options. Water is less viscous that oil, therefore it introduces less friction. However, oil's high viscosity makes it more difficult to force through small gaps making leakage less likely. Finally, several different cylinders were purchased. These cylinders ranged in piston area and friction levels.

It should be noted that the experimental plans changed significantly over the course of testing. This was due to a variety of difficulties that were encountered and will be discussed in the next section.

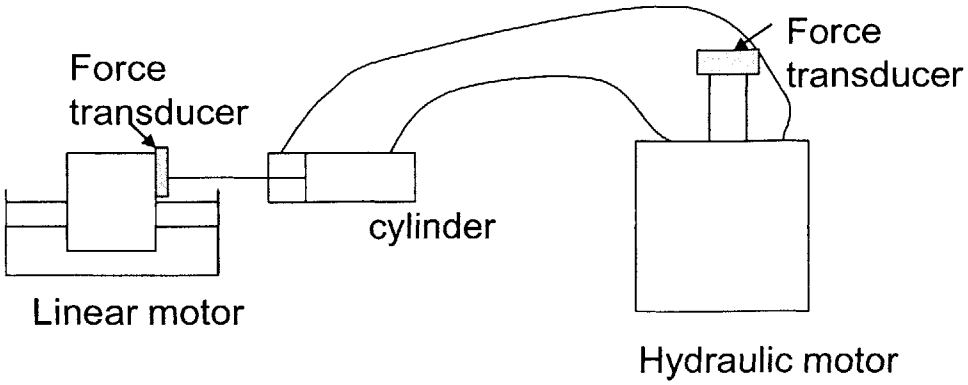

Figure 3-19: Setup for running the experiment to test the force/torque relationship

Force to Torque Relationship

This experiment was designed to determine the relationship between the input force provided by the linear motor and the output torque from the hydraulic vane motor. The setup for this test is shown in Figure 3-19. This test requires the use of two force transducers: one on the linear motor and a second on the hydraulic motor. The hydraulic motor is locked to the force transducer so that it is unable to rotate. The linear motor was then forced by hand. The force from the linear motor and the torque at the hydraulic motor were measured. Based on the size of the components in the system the theoretical relationship between force and torque can be calculated. The ratio of force to torque is based on the fact that the pressure in the system is constant. The equation governing this ratio is

$$\frac{T}{F} = \frac{A_v R_{eff}}{A_c} \tag{3.30}$$

where A_c is the area of the cylinder, A_v is the area of the vane, R_{eff} is the effective radius of the hydraulic motor. The effective radius is determined by the following equation

$$R_{eff} = \frac{R + r}{2} \tag{3.31}$$

where R is the maximum internal radius of the motor and r is the minimum internal radius of the motor.

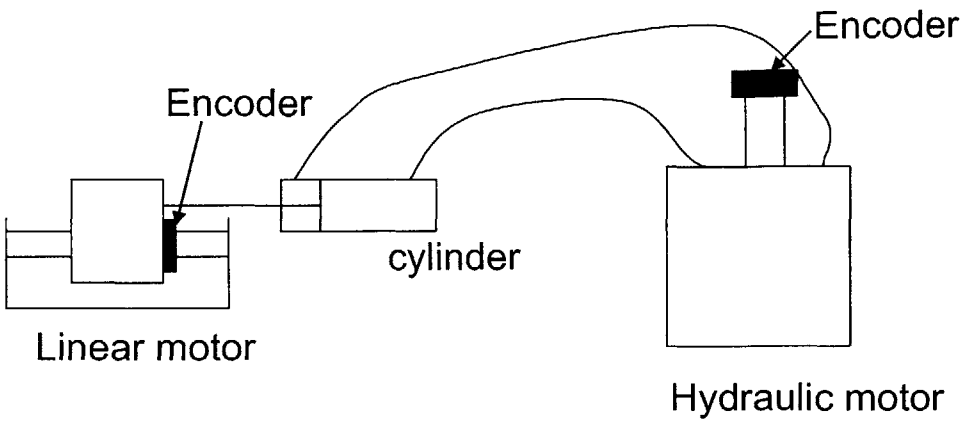

Figure 3-20: Experimental setup for testing the relationship between linear displacement and rotary displacement

Linear Displacement to Rotary Displacement Relationship

This test was designed to determine the relationship between the linear displacement of the linear motor and the rotary motion of the hydraulic motor. The setup for this experiment is illustrated in Figure 3-20. An encoder is placed at the linear motor and a second at the hydraulic motor. The linear motor is moved and its motion is recorded. The corresponding motion in the hydraulic motor is similarly recorded. The relationship between the linear motor displacement and the hydraulic motor displacement is based on the size of the components in the system. The theoretical ratio between linear displacement and rotary displacement is governed by

$$\frac{x_{linear}}{x_{rotary}} = \frac{L(R^2 - r^2)}{2A_c} \tag{3.32}$$

where x_{linear} is the displacement of the linear motor and x_{rotary} is the displacement of the hydraulic motor in radians.

Static Friction

The static friction in the system was tested in the following fashion. A force transducer is placed at the linear motor and an encoder is placed at the hydraulic motor, as shown in Figure

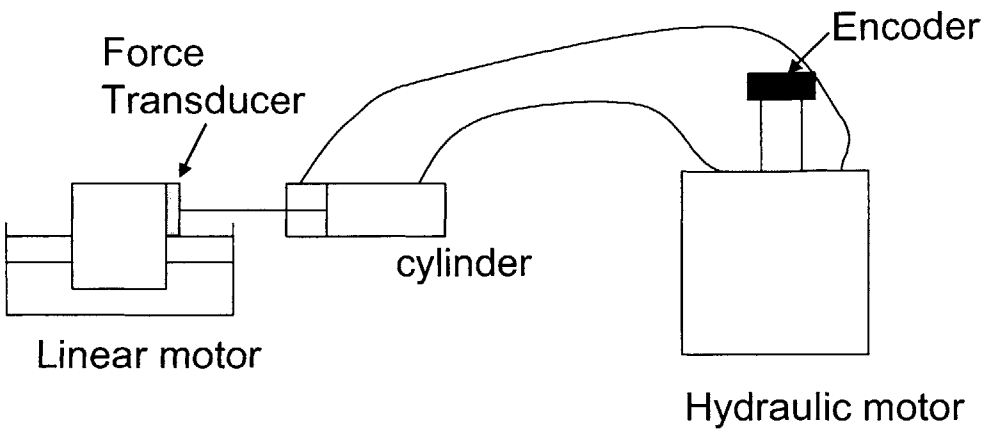

Figure 3-21: Experimental setup for testing static friction

3-21. The computer was programmed to linearly increase the force output by the linear motor until the hydraulic motor began to rotate. The force required to set the hydraulic motor into motion is equal to the static friction in the system.

The individual components of the system can be tested for static friction in a similar manner. For example, the static friction in the linear motor alone and the linear motor and hydraulic cylinder were tested. In this case, a force transducer and an encoder were placed at the linear motor. The force commanded to the linear motor was linearly increased until the encoder register that motion had occurred. These additional static friction tests allowed the source of the friction to be determined.

3.3.3 Experimental Results

This section discusses the experimental results that were obtained during the testing of the hydraulic vane motor. The main goal of the testing is to determine the trade-off between using a low-friction but high-leakage approach compared to a high-friction and low-leakage approach. Extensive troubleshooting was required to get the hydraulic motor functioning properly. This process is outlined first, as it provides valuable knowledge as to how future designs must be structured.

Troubleshooting

The hydraulic vane motor was initially set up to test the lowest friction design. Therefore, the lowest friction option for each of the design variables was selected as a starting point. No shaft seal was used; instead a plain bearing was the only component contacting the rotating shaft. Water was chosen as a hydraulic fluid. The vane was installed such that it was not touching the motor wall. Finally, the lowest friction hydraulic cylinder purchased from Airpot was used in the system. The Airpot cylinders are low friction because there is no seal between the piston and the cylinder. Instead a tightly held tolerance is used to minimize leakage. Inevitably some fluid loss exists, however the exact amount of leakage is unknown.

The low friction system was unsuccessful. Making any changes to the lowest friction design requires a friction element to be introduced. Therefore, the approach to finding a working system was to gradually and systematically add friction into the system. It was immediately obvious that leakage through the plain bearing was significant. Therefore, the first step in the attempt to get the system working was to remove all external leaks. To solve the problem, of fluid loss through the shaft seal the rubber and spring loaded Teflon seals were tested. Both seals solved the leakage problem; however the Teflon seal added less friction than the rubber seal. It was therefore concluded that the shaft does require a seal and that a spring loaded Teflon seal works best. Additionally, Teflon tape was added to the fittings to minimize the external leakage occurring through the connections.

Eliminating external fluid loss still did not solve the problem. The next step was to eliminate internal fluid loss in the hydraulic cylinder. A small amount of leakage was occurring where the shaft of the cylinder exits the housing. Based on this observation, it was presumed that leakage was also occurring inside the cylinder around the piston. To eliminate this internal fluid loss, the Airpot cylinder was replaced with a cylinder that contained contact seals. The higher friction cylinder ensured that no fluid leakage was occurring internal to the cylinder. Still, the system was unsuccessful.

At this point the only leaks remaining were internal to the hydraulic vane motor. There were several places inside the hydraulic motor where fluid loss could occur. The most obvious were between the shaft and the stop and between the vane and the motor wall. Little could be done to minimize the gap between the stop and the motor shaft. However, sealant was used to

ensure that all gaps around the stop due to manufacturing errors were filled. For example, a small gap between the stop and the motor wall was filled with sealant. Additionally, the vane was altered so that it was touching the motor wall. Unfortunately, eliminating these internal leaks in the hydraulic vane motor did not eliminate the problem.

The next step in the troubleshooting process was based on an observation made during testing with the Airpot cylinder. It was noticed, that when the Airpot cylinder was used, the system would work when the hydraulic motor was turned, however it would not work when the hydraulic cylinder was pushed. Two possible explanations for this observation were developed. First, the volume of liquid in the hydraulic motor was much larger than that in the hydraulic cylinder. It was possible that the momentum of the fluid moving from the hydraulic motor to the cylinder was larger and therefore inducing more motion. Comparatively, the momentum of the fluid moving from the hydraulic cylinder to the hydraulic motor was so small that it was having no effect. The second explanation was that the Airpot cylinder had very low friction so a smaller force was needed to put it into motion. However, the hydraulic motor had a larger amount of friction and therefore required more force to put it into motion. Based on this observation, possible solutions were to use a hydraulic cylinder with a larger diameter to increase the flow or to decrease the volume of the hydraulic motor. The quickest solution was to add a spacer to the hydraulic motor to see if the concept was worth pursuing. At this point a small amount of motion was being witnessed however the performance was far from suitable.

Another idea for reducing the amount of internal leakage was to use a more viscous fluid. A fluid with a larger viscosity will be more resistant to moving through small gaps. The flow through a gap is resisted by the wall shear stress.

$$\tau_w = \mu \frac{du}{dy} \tag{3.33}$$

where τ_w is the wall shear stress, μ is the fluid viscosity, and $\frac{du}{dy}$ describes the velocity profile through the gap. The shear stress is proportional to the fluid viscosity, so increasing the viscosity by a factor of two will increase the shear stress by a factor of two thus making it twice as difficult for fluid to flow through the gap[29]. An alternative way of approaching the problem would be to look at the velocity of the flow through the channel. Reducing the velocity of the flow will likewise reduce the rate at which the fluid is leaking through the gap. The velocity

of fluid through two parallel plates is

$$V = \frac{Plh^2}{3\mu} \tag{3.34}$$

where h is the thickness of the gap, l is the length of the gap, and P is the pressure drop along the length of the gap. The fluid viscosity is inversely proportional to the flow velocity. Thus, an increase in the viscosity will result in a proportional decrease in the fluid velocity. Both equations indicate that increasing the viscosity of the fluid should reduce the problem of internal leakage. Water has a viscosity of 0.89×10^{-3} Pa·s and oil has a viscosity of 32×10^{-3} Pa·s, which is nearly a 36 fold increase in viscosity. This should similarly reduce the fluid loss 36 times. Therefore, the water in the system was replaced with oil.

At this point the system was working well enough to take some initial data. Figure 3-22 shows data from a test to measure the ratio of linear displacement to rotary displacement. There are three obvious problems occurring in the system. First, the slope of the line is not that which was theoretically predicted by Equation 3.32. Second, there are some mysterious end effects in which the hydraulic cylinder is being forced but no motion is induced in the hydraulic motor. Finally, the motion is not repeatable. The curve starts and stops at a different place for each cycle. This means that if the displacement of the cylinder is known the angle of the hydraulic motor can not be inferred. Clearly something within the hydraulic vane motor is still not functioning properly.

Due to the systematic approach that was taken to troubleshooting the hydraulic vane motor, it was clear that the problem was occurring inside the hydraulic motor. However, the housing of the motor was composed entirely of aluminum. It was therefore impossible to see inside the motor and assess the problem further. Thus, a new motor housing composed of a clear plastic was machined. This component would allow the internal workings of the motor to be witnessed and hopefully the problem could be spotted. As soon as this clear motor housing was employed the source of the problem was obvious. There were gaps between the vane and the shaft due to manufacturing inaccuracies. These gaps were filled with sealant. Finally, the hydraulic motor was functioning properly and quality data could be collected.

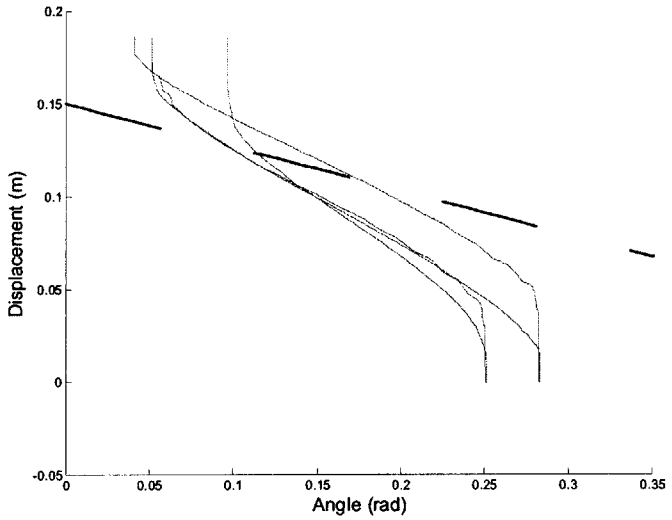

Figure 3-22: Data for the displacement ratio when internal leakage is occuring. The dashed line represents the theoretical displacement ratio.

Static Friction

The first test performed was to characterize the static friction in the system. Three static friction measurements were taken. First, the linear motor alone was tested for static friction. Figure 3-23 shows the results from this testing. The static friction in the linear motor is dependent on location. This is due to the construction of the motor, which consists of a series of magnets. The static friction can vary depending on where the forcer is located relative to the magnets. The average static friction in the linear motor is approximately 1.2 N and the maximum is 1.9 N.

The second static friction test that was performed was to test the friction in the hydraulic cylinder. The hydraulic cylinder was not filled with fluid during this test. Additionally, the linear motor was used to perform this test; therefore, the static friction of the linear motor is also measured. Two different cylinders were tested: a small cylinder with a diameter of 1.0625 inches and a medium sized cylinder with a diameter of 2.5 inches. A large cylinder, with a 4.5 inch diameter, was also purchased; however, its static friction level was so high that it was impossible to actuate with the available linear motor and thus was not tested. The data from

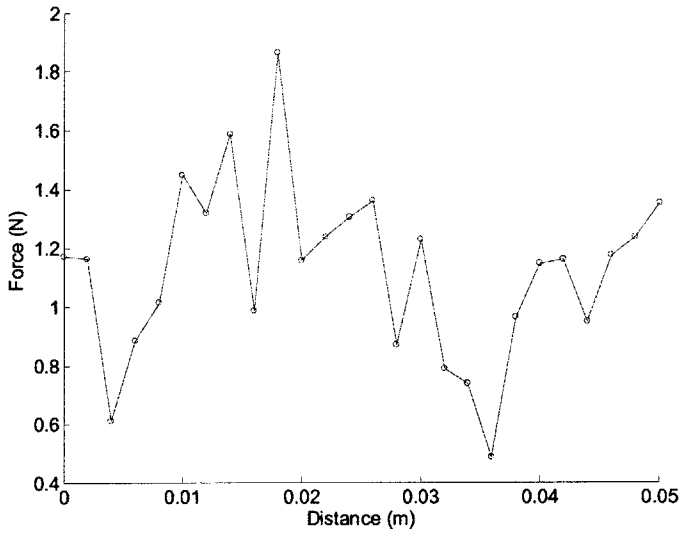

Figure 3-23: Static friction in the linear motor

this test is shown in Figure 3-24. The small cylinder contained approximately 12 N of static friction and the medium sized cylinder contained 25 N of friction. This is clearly a large source of static friction compared to that of the linear motor alone.

Finally, the static friction test was performed on the whole system filled with oil. It was discovered that the medium sized cylinder was too difficult to actuate when filled with fluid. Thus, further test data for the medium cylinder could not be obtained. All of the remaining test data refers to the system utilizing the small cylinder. The static friction test for the whole system was tested with the vane touching the motor wall and then with the vane not touching the motor wall. The result of these tests can be seen in Figure 3-25 and Figure 3-26. The pushing and pulling motions of the cylinder are separated on the graphs. This is because the area of the piston is different depending on which way it is being actuated, due to the presence or absence of the piston rod. A larger area piston will require more force to produce an equivalent amount of pressure in the system. This is reflected in the experimental data. Pushing on the piston rod means the larger piston area is forcing the fluid and a larger force is expected. In both vane configurations pushing the cylinder required more force to overcome the static friction.

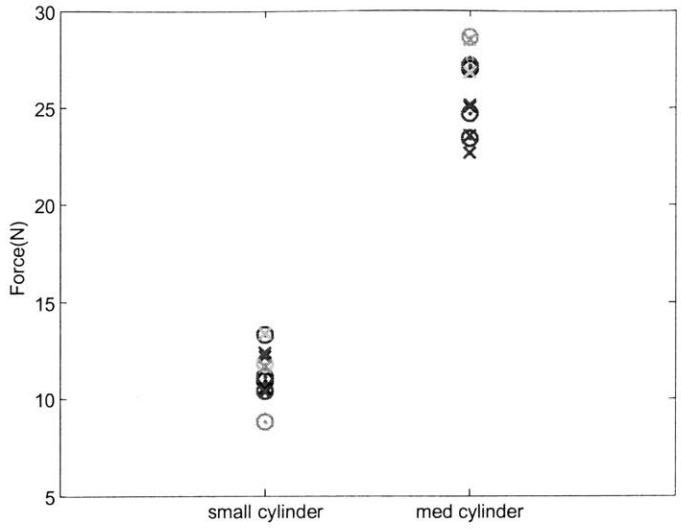

Figure 3-24: Static friction in the cylinders, where x indicates a measurement from the force sensor and o is the force calculated from the motor voltage

One unusual result is that less static friction was present in the system when the vane was touching the motor wall. This result is opposite of what was expected. The static friction was expected to decrease when the vane was not touching the motor wall due to the removal of sliding friction. There is no elegant explanation for this result. The system had to be taken apart, the fluid changed, and the system reassembled to change the motor vane. Some additional friction could have been introduced during this process. For example, dirt could have entered the system or the alignment of the components could have been altered slightly.

The more useful piece of data is the relative increase in friction compared to the previous test in which only the cylinder and linear motor were included. Recall that the cylinder and linear motor system contained 12 N of static friction. The static friction results of the whole system are summarized in Table 3.1. According to the test data the hydraulic vane motor, fluid lines, fittings, and fluid add an additional 1-8 N of static friction. This is a promising result because it indicates that the prototype hydraulic vane motor contributes only a small portion of the overall static friction. This, in fact, was the goal in specially designing a hydraulic motor.

The biggest contribution to the static friction in the system comes from the hydraulic

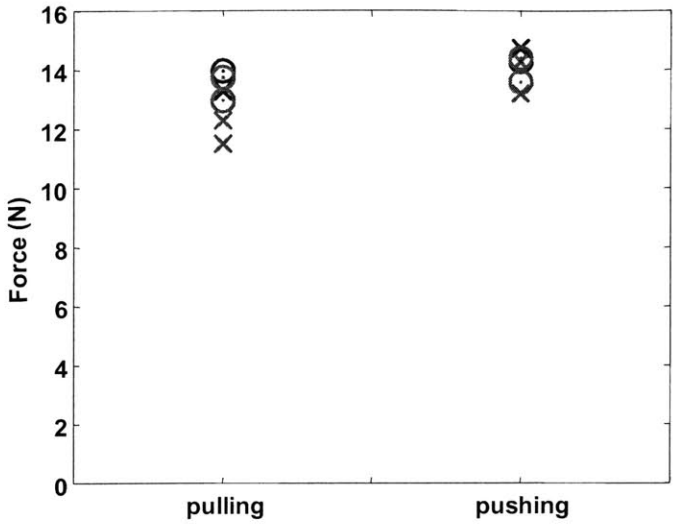

Figure 3-25: Static friction in the system when the vane is touching the motor wall

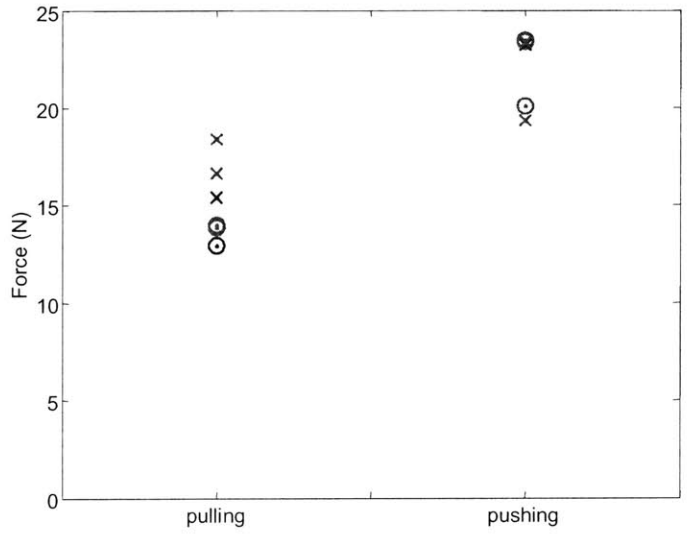

Figure 3-26: Static friction in the system when the vane is not touching the motor wall

	Pulling Force (N)	Pushing Force (N)
Vane touching	13	14
Vane not touching	15	20

Table 3.1: Static friction in test setup

cylinder. In the final design, the friction in the hydraulic cylinder can be dealt with in several ways. First, the cylinder was a purchased component for which many different alternatives exist. The solution could be as simple as purchasing a lower friction cylinder from a different manufacturer. Additionally, there is no reason a hydraulic cylinder must be used at all. Instead, the system could be composed of two hydraulic vane motors driven by a rotary electric motor. This could be a very effective option considering the low friction measured from the hydraulic motor during this testing. Hopefully in the final design this friction can be reduced even further.

Displacement Relationship

The next set of data presented here will report on the relationship between the input displacement from the linear motor to the output rotation of the hydraulic motor. Based on the size of the components in the system and Equation 3.32, the ratio of linear displacement to rotary displacement should be 0.24 m/rad. The test was run with the vane touching the motor wall and the vane not touching the motor wall. The data obtained for these tests is shown in Figure 3-27 and Figure 3-28. In both situations the displacement ratio matched the theoretical value.

Force to Torque Relationship

The final set of test results are regarding the relationship between in input force from the linear motor and the output torque from the hydraulic vane motor. Figure 3-29 shows the experimental data for the torque to force ratio when the vane is touching the motor wall. There is a section of the plot in which the linear motor is being forced but the hydraulic motor is not producing any torque. This result was due to the method the hydraulic motor was manufactured and assembled. When the vane was touching the motor wall, it was placed in a slot machined into the motor shaft and preloaded against the motor wall with a piece of rubber.

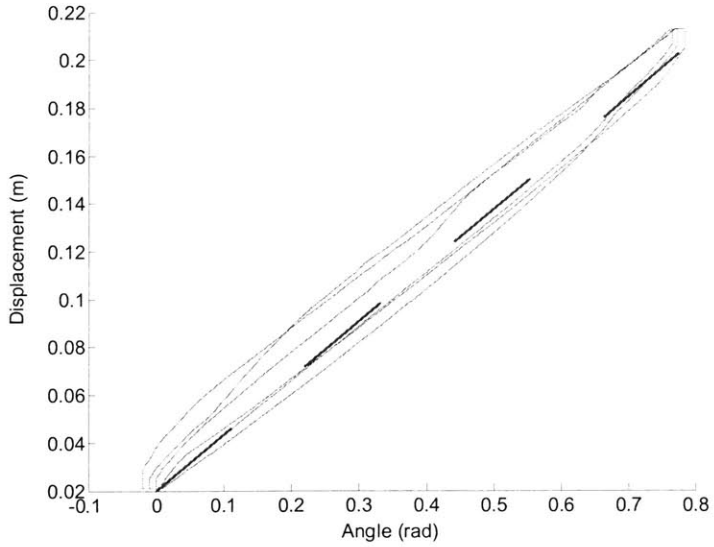

Figure 3-27: The displacement ratio when the vane is touching the motor wall, where the dashed line is the theoretical relationship

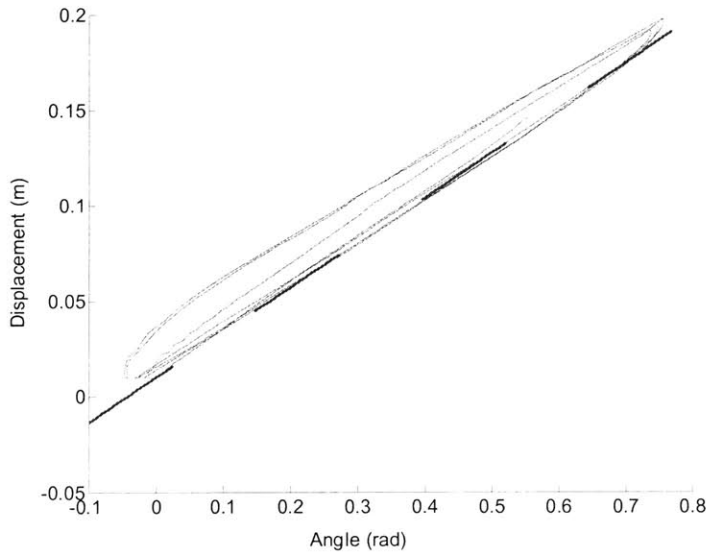

Figure 3-28: The displacement ratio when the vane is not touching the motor wall, where the dashed line is the theoretical relationship

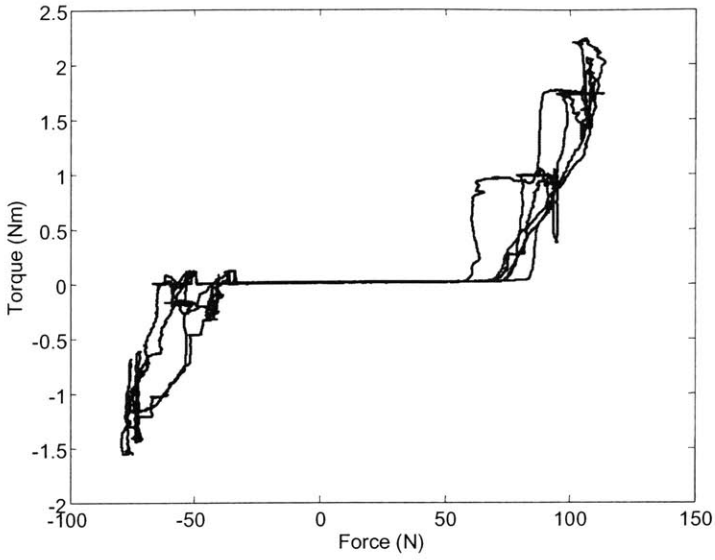

Figure 3-29: Torque to force relationship when the vane is touching the motor wall

However, the vane was not rigidly attached to the shaft. Therefore, it was observed that the vane would move within its slot rather than produce a torque on the shaft. Only after the vane was cocked securely in the slot would it begin to transfer torque to the shaft. This can be seen on the graph as the region above 75 N and below -50 N. The torque producing region of the data has a slope of 0.07 Nm/N. The theoretical ratio of torque to force is indicated by Equation 3.30 and should be 0.24 Nm/N for this particular setup. Therefore, 29 percent of the force input to the system is being converted to output torque.

The data for the experimental setup in which the vane was not touching the motor wall can be seen in Figure 3-30. In this case, the vane is rigidly connected to the shaft so there is no region where the torque is not being transmitted. The slope of this data is 3.5×10^{-5} Nm/N. Therefore, 0.01 percent of the input force is being converted to output torque. The poor torque output when the vane is not touching is discouraging. However, one must consider the dependence of the torque output on the gap size. The pressure acting on the motor vane is inversely proportional to the square of the gap size according to the following equation

$$P = \frac{3\mu L v}{h^2} \tag{3.35}$$

where L is the length of the gap, v is the velocity, and h is the gap thickness. However, the gap width is not precisely known. When the vane is touching the motor wall the gap width at the wall is assumed to be zero. For the vane not touching the motor wall the gap was made as small as possible considering the manufacturing skill and technique available. The gap was measured to be approximately 0.03 inches. In both cases the top and bottom of the vane is not touching the motor housing. In reality the vane is never completely sealed. Additionally, the gap size when the vane is not touching is much larger than a typical machine shop can produce if the parts had been outsourced.

To get a better estimate of the actual gap width, Equation 3.35 was solved using the velocity data obtained from testing. The gap width, h, was adjusted until the solution to Equation 3.35 matched the best fit line obtained from the experimental plots for the torque to force relationship. This method makes use of the experimental data to estimate the gap width. The fit for the vane not touching the motor wall is shown in Figure 3-31 and corresponds to a gap width of 0.12 in. The fit for the vane touching the motor wall is shown in Figure 3-32 and corresponds to a gap width of 0.004 in. According to these results, the vane touching the motor wall actually has a gap width that is close to what is expected to be achieved when the motor is manufactured with stricter tolerances. In fact, if the machining of the motor is outsourced and manufactured using wire EDM the tolerances can be held to 0.0005 in. This is significantly smaller than the gap width that was achieved using in house manufacturing.

3.4 Actuator Conclusions

Hydraulic actuation was deemed the most promising of the actuator options. A novel idea was developed for a low friction hydraulic motor. Therefore, a proof of concept prototype of the motor was designed and constructed. After evaluating the prototype hydraulic motor, it was determined that a low friction hydraulic motor is a feasible option. However, the gap size must be carefully controlled. The motor concept is capable of maintaining the proper relationship between the input and output displacements under low loads. This capability seems to be true

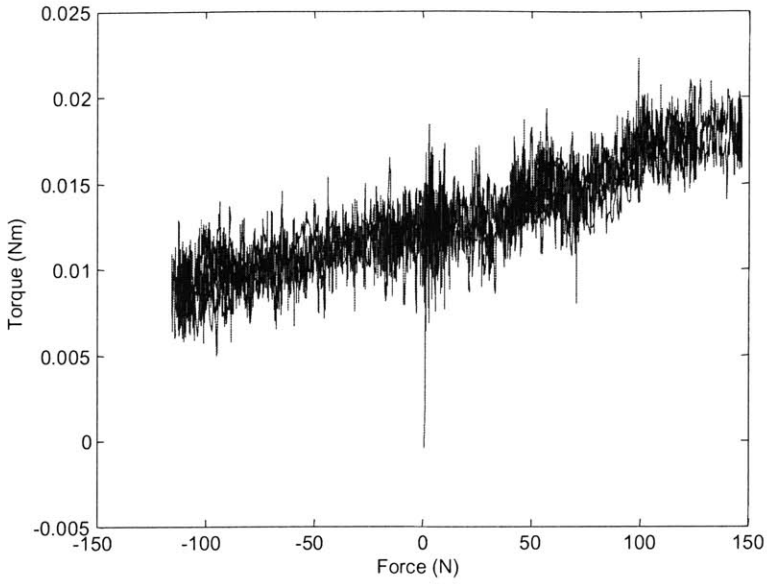

Figure 3-30: Ratio of force to torque with the vane not touching the motor wall

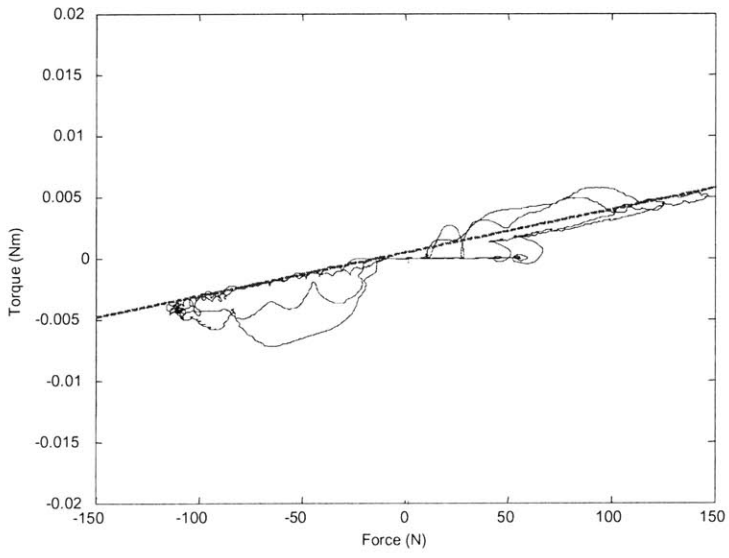

Figure 3-31: Data fit to determine the gap size for the vane not touching, where the dashed line is the theoretical line for a gap width of 0.12 inches

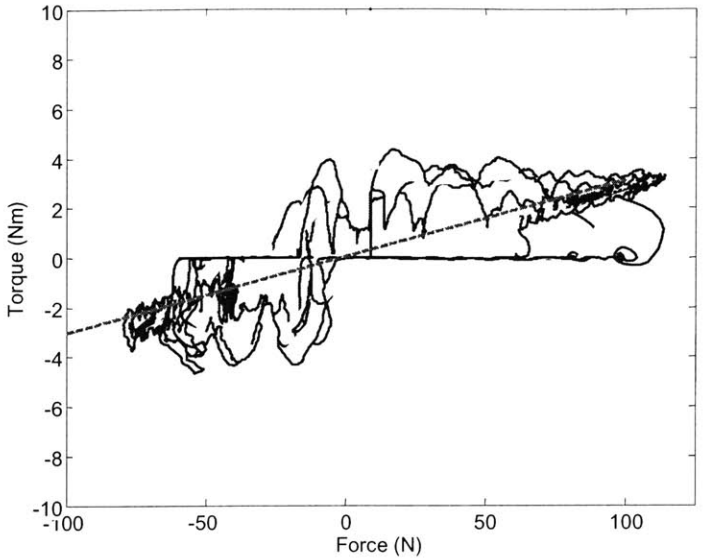

Figure 3-32: Data fit to determine the gap width for the vane touching the motor wall, where the dashed line is the theoretical line for a gap width of 0.004 inches

regardless of the gap between the motor housing and the vane. On the contrary, the input and output force relationship is highly dependent on the gap between the motor housing and the vane. Suitable torque values can be obtained with little to no gap; however, a large gap produces a negligible amount of torque. Therefore, this actuator option will be pursued by altering the motor design and improving the manufacturing technique to minimize the gaps internal to the motor.

Chapter 4

Transmission Selection

The existing wrist robot uses a differential as a transmission to produce the two degrees of freedom required for abduction/adduction and flexion/extension. This transmission was reevaluated for two reasons. First, it was necessary to find out if a differential is a feasible option with MRI compatible components. Second, there might be an alternative transmission that is better suited for this application. Based on the functional requirements the transmission must allow for two degrees of freedom. Additionally, one advantageous aspect of the original wrist robot is that both actuators are attached to ground. Therefore, the transmission for this application aims to preserve this characteristic. Five different transmission alternatives were considered: differential, cables and belts, geared rings, friction drive, and spatial kinematics. The differential was evaluated first to show that it is still a feasible option for this application. Because the differential was used successfully in the wrist robot, it was used as a benchmark to which the other alternatives were compared.

4.1 Differential

A differential is a transmission in which a set of three or four miter gears are arranged to produce two degrees of rotary motion as seen in Figure 4-1.

The motion is related to the relative motion of the two actuators. If the two drive gears are rotated in the same direction than the spider gears will rotate about axis "B". However, if the drive gears are rotated in opposite directions the spider gear will rotate about axis "A".

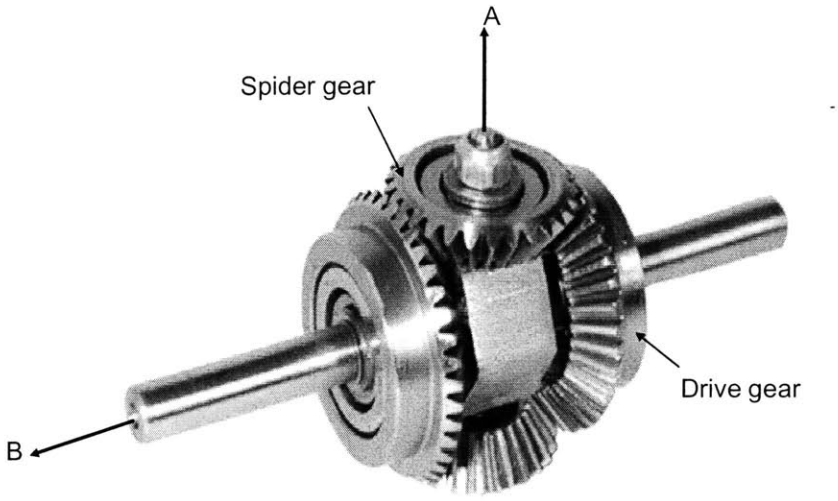

Figure 4-1: Differential gear transmission[33]

Thus, the spider gear can move with any combination of the two rotary motions by varying the relative rotation between the two drive gears. The rotation achieved by a differential gear is given by the following equations

$$\theta_a = \frac{\alpha + \beta}{2} \tag{4.1}$$

$$\theta_b = \frac{\alpha - \beta}{2} \tag{4.2}$$

where θ_a and θ_b are the angles of rotation about axis A and B respectively, and α and β are the angles of rotation of the drive gears.

For the differential gear transmission to work in this application the gears must be made out of an MRI compatible material rather than the standard steel material. Plastic gears are common however they are significantly weaker. To determine if the differential gear transmission will work in the MRI compatible wrist robot it is necessary to examine if plastic gears will be capable of withstanding the required torque. Recall from the functional requirements that the required torque for each degree of freedom is 1.2 N-m. The differential was assumed to provide a 1:1 transmission ratio. This assumption is made because the hydraulic motor

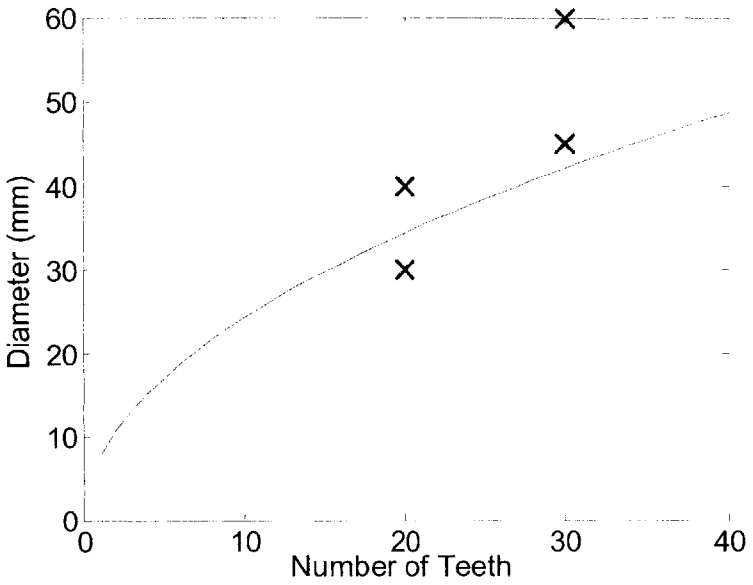

Figure 4-2: Plot to determine gear size and number of gear teeth required to withstand applied forces

can be designed to produce any desired torque or transmission ratio eliminating the need for a transmission ratio in the gears. The analysis also assumes the worst case scenario for unknown parameters. The following equation determines the maximum stress in a gear tooth

$$\sigma = \frac{TNs}{rdFY} \tag{4.3}$$

where T is the applied torque, N is the number of teeth, r is the radius, d is the diameter, F is the face width, Y is a geometrical factor, and s is a safety factor which was conservatively set equal to 2 for this estimation[30]. The yield stress used in this calculation was 45 MPa, which is that of nylon, a common material used in gears however comparably one of the weaker plastic materials. A weak material was used in this scenario for safety. F was set at 0.009m which was the lowest value found in the gear catalog. Y was set at 0.2, which was again the lowest value found on the chart used to determine Y. The equation was then solved for r in terms of N. The result is shown in Figure 4-2.All points above the curve represent gears that could be

safely used in this application. An "x" on the plot represents gears found in a catalog. There are certainly gears that are strong enough to be used in the MRI compatible wrist robot.

Another issue for a design that utilizes gears is backlash. Backlash is the error in the mate of the gear teeth. This error means that the endpoint of the mechanism will move prior to the engagement of the gears. Backlash has been shown to negatively affect the performance of a machine. According to the catalog, the backlash in plastic gears is between 0.1 and 0.2 mm. The existing wrist robot, for comparison, has between 0.055 and 0.14 mm. That is an increase in backlash of 30-45%. The problem with backlash was solved by allowing the gears to be adjustable in the existing wrist robot. This is certainly an option for the MRI compatible robot. Another option is to purchase precision designed plastic gears. For example, injection molded gears give the designer increased flexibility in material choice and tolerances. However, because the mold must be specially designed the price can range from $5000-$50,000. Comparatively, a high quality gear purchased from a catalog only costs approximately $50.

4.2 Cables and Belts

Cables and belts were considered as an option for the transmission of this device. The Phantom®, shown in Figure 4-3, is one example of a device that has successfully utilized cables in its transmission design. Cables are generally made out of steel; however, bronze cables are commercially available. The susceptibility of bronze is not directly available. Bronze is a copper alloy that can contain concentrations of lead, zinc, tin, and iron. Although, copper has a favorable susceptibility this is not the case with all of the other components of bronze. For example, iron is a ferromagnetic material that is not MRI compatible. Therefore, bronze should be used in the MRI machine only if the exact chemical composition is known. Belts, on the other hand, come in a variety of materials. Plastic belts are common and have the advantage of being MRI compatible. One disadvantage to cables and belts is their compliant nature. Cables and belts can act as springs in the system introducing compliance and complicated dynamics. These dynamics can have negative effects on the performance of the robot. Finally, no configuration utilizing cables or belts could be conceived that would be advantageous over the differential.

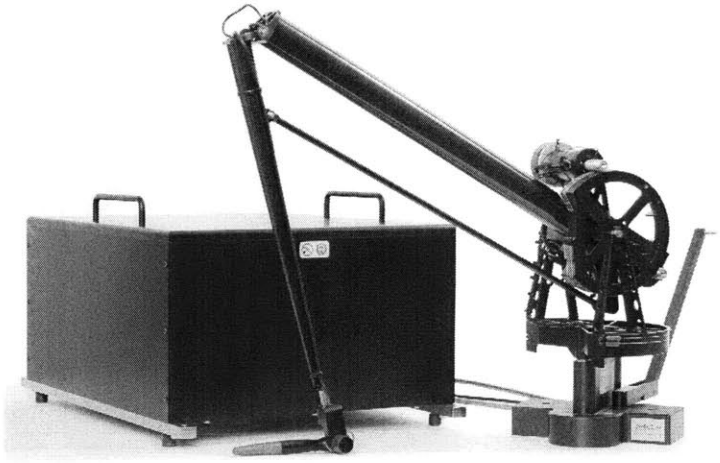

Figure 4-3: Phantom® utilizes cables as its transmission system

4.3 Geared Rings

Geared rings are another transmission alternative. A geared ring was used as the transmission of the pronation/supination degree of freedom in the original wrist robot. The geared rings would have to be made out of an MRI compatible material. However, no MRI compatible geared rings were found in catalogs; therefore, it is likely that this component would have to be specially designed leading to high costs. Additionally, a plastic gear ring would have the same problems with backlash as the plastic differential. Finally, the ring configuration is bulky and limits the amount of space around the patient's hand and wrist. There is no clear advantage to using geared rings over a differential gear transmission.

4.4 Friction Drive

A friction drive is a possible transmission design. A friction drive uses preloaded rollers to produce friction through which torque can be transferred. A Parker positioning system shown in Figure 4-4 is an example of a commercially successful friction drive application. The rollers of a friction drive can be oriented in any way. The idea for this application is to design friction drive rollers to replace the differential gears. The rollers can be shaped and sized the same

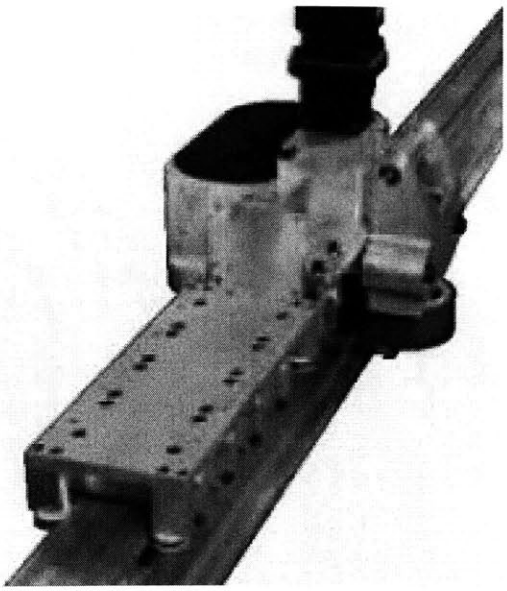

Figure 4-4: Parker positioning system utilizing a friction drive[35]

as the differential gears. However, the torque would be transmitted through friction rather than gear teeth. The advantage of a friction drive is that it contains zero backlash. The disadvantage is that the required preload force adds additional stress to the robot. Because MRI compatible materials are generally weaker, added stress means that the structural supports will have to be larger which will contribute additional size to the robot.

4.5 Spatial Kinematics

The final transmission alternative is the use of spatial kinematics. These devices use a variety of joints and linkages to obtain the necessary degrees of freedom. Figure 4-5 shows an example of spatial kinematics used to give a fan more rotational freedom. The fan is capable of tracing a figure eight pattern in a spherical space. In this application, each joint would need an MRI compatible bearing. Spatial kinematics are more complicated than the other transmission options. Additionally, it is not clear that spatial kinematics can be achieved in a compact space. It was determined that the added complexity of spatial kinematics is undesirable compared to some of the more elegant transmissions designs. Therefore, spatial

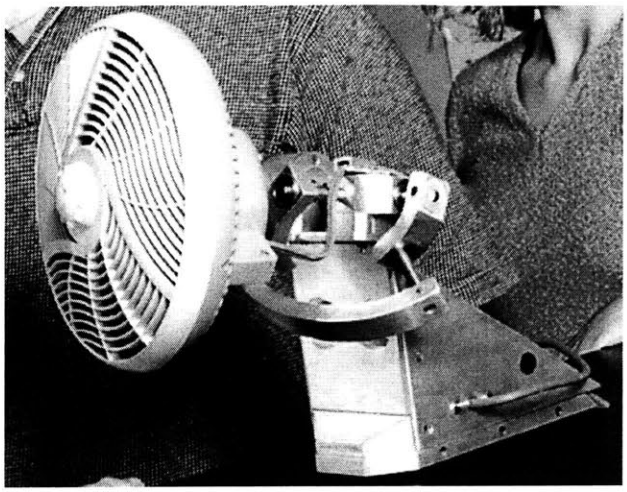

Figure 4-5: Spatial kinematics applied to a fan[36]

kinematics were not pursued further.

4.6 Transmission Conclusions

It has been shown that using plastic gears to create a differential is a viable option for the MRI compatible wrist robot. In terms of strength the plastic gears are suitable. However, it is uncertain if the amount of backlash in plastic gears can be tolerated. Among the alternative transmissions that were considered only the differential gears and the friction drive seem valuable options to pursue. Because these two transmissions can be designed in the same orientation and size, it would be easy to replace one with the other. Therefore, it was decided that both transmission designs would be pursued. The design would be made such that the transmission can be easily exchanged. This will allow the best transmission option to be determined through testing.

Chapter 5

Other Design Considerations

There are several other components in the design that required investigation. These design considerations include the materials, bearings, electric motor, hoses and fittings, and seals. This chapter discusses the various options explored for these components.

5.1 Materials

An important aspect of designing an MRI compatible robot is material selection. The materials determine the safety of the robot within the MRI machine as well as the quality of the images that the MRI machine will produce. In addition, the materials must be able to provide support that can withstand the forces applied to the robot. In general, three factors determine a material's effectiveness in the MRI machine: susceptibility, yield strength, and elastic modulus.

Several metals, such as copper and carbon, have good MRI compatibility. However, when using metal in the MRI machine one must be careful to avoid eddy currents. Additionally, carbon, for instance, has a different susceptibility based on its orientation within the MRI machine. The benefit of metals is they generally have a high yield strength and elastic modulus.

Plastics have been shown to have excellent MRI compatibility. Most of the components in previous MRI compatible robots have been constructed of plastic with great success. The drawback to using plastics is their low yield strength and elastic modulus.

A third option for materials is a filled plastic, which are available in virtually all polymers

Material	Yield Strength (MPa)	Elastic Modulus (GPa)
Copper	275	115
Carbon fiber	3800	228
Nylon	70	2
Lexan	72	2.2
G10 (glass filled epoxy)	241	18
Glass filled nylon	190	12

Table 5.1: Material properties of several MRI compatible materials

and a variety of fillers. The most common fillers are carbon and glass, both of which are MRI compatible. However, carbon again has a different susceptibility based on its orientation within the MRI machine. One drawback when using filled plastics is their poor machinability. They can be abrasive, hard to clean up, hard on the machines, and result in a poor surface finish. However, the filled plastic materials have increased yield strength and elastic moduli compared to standard plastics. Table 5.1 summarizes a few of the MRI compatible materials that were researched and their material properties.

It was decided that metals should be avoided whenever possible so that eddy currents and orientation would not be an issue. There are, however, several parts that will be machined via wire EDM. These parts must be made out of a conductive material for the EDM process. Therefore, these parts will be constructed out of copper, which has an excellent susceptibility compared to carbon. All parts taking a significant structural load will be machined out of G10, which is a glass filled epoxy resin. This is a non-conductive material that has good material properties. It is also one of the easiest to machine of the glass filled composites. It is difficult, however, to machine small radius rods in G10 because of the fibrous nature of the material. Therefore, all parts which do not take significant loads or have small radius rods will be made out of Lexan, a more machine friendly material.

5.2 Bearings

The bearings of a machine support the applied forces and torques. There are a variety of different types of bearings depending on the types of loads it must support. In general, there are two forces that a bearing could experience: radial forces and axial forces. An axial force acts down the rotational axis of the bearing. A radial load acts perpendicular to the rotational

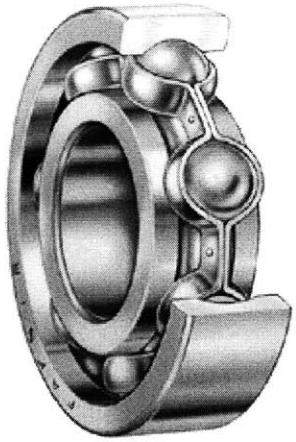

Figure 5-1: Ball bearing[37]

axis of the bearing.

Different bearing varieties are better at supporting different loads. Ball bearings, as shown in Figure 5-1, can be purchased in varieties such as deep groove, angular contact, or four point contact [42]. Deep groove ball bearings can support moderate radial and axial loads. Angular contact bearings are capable of supporting higher axial loads than deep groove ball bearings. Finally, four point contact bearings are the best ball bearing at supporting axial loads.

Roller bearings are an alternative to ball bearings. The cylindrical roller bearing, shown in Figure 5-2, can support very high radial loads but only light axial loads. The tapered roller bearing, shown is Figure 5-3, can support very high loads in both the radial and axial directions.

An additional variety of bearing is the plain bearing. A plain bearing has no rolling elements. Instead a plain bearing is a sleeve composed of a low friction material on which a shaft rotates. Plain bearings generally have higher friction than rolling element bearings because sliding friction is higher than rolling friction. Figure 5-4 illustrates some examples of plain bearings. Plain bearings come in varieties that are only suitable for radial loads and varieties that are suitable for radial and axial loads.

Using bearings in an MRI machine limits the variety of bearings that can be chosen. Standard bearings are composed of steel, which is not MRI compatible. Ball bearings do exist in MRI compatible materials, however not all of the varieties listed above are available and the

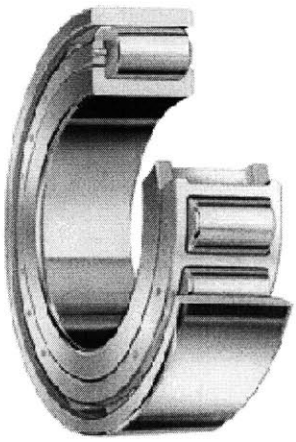

Figure 5-2: Cylindrical roller bearing[37]

Figure 5-3: Tapered roller bearing[37]

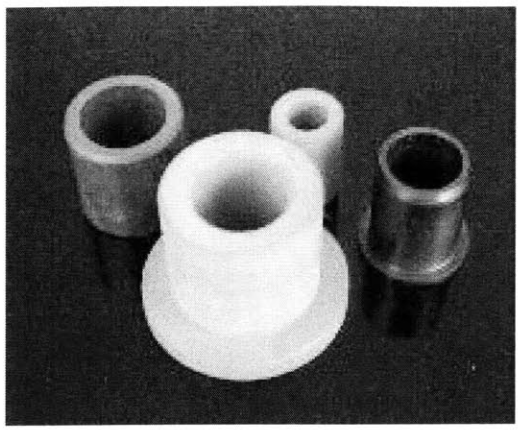

Figure 5-4: Plain bearings

sizes are limited. MRI compatible ball bearings are composed of plastic raceways and glass balls. Two varieties were identified: deep groove and four point contact. An abundance of plain bearings are available in MRI compatible materials. Plastics, for instance, are a common material for plain bearings due to their low coefficient of friction.

Friction is a major concern in this application. Therefore, ball bearings should be used in this design whenever possible to reduce the friction in the robot. In the case that a suitable ball bearing can not be found due to size constraints or load capacity, plain bearings should be employed.

5.3 Hoses and Fittings

There are a great variety of hoses and fittings that can be used to connect the components in the hydraulic system. This section will examine these different options. The most appropriate option for this application will be selected.

The discussion of hoses is limited to plastic hoses. Plastic is MRI compatible and a common material for fluid hoses. Plastic hoses come in two basic options: reinforced or non-reinforced. Reinforcement can be added to a plastic hose with the addition of a variety of materials such as steel wire or plastic braid. Only plastic reinforced hoses will be considered because of their MRI compatibility. A reinforced hose can be stiffer and thus less compliant than a non-reinforced

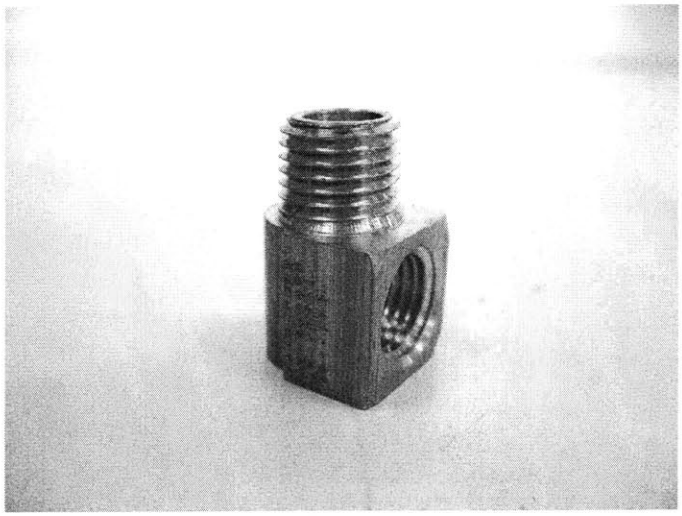

Figure 5-5: Threaded brass fitting

hose, which is good for the dynamics of the system. However, the hoses must be flexible enough to bend and fit in the MRI machine. A hose's flexibility is qualified by its minimum radius of curvature. The ideal hose for this application will have a small radius of curvature and high stiffness.

This design requires a fitting that is easy to assemble and disassemble. It is also advantageous to use fittings that do not minimize the area inside the hoses. Fittings that constrict the flow will create pressure losses. There are some fittings that go outside the hose and others go inside the hose. The flow will be constricted more by fittings that must go inside the hose. Finally, one must be aware of the type of hose with which a particular fitting can be used.

The initial prototype of the hydraulic vane motor used threaded brass fittings, as shown in Figure 5-5. The threaded fittings were extremely difficult to work with because they were not conducive to assembling and disassembling the system. Additionally, the threaded fittings had a tendency to leak. The diameter inside the threaded fitting was also much smaller than the hose diameter.

The best option for fittings seems to be quick connect fittings, as shown in Figure 5-6. These go on the outside of the hose so the diameter is not decreased. They also are designed for easy assembly and disassembly. Unfortunately, they make use of steel teeth to grasp the

Figure 5-6: Quick connect hose fitting[38]

outside of the hose. Therefore, these fittings are not MRI compatible.

The next option for fittings is a compression fitting, as shown in Figure 5-7. These fittings are designed so that the hose is clamped by tightening a threaded nut around the hose. They also do not minimize the hose diameter. However, they are recommended for use only with unreinforced hoses. Additionally, they are somewhat difficult to disconnect.

The final fitting option is barbed fittings, as shown in Figure 5-8. These are fittings that fit inside the hose and are secured with a hose clamp. Because the fittings go inside the hose, the diameter gets restricted. Additionally, standard hose clamps are composed of steel and non-MRI compatible material. There are nylon hose clamps available however their effectiveness is unknown. The advantage of barbed hose fittings is they can be used with either reinforced or non-reinforced hoses.

It was decided that two options for hoses and fittings would be purchased. First, unreinforced hoses with compression fittings can provide a piping system that does not constrict the flow; however, the compliance of the hoses could affect the system dynamics. The second option uses reinforced hoses with barbed fittings. This option is less compliant however the barbed fittings restrict the flow creating increased pressure loss. The two systems can be compared experimentally to determine the best option.

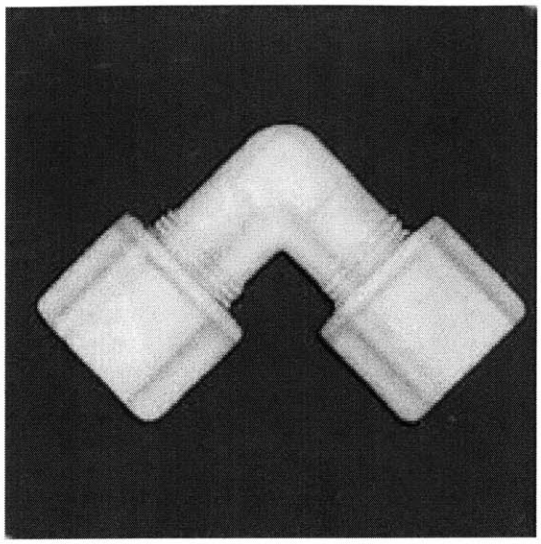

Figure 5-7: Compression hose fitting[38]

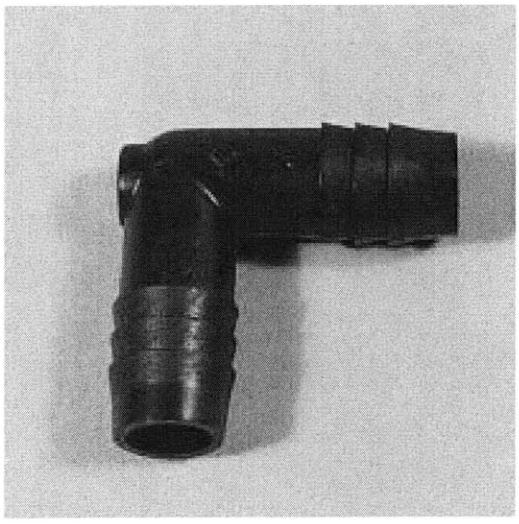

Figure 5-8: Barbed hose fitting[38]

5.4 Seals

Several seals are required within the hydraulic vane motor. There are static seals, for parts that are not meant to move after assembly. For example, a static seal is required between the motor top and motor housing. Dynamic seals are required at the rotating shaft of the motor. Selecting seals for this design is a difficult task. There are a variety of seals for dynamic and static applications. However, few seals are considered low friction. The goal of the seals in this design is to have all dynamic seals retain as much fluid as possible while adding as little friction as possible. The friction in a static seals is not important; therefore, these seals should not leak.

The most common static seals used in hydraulic applications are o-rings. O-rings were used as static seals in the first prototype of the hydraulic vane motor with great success. As a result, o-rings will again be used in the same fashion for the final prototype. The groove for an o-ring is well specified based on the type of seal required. The important aspects of the o-ring groove are the amount of squeeze and the amount of space. The o-ring needs to be squeezed a certain percentage to create a good seal. However, the groove needs to allow space for the deformed o-ring.

Dynamic seals are a more challenging problem. Testing of the initial prototype of the hydraulic vane motor showed that Teflon spring seals were very effective and added a low amount of friction. Unfortunately, these seals are not MRI compatible because the spring is made of steel. Therefore, the ideal seal seems to be composed of Teflon, or a similar material, but does not have a spring.

Several varieties of dynamic seals were identified. First, there are a variety of rubber seals. However, testing with the prototype hydraulic vane motor revealed that these seals have high friction. Another option is lip seals, which come in a variety of plastics. However, most lip seals come with a steel backing which is not MRI compatible. Only one variety of lip seal was found made of PTFE and had no steel backing. This is the Flexilip^{TM} seal from Parker, as illustrated in Figure 5-9. Unfortunately, these seals are not a standard part and must be custom designed for the particular application. This option is too costly for an initial prototype, but could be pursued in a later design if needed.

The final option is the use of o-rings. PTFE o-rings exist and can be used for rotary

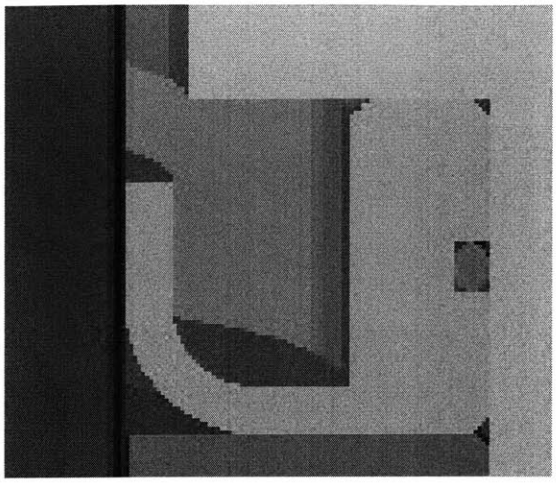

Figure 5-9: Parker Flexilip^{TM} seal[39]

applications if a few design details are addressed. A PTFE o-ring is not a able to stretch like a typical rubber o-ring; therefore, a groove can not be used as it is in typical o-ring design. Instead, the groove is more like a channel that is open on top. The channel is closed with a backup o-ring, which keeps the o-ring from sliding out. An additional design consideration is the amount of squeeze a PTFE o-ring requires. Because the PTFE material is not flexible, the design of the groove must account for little to no squeeze.

It was decided that the PTFE o-ring was the best dynamic seal option for this application. However, it should be noted that a more suitable lip seal is available. If the o-ring seal proves to be ineffective the lip seal could be pursued for a greater cost.

5.5 Electric motor

An electric motor is required in this design to drive the hydraulic system. Several factors were important for the selection of the electric motor. As always in this design friction should be kept as low as possible. Additionally, a low inertia motor is desirable. Finally, the electric motor must be able to produce the required torque.

First, a decision was made to create a 1:1 transmission ratio between the hydraulic motors in the system. Recall that if each hydraulic motor has a different area a transmission ratio can

be produced. For example, if the hydraulic motor at the endpoint of the robot has a smaller area than the hydraulic motor attached to the electric motor the patient will need a smaller torque to backdrive the system. However, the electric motor will have to produce more torque to provide the same endpoint torque. This technique can be useful in reducing the apparent friction or inertia in the system. For this concept to be useful the benefit gained from the hydraulic motor transmission ratio must be greater than the loss acquired by increasing the size of the electric motor.

It was determined that the negative effects of using a larger electric motor out weigh the benefits of the hydraulic motor transmission ratio. For example, assume a 2:1 transmission ratio is built into the hydraulic system. This means that the motor must be twice as large. The friction in the hydraulic system will not be affected significantly by change in area. Likewise the added friction due to increased electric motor size will be small according to values found in the catalogs. This means there will be a slight benefit in terms of apparent friction. However, the inertia of the system will be affected negatively. First, it was assumed that the hydraulic motor can be designed such that the area of the motor will change but the inertia will not. Therefore, a 2:1 ratio between the areas of the hydraulic motors means the electric motor inertia must be less than twice as large to benefit from the transmission ratio. However, according to the catalogs the inertia will increase 3 to 6 times for a motor that produces twice as much torque. Therefore, it was decided to use a 1:1 transmission ratio for this initial prototype. It should be noted, however, that if friction proves to be a significant problem for the robot and inertia is not an issue, employing a transmission ratio between the hydraulic motors may be an appropriate solution.

The torque required from the electric motor was determined based on test results from the prototype of the hydraulic vane actuator. The test results showed that while the vane was touching the motor wall and leakage was assumed to be zero, there was in fact fluid loss occurring as if a gap of 0.004 inches existed. This was not unlikely because the top and bottom edges of the vane were not touching the motor wall. As a result of this gap width the torque output from the hydraulic vane motor was only 29 percent of the input force. Therefore, the input torque must be higher than the desired output torque. For this design it was assumed that a gap of 0.004 inches could be obtained or improved by using better manufacturing techniques.

Motor	Cont. Stall Torque (Nm)	Friction (Nm)	Inertia (kg-m^2)
Bayside BM115-1	4.65	not available	2.32×10^{-4}
Parker BE344J	4.8	0.035	8.1×10^{-5}
Kollmorgen AKM43E	4.7	0.038	2.09×10^{-4}

Table 5.2: Comparison for brushless motors

Specifically using wire EDM, which is capable of tolerances as low as 0.0005 inches. Therefore, the electric motor must provide a torque of 4.1 Nm so that the output hydraulic motor will be capable of providing 1.2 Nm.

Two varieties of electric motors were investigated for this application: brushed and brushless. Brushed motors are mechanically commutated by the use of brushes. While brushless motors have no mechanical contact and are commutated through the use of position sensors. There are several advantages and disadvantages to each motor.

Brush motors have limits based on the mechanical contact of the brushes. They are generally run at lower speeds to avoid wear and sparking of the brushes. They have a shorter life because the brushes can wear out. However, they are generally much cheaper than brushless motors. Additionally, brushed motors require a simple electronic interface for operation.

Brushless motors do not have any mechanical contact which eliminates many of the problems that exist with brush motors. Brushless motors have a longer life and can be run at higher speeds. Additionally, brushless motors typically have lower inertia because of their construction. A position sensor is required to commutate the motor, which increases the cost of brushless motors and makes the electrical interface more complex.

Both motors were explored for this application. However, no brushed motors could be located that had a sufficient torque. As a result only brushless motors were compared. Several companies were considered to provide the brushless electric motor. The motors considered and their important characteristics are summarized in Table 5.2. The best options for brushless motors were either the Parker or Kollmorgen models. A quote was received for both motors and the Kollmorgen motor was approximately four-hundred dollars cheaper. Therefore, the Kollmorgen motor was selected.

The next step was to decide on the sensor that will be used with the motor. The sensor comes with the motor because it is required for commutation; however, there are several sensor

options to choose from. Kollmorgen offers four options for position sensors: resolver, Smart Feedback Device (SFD), absolute sine encoder, or incremental encoder.

A resolver is a position feedback device consisting of a set of windings. The voltage in the windings varies in amplitude depending on the position of the motor. This change in voltage provides information about the rotation angle of the motor. A SFD is a position sensor that communicates with the drive not only position information but also motor parameters. This allows the system to be tuned for the particular motor and position sensor[40]. An absolute sine encoder uses a disk in which each position has a unique pattern of light and dark. Light is shown through the disk and detected on the other side by light sensors. The exact position of the disk is known based on the pattern of light that is detected. Because each position has a unique pattern, the shaft location is known even when the sensor is first turned on. An incremental encoder uses the same light sensing technology. However, the disk contains a pattern of evenly spaced light and dark regions. As an incremental encoder passes through the light and dark regions the light sensor will produce a square wave. Each pulse in the square wave corresponds to a set angle of rotation. A technique call quadrature encoding can increase the resolution of the incremental encoder. Instead of counting pulses of the square wave, quadrature encoding counts the edges of the wave between each pulse. This technique increases the resolution by a factor of four. The drawback of incremental encoders is that the position is not unique. Therefore, when the sensor is turned on the exact position is not known.

The incremental encoder was chosen for this application for its simplicity. Many of the advantages of the more complex position sensors are not necessary in this application. For example, knowing the exact location of the motor is possible if an absolute encoder was chosen. However, knowing the exact position of the electric motor does not necessarily give accurate information about the endpoint of the device. Most likely fluid leakage will occur over time and alter the relationship between the electric motor location and the hydraulic vane motor position. This makes the exact position of the electric motor irrelevant.

Kollmorgen offers several incremental encoders with varying degrees of resolution. A higher resolution will give more accurate position information and a higher apparent stiffness of the robot. The highest resolution the electrical system can handle is 10,000 counts per revolution

according to the manufacturer. The highest available incremental encoder has 5000 counts per revolution. After quadrature decoding that is a resolution of 20,000 counts per revolution. This corresponds to angular position accuracy of 0.018 degrees.

Chapter 6

Detailed Design

The overall design of the MRI compatible wrist robot is introduced here, followed by the detailed calculations that went into the design. A solid model of the overall design that will be placed in the MRI machine can be seen in Figure 6-1. The overall design is composed of several subassemblies, which include two hydraulic vane motors, handle mechanism, transmission, and stand. There is an additional subassembly that is placed outside the MR room. The non-MRI compatible portion of the design can be seen in Figure 6-2. This subassembly consists of a hydraulic motor, electric motor, and mounting structure. Two of the non-MRI compatible subassemblies are required in the design.

6.1 Differential Gear Transmission

The differential gear transmission is pictured in Figure 6-3 and Figure 6-4. The differential transmission consists of several components. These components include gears, bearings, shafts, side supports, a center cube, and a connecting rod. Each component included in the differential gear transmission will be discussed in this section along with the analysis that was performed upon it.

6.1.1 Forces

The forces applied to each component in the differential gear transmission are the basis for much of the design analysis in this section. Therefore, the first step is to evaluate and

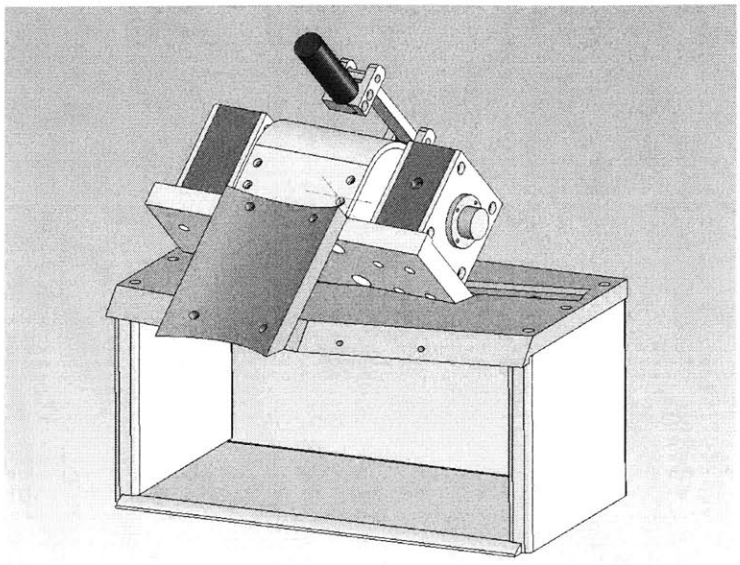

Figure 6-1: Solid model of the MRI compatible wrist robot

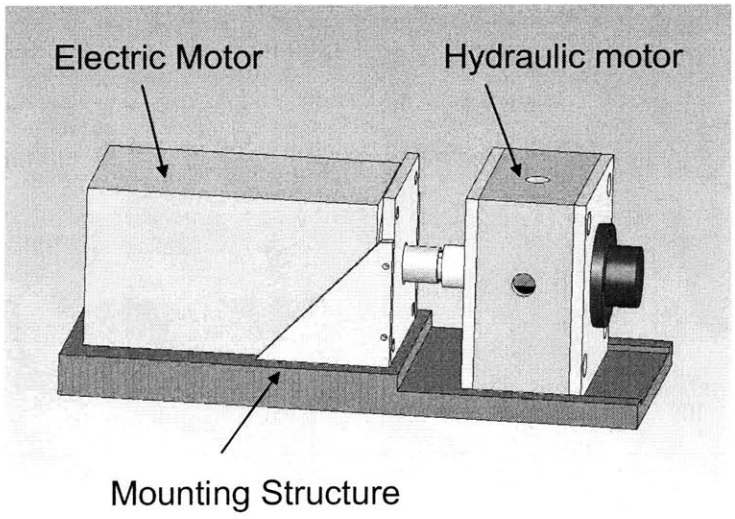

Figure 6-2: Solid model of the non-MRI compatible portion of the robot

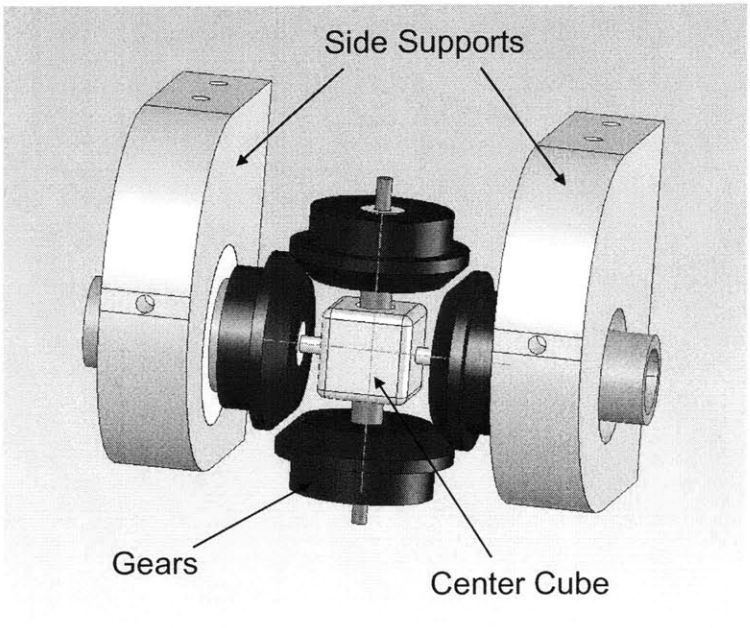

Figure 6-3: Solid model of the differential gear transmission

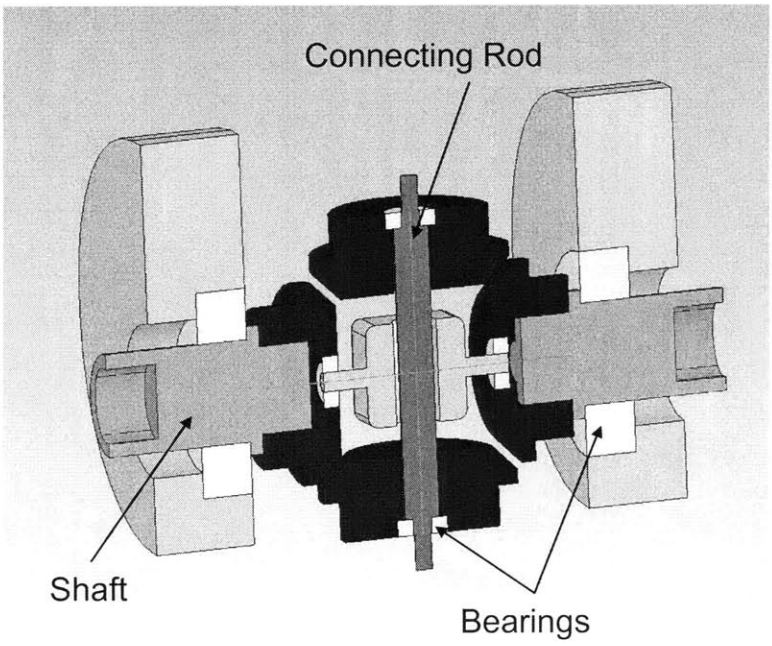

Figure 6-4: Section view of the differential gear design

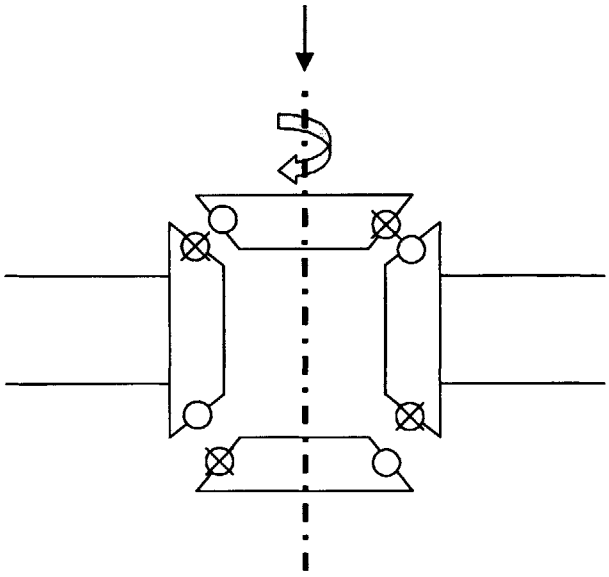

Figure 6-5: Free body diagram of differential gear transmission

quantify the forces in the differential gear transmission. There are two axes of rotation that the transmission can experience. The free body diagrams for these motions are shown in Figure 6-5 and Figure 6-6. The $\otimes$ symbol indicates a force pointing into the page and the $\bigcirc$ symbol indicates a force pointing out of the page. In fact, this notation will be used consistently throughout this thesis. It is assumed that the gears are not preloaded against each other. Based on the diagrams, both rotations place torsional moments on the gears. This in turn puts a torsional moment on the shafts supporting the gears. The torsional moment is equal in magnitude to the applied torque of 1.2 Nm.

An additional force due to the weight of the handle mechanism is also applied to the differential gear transmission. The weight of the handle mechanism was determined to be 2.6 N based on the volume of the solid model. This weight is distributed among two shafts each of which support 1.3 N. This weight is acting over a moment arm equal to 0.91 inches, which corresponds to a bending moment of 0.03 Nm.

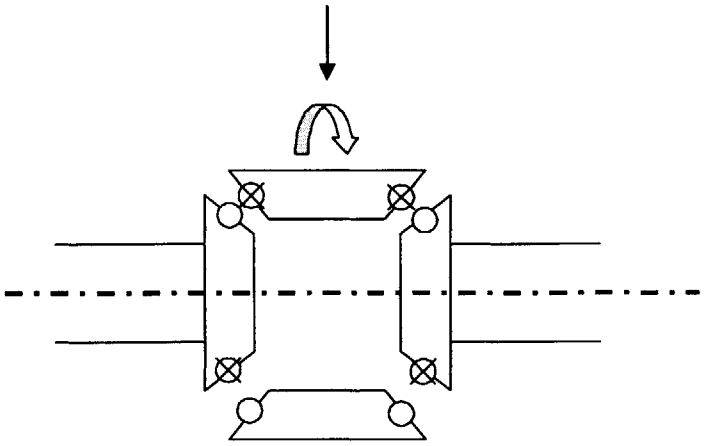

Figure 6-6: Free body diagram of transmission subject to a different motion

6.1.2 Gears

The gears used to create the differential gear transmission were purchased from Quality Transmission Components. The gears are plastic miter gears model PM2-25. They are made of Nylon MC901 and the tooth profiles are machined. The allowable torque of these gears was listed in the catalog as 2.359 Nm[41]. This value was checked with the following equation used for bevel gear strength

$$T = \frac{d_m}{2} m \frac{R_a - b}{R_a} y b \sigma_b K_v \tag{6.1}$$

where m is the module equal to the pitch diameter divided by the number of teeth, b is the tooth width, y is the form factor based on the number of gear teeth, σ_b is the bending strength of the material, K_v is a speed factor, R_a is the outer cone distance, and d_m is the central pitch circle diameter given by

$$d_m = d - b \sin(\delta) \tag{6.2}$$

where d is the pitch diameter and δ is the cone angle. Plugging in the proper values this equation yield an allowable torque of 2.097 Nm. This is slightly lower than the catalog value. The equation used to calculate the allowable torque in the catalog was a simplified equation

accurate for spur gears. This could account for the different result.

The differential gear transmission requires four of these gears. Note that three gears could also be used; however, this would produce an asymmetrical forcing on the system. The asymmetry is not a significant problem for the differential gear design; however, it would be difficult to implement with the friction drive transmission. The goal here was to keep the transmission design interchangeable between the differential gears and friction drive as much as possible.

6.1.3 Bearing

The next set of design calculations that was performed for the differential gear transmission was for the bearings. There are six bearings in the differential transmission. There are two large bearings that support the applied loads and the shafts on which two of the gears are located. There are four additional bearings one inside each of the four gears. These bearings facilitate relative rotation of the four gears. They are not anticipated to support any load but rather reduce friction in the system. All of the bearings help to locate the gears relative to each other. It is important to keep the gears properly spaced to avoid unwanted forces and to avoid adding friction.

The bearings were purchased from KMS Bearings. They are ball bearings with plastic raceways and glass balls. They come in two varieties: deep groove or four point contact. Because none of the bearings must support an axial load deep groove ball bearings were selected. The large bearings are model AR16-G and the small bearings are model AR3-G.

Ball bearings are rated based on their life. A bearing catalog will publish a rating C_r. This rating can be used to determine the life of the bearing based on the particular speed and loading conditions of the application. The following equation is used to determine a bearings life in hours, L_h,

$$L_h = \frac{10^6}{60n}\left(\frac{C_r}{P_r}\right)^3 \tag{6.3}$$

where n is the speed in revolutions per minute and P_r is the load on the bearing.

In the case of the large bearings, only radial loads are placed on the bearing therefore P_r is simply equal to the radial force. If an axial load exists the expression for P_r is more

complicated, as will be seen later. In this case, the radial load is due to the weight of the handle mechanism, which was estimated to be 2.6 N. This force is shared by two bearings; therefore, each bearing only supports half of the weight or 1.3 N. The speed is based on the motion of the patient and is 192 rev/min[3]. The catalog rating is based on the largest bearing available, which is 271 N. Although the load on the bearing is not great, the bearing must be able to accommodate an appropriately sized shaft as well. As will be seen in the next section, a large bearing is required based on the required shaft size. Using these values in Equation 6.3 yields a life of 7.9×10^8 hours. This is an immense amount of time and one can be confident that the large bearings in the differential gear transmission will not fail.

Because the small bearings are not expected to support any load, they were selected for their size rather than life. The bearings had to be small enough to be placed in the gears. In fact, the bearings chosen are the smallest offered by KMS Bearings.

All of the bearings are retained in their housing by incorporating shoulders into the design. Standard retaining techniques, such as snap rings, were not possible due to the MRI compatibility requirements. Shoulders can be machined into any part; however, they can make assembly more difficult.

Finally, the fit of the bearing into the housing is important. The bearing manufacturer recommends that one surface of the bearing receive a press fit while the other surface receives a slip fit. In this design, the outer diameter of all bearings was press fit into its housing. The inner diameter of all bearings was slip fit to its shaft.

6.1.4 Shaft

The shafts in the differential gear transmission are designed to connect the gears to the hydraulic vane motors. They are also required to support the gear transmission. The shafts are an important structural component of the robot therefore they need to be properly sized. This section describes the analysis that was done to determine the size of the shafts in the differential gear transmission.

There are two important aspects of shaft design. First, the shaft must be capable of supporting the applied loads. Second, the shaft must be stiff to aid proper alignment of the gears. Specifically, a shaft that is supporting a gear should not have an endpoint slope greater

than 0.0005 radians[30]. This will ensure that the gears will be properly aligned. Generally, the stiffness of the shaft is a much stricter requirement than the shaft strength.

The shaft strength is determined by the following equation

$$\sigma = \frac{32M}{\pi d^3} \tag{6.4}$$

where σ is the yield strength of the material, M is the bending moment applied to the shaft, and d is the diameter of the shaft. The bending moment on the shaft is due to the weight of the handle mechanism, which was determined to be 0.03 Nm. The shaft material is G10, which has a yield strength of 241 MPa. Plugging this information into the equation yields a minimum shaft diameter of 0.042 inches.

The shaft must also support a torsional load, which has the following strength equation

$$\sigma = \frac{16T}{\pi d^3} \tag{6.5}$$

where T is the torsional moment. Again, plugging the relevant values into this equation yields a minimum shaft diameter of 0.116 inches. Clearly the requirements of shaft diameter based on material strength are not particularly strict for this design. However, the design must also be checked for shaft stiffness.

The angle of shaft deflection must be kept under 0.0005 rad at the endpoint. However, this value is cumulative among all the structural elements in the design. Therefore, half of this angle, 0.00025 rad, was allotted to the shaft. The equation for shaft deflection is

$$\theta = \frac{Ml}{2EI} \tag{6.6}$$

where θ is the angle of deflection, l is the shaft length, E is the elastic modulus of the material, and I is the moment of inertia. For a circular shaft the moment of inertia is

$$I = \frac{\pi d^4}{64} \tag{6.7}$$

Solving these equations for shaft diameter yields a minimum diameter of 0.26 inches based on shaft deflection criteria. Finally, the shaft must be capable of meeting the deflection

Type of Analysis	Shaft size (in)
bending strength	0.042
torsional strength	0.116
bending deflection	0.26
torsional deflection	0.65

Table 6.1: Summary of shaft sizing analysis

requirements while under a torsional load. The equation for shaft deflection due to torsion is the same as Equation 6.6. Solving this equation for torsion means that the minimum shaft diameter is 0.65 inches. The summary of this shaft analysis is shown in Table 6.1.

According to this analysis the shaft must have a minimum diameter of 0.65 inches. This, however, includes no safety factor. Therefore, the shaft was made with a diameter of 1.00 inch, which is the largest diameter possible based on the limited bearing sizes. The selected shaft diameter allows for a safety factor of 1.5.

6.1.5 Side Support

The side supports serve several purposes. They are required for housing the bearings, attaching the gear transmission to the robot assembly, and supporting the loads applied to the differential gears. The loads transferred to the side supports through the differential gear transmission are due only to the weight of the handle mechanism. However, it should be noted that the side supports will also be used in the friction drive transmission, which has higher applied loads. The side supports were thus sized to support loads from either the differential gear or the friction drive transmissions. This section will examine the required sizing of the side supports based on the loads experienced when the differential gear transmission is employed.

The analysis of the side support involves determining the size of the support based on the same two factors analyzed for the design of the shaft. These factors are the deflection of the supports and the strength of the material. First, the deflection of the supports will be determined. The same equation used in shaft deflection, Equation 6.6, is used here. However, the moment of inertia, I, is different for a rectangular cross section

$$I = \frac{bh^3}{12} \tag{6.8}$$

Type of Analysis	Support Thickness (in)
deflection	0.11
strength	0.003

Table 6.2: Summary of result for side support thickness

where b is the length of the side support and h is the thickness. In this analysis the length b was set to 4 inches and l was set to 2 inches. This is the amount of space that is required for the differential gear transmission to rotate inside its housing with out interference. The allowable deflection for the supports was set to half of the total deflection requirement, or 0.00025 rad. The deflection equation was then solved for h, the thickness of the support. The results found that the thickness of the supports should be at least 0.11 inches.

The side supports were then analyzed to determine the minimum thickness based on the strength of the material. This calculation was performed with the following equation

$$\sigma = \frac{M}{I}\frac{h}{2} \tag{6.9}$$

This equation was solved for h to determine the thickness of the side supports. The result was that the thickness should be a minimum of 0.003 inches. The results of this analysis are summarized in Table 6.2.

In reality the support side was made a thickness of one inch. This is based on the analysis done for the friction drive transmission, which can be found in Section 6.2. The important point here is that the side support is sized to appropriately handle the forces generated in the differential gear transmission. There is little risk of failure due to the deflection or strength of the side supports.

6.1.6 Connecting Rod

The connecting rod is designed to locate the gears in the differential transmission and assist in holding them in place. The connecting rod is not designed to undergo any loading; therefore, it was constructed out of Lexan. The rod has a shoulder on each end that properly spaces two of the gears in the transmission. The ends of the rod are threaded so that the rod and gear assembly can be held together by a set of nuts. The rod must be able to rotate relative to the

gears. This is because the two gears that it connects rotate in opposite directions from one another. Therefore, the rod passes through the center cube and gears without making contact. The connecting rod only makes contact to the system at the bearings.

6.1.7 Center Cube

The center cube is again designed to aid locating the gears in the differential transmission. The center cube is not anticipated to take any loads; therefore, it is composed of Lexan. The cube must be free to rotate relative to the gears. As a result it only contacts the system via a set of bearings. In reality the center cube could be eliminated; however it is included for safety. Its main function is to assist alignment and prevent any shifting in the components. For example, the center cube could be useful in the case of the friction drive if there is slippage between the friction cones.

The drawback of including the center cube is the alignment of the bearings. The cube forces the alignment of four bearings plus any bearings that are included in attaching components, such as the hydraulic vane motor. Standard practice is to include only two bearings in a line. The more bearings that are included the more difficult they become to align. Any misalignment of the bearings can lead to additional stress or friction in the system.

If the alignment of the system proves to be a problem several options can be pursued. A flexible coupling could be used to connect various components, which will compensate for alignment errors. Additionally, the center cube could be eliminated if it is deemed unnecessary. This is an issue that must be addressed through testing.

6.2 Friction Drive Transmission

The friction drive transmission, shown in Figure 6-7 and Figure 6-8, was designed as an alternative to the differential gear transmission. The two transmissions were made easily interchangeable. Many of the parts are identical to those used in the design of the differential gear transmission. The center cube, for instance, was not altered for the friction drive design. Therefore, this component will not be discussed in this section. All other components, which include the friction cones, bearings, side supports, and connecting rod, will be described here

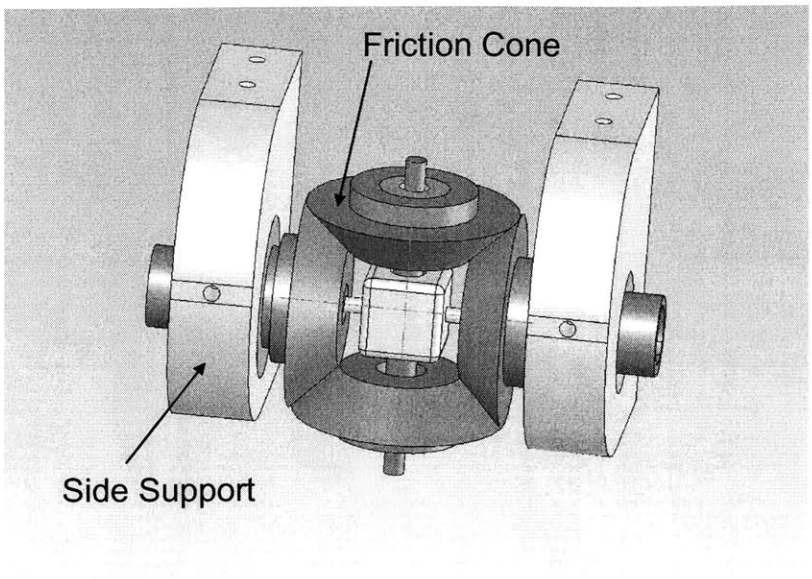

Figure 6-7: Solid model of the friction drive transmission

along with any analysis that was performed.

6.2.1 Forces

Again the first step for the analysis of the friction drive transmission is to identify and quantify the applied forces. First, it must be noted that the same forces that are present in the differential gear transmission are also present in the friction drive transmission. However, in the case of the friction drive transmission it is necessary to use an additional preload force illustrated in Figure 6-9. Applying a clamping force, indicated by the big arrows, creates a preload force, indicated by the small arrows. The preload force is normal to the contact surface and based on the following equation

$$F_f = \mu P_f \tag{6.10}$$

where F_f is the frictional force required to keep the friction drive from slipping, μ is the coefficient of friction, and P_f is the preload force. In this case, the friction force must be greater than the torque applied to the transmission acting at a moment arm equal to the radius

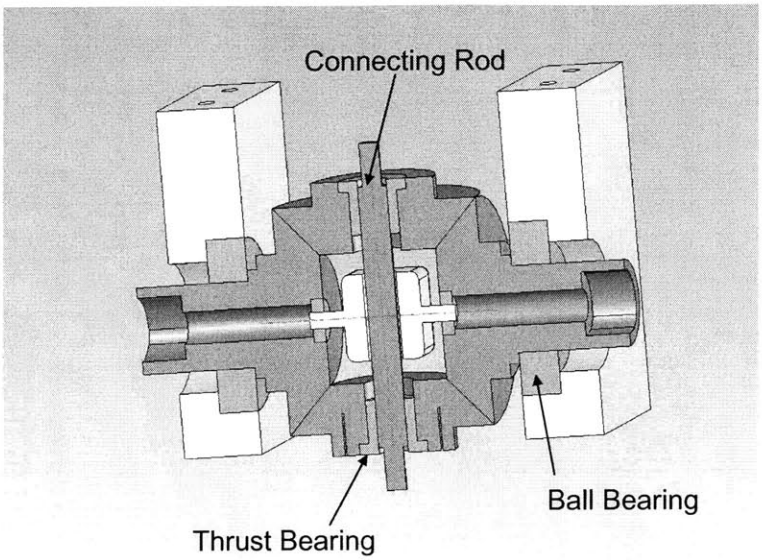

Figure 6-8: Section view of the friction drive transmission

of the drive cone. The torque is 1.2 Nm and the maximum cone radius is 0.033 m. This corresponds to a frictional force of 36 N. The friction drive cones are to be coated in rubber. Therefore, the coefficient of friction for rubber on rubber is 1.16. Using these values to solve Equation 6.10 results in a preload force of 31 N. To achieve this amount of preload the clamping force placed on the friction drive must be 22 N.

The preload force can be decomposed as shown in Figure 6-10. This free body diagram indicates that adding a preload force contributes an additional thrust force to the system. The magnitude of the thrust force is governed by

$$F_t = 2P_f \sin(\frac{\pi}{4}) \tag{6.11}$$

where F_t is total thrust force. In this case F_t is equal to 44 N.

6.2.2 Friction cones

The friction cones are designed to act much like the differential gears. However, instead of using teeth the friction cones transmit torque through friction. A preload force is applied

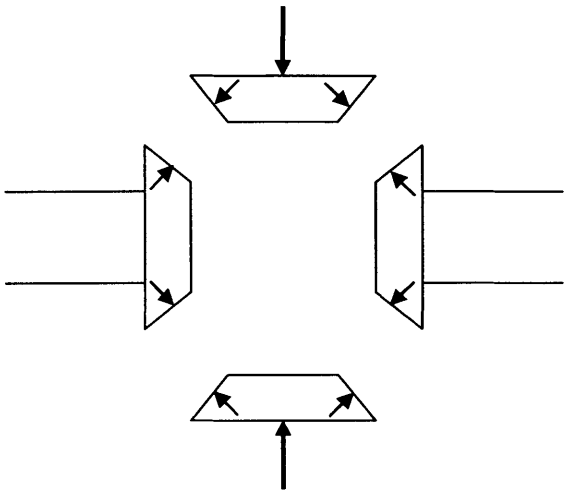

Figure 6-9: Free body diagram of transmission subject to a preload

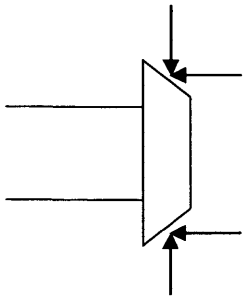

Figure 6-10: Free body diagram of the decomposed preload forces

to the cones to supply this friction. The preload force is relatively high therefore the strength and the life of the cones must be evaluated.

First the geometry of the contact area was selected. There are two basic options for the contact geometry: an elliptical contact or a line contact[43]. An elliptical contact is essentially a point contact that when placed under stress flattens into an elliptical shaped contact area. This type of contact is created by two cones that have rounded profiles. A line contact is created by two cones with a straight profile. The line contact has a uniform stress along the length of the contact area. In general, the pure line contact friction drive is not recommended. This is because the stress tends to concentrate at the edges of the cones, which causes the device to wear more quickly. However, line contact was chosen for this prototype due to the simplicity of design and analysis. A radius of curvature can be added to the cones if wear proves to be a significant problem.

The friction cones were designed dimensionally so that they could easily be exchanged for the gears in the transmission design. However, these dimensions were checked to ensure they were strong enough to withstand the anticipated loads. The preload creates a contact stress that is governed by the following equation when the friction elements experience line contact

$$\sigma_o = \frac{2Q}{\pi l b} \tag{6.12}$$

where σ_o is the maximum contact stress, Q is the preload force, l is the length of the contact line, and b is given by the following expression

$$b = \left[\frac{4Q}{\pi l} \left(\frac{1-\xi_A^2}{E_A} + \frac{1-\xi_B^2}{E_B} \right) \frac{1}{\left(\frac{1}{r_{A,x}} + \frac{1}{r_{B,x}} \right)} \right]^{1/2} \tag{6.13}$$

where ξ is the Poisson's ratio, E is the Young's modulus, and r is the principal radius. Solving the stress equations with the relevant parameters for this design one finds that the maximum contact stress is 16 MPa. This is well below the yield strength of the material, which is 240 MPa.

Another consideration in the design of a friction drive transmission is the life of its elements. The life of a friction drive element with line contact is given by

$$L = K_6 Q^{-4} R_A^{4.30} l^{3.11} \left(1 + \frac{R_A}{R_B}\right)^{-5.19} \tag{6.14}$$

where L is the life in millions of stress cycles, K_6 is a constant equal to 2.15×10^{34}, and R is the rolling radius. The life of the friction drive can be converted to units of time with the following equation

$$H = \frac{10^6 L}{60 \nu n} \tag{6.15}$$

where H is the life of the component in hours, ν is the number of stress cycles per revolution, and n is the speed in revolutions per minute. Plugging in the relevant parameters the life of the friction drive in this design is expected to be 6.6×10^{16} hours. This is an enormous life that ensures the robot has little risk of failure due to the friction drive.

6.2.3 Bearings

The bearings in the friction drive transmission are described and analyzed in this section. There are six bearings in the design of the friction drive. Two large ball bearings with plastic raceways and glass balls were purchased from KMS Bearings. These bearings are used to support two of the friction cones. As a result the large bearings are undergoing two forces in this design: an axial force and a radial force. Two small ball bearings from KMS Bearings are located inside two of the friction cones. These bearings are not anticipated to carry any loads; rather they provide a low friction rotational surface. The small bearings are therefore the same as those used in the design of the differential gear transmission, which was model AR3-G. Finally, two plain thrust bearings are located in the remaining friction cones. These bearings must be capable of carrying a substantial axial load. The plain bearings were purchased from McMaster-Carr and are composed of Rulon J.

First, the analysis required for the large ball bearings will be presented. These bearings must be capable of supporting a radial load of 1.3 N and an axial load of 44 N. The same bearings used in the differential gear design, KMS Bearing model AR16-G, would be ideal; however, these bearings are deep groove ball bearings, which are not the best option to support high axial loads. If deep groove ball bearings prove not to be sufficient there is an option to

use four-point contact ball bearings.

The life of the bearings was determined with Equation 6.3. Because there is an axial and radial load on these bearings, the following equation must be used to determine the equivalent value for P_r

$$P_r = XF_{radial} + YF_{axial} \tag{6.16}$$

where X and Y are determined from a chart found in any design textbook[30]. These values are based on relationships between the axial load, radial load, and catalog static load rating of the bearing. In this situation X is 0.56 and Y is 1.31. Solving Equation 6.3 with these values yields a bearing life of approximately 30000 hours. This bearing life should be more than sufficient for this application. If the bearing is problematic it can be easily exchanged with a four-point contact bearing of equal size.

A decision was made to exchange two of the small ball bearings to plain thrust bearings when the friction drive transmission is utilized. This decision requires some explanation. If possible it is desired to use ball bearings because of their low friction. Therefore, ball bearings were first analyzed for use as thrust bearings in this design. Due to size constraints in the design a small bearing must be used as the thrust bearing. Unfortunately, small bearings have a smaller load rating. The deep groove ball bearings are not intended for use with purely axial loads. However, as an estimate Equation 6.3 was solved with the thrust load, 44 N, as P_r. One finds that using a ball bearing in this situation is not suitable as it will only last 450 hours. This is much smaller than the life of the other components analyzed for this design. It is therefore not wise to pursue a ball bearing for this design component. If a rolling element bearing is to be used, it should have a larger load rating or be of a variety more suited for axial loads such as a tapered roller bearing. Unfortunately, neither of these options is feasible in this design due to size constraints and material limitations.

The alternative to ball bearings that was pursued was a plain thrust bearing. This type of bearing has no rolling elements. Instead a plain bearing is simply composed of a low friction material. In this case the material is Rulon J, a type of low friction plastic. The analysis required for this bearing was to simply check that the material could withstand the axial force. The yield strength of the material is 14 MPa and the applied force is 44 N. Therefore, the

Type of Analysis	Support Thickness (in)
deflection	0.48
strength	0.029

Table 6.3: Summary of result for side support thickness in the friction drive transmission

diameter of the thrust bearing must be a minimum of 0.078 inches in diameter. In fact, the diameter of the thrust bearing is 0.875 inches. The plain bearing is a much safer design than the ball bearing although it may introduce more friction.

6.2.4 Side Support

The analysis of the side supports for the friction drive transmission was performed in a similar fashion to the analysis for the differential gear transmission. However, the friction drive transmission has an additional force that must be accounted for. This force is due to the preload on the friction cones. This section will describe analysis done to determine the size of the side supports required for the friction drive transmission.

There are two important considerations that will determine the size of the side supports. First, the deflection of the supports due to the applied loads must be kept less than 0.00025 rad. Second, the material strength of the side supports must be capable of withstanding the applied loads. There are two loads applied to the side supports in the friction drive transmission. The weight of the handle mechanism creates a small moment load and the preload force creates a greater load. The effects of the handle weight were analyzed in the previous section; therefore, the effects of the preload force will be determined here.

First, the thickness of the side supports to meet the deflection requirements will be determined. This is done using the same equations used in the analysis of the side supports for the differential gear transmission, Equation 6.6 and Equation 6.8. The difference here is that the applied force is 44 N which acts over a 2 inch moment arm. Solving the equations, one finds that the thickness of the side supports must be a minimum of 0.48 inches.

Next the thickness of the side supports was determined based on the material strength. Again, Equation 6.9 and Equation 6.8, from the previous section were used in this analysis. In this situation the side support thickness must be a minimum of 0.029 inches to meet the design requirements. The thickness results for this component are summarized in Table 6.3.

The forces generated by the friction drive transmission are greater than those present in the differential gear transmission. This explains why the thickness requirements in Table 6.3 exceed those in Table 6.2. As a result, the side supports were sized to meet the design requirements for all cases. Namely, the thickness of the side supports must be greater than 0.48 inches the largest value in the analysis. In reality the side supports were designed with a thickness of one inch, providing a safety factor of two.

6.2.5 Connecting Rod

The connecting rod for the friction drive transmission is similar in design to that used in the differential gear transmission. The function of the connecting rod is the same. It provides a means of attaching the friction cones and locating them relative to each other. However, there are a few differences in the component, which will be discussed in this section.

First, the connecting rod for the friction drive transmission must allow for the friction cones to be preloaded together. Therefore, the friction cones do not have a precise spacing as the gears in the differential design. Instead the friction cones will be pulled together until the proper preload is applied. This means that the connecting rod must be able to accommodate this unpredictable spacing. Therefore, the connecting rod does not have a shoulder on which the bearings or friction cones must sit. Instead the bulk of the connecting rod was made shorter than the length of the friction cone assembly. The ends of the rod were then threaded so that a set of nuts can tighten the assembly together. The shorter connecting rod ensures that it will not interfere as the friction cones tighten together.

Another consideration for the connecting rod is the applied forces. In the differential gear transmission the connecting rod was not anticipated to support any loads. However, this is not the case for the friction drive transmission. The connecting rod is used to apply the preload force; therefore, it is important that it is sized accordingly. The clamping force used to apply the preload is 22 N. The stress in the rod is governed by the following equation

$$\sigma = \frac{F}{A} \tag{6.17}$$

where F is the clamping force and A is the cross-sectional area of the rod. It is desired to make the connecting rod out of Lexan although it is a weaker material than G10. Solving this

equation, leads to a minimum connecting rod diameter of 0.025 inches. This is much smaller than the minimum diameter of 0.25 inches that was used in the design. Therefore, Lexan is an appropriate material for this component and the connecting rod is sized appropriately for the anticipated loads.

6.3 Handle mechanism

The handle mechanism is the subassembly of the robot that connects the patient's hand to the robot transmission. The idea behind the handle mechanism is to create a four-bar linkage between the differential and the wrist joint, as shown in Figure 6-11. This will accommodate for the fact that the two joints are not coincident. The original handle design was much different from this mechanism, as it contained a linear bearing rather than a four-bar linkage. The linear bearing was discovered to create a bias for a particular path of motion. As a result the patient found it much easier to move the handle in one direction compared to another. Due to this bias, a redesign of the robot handle was performed by Interactive Motion Technologies (IMT). IMT is the company that has commercialized the wrist robot. The design of the handle mechanism presented here utilizes the same concept. However, the design details, including bearings, materials, and structure, have been altered to meet the requirements of this application.

There are two design components in the handle mechanism that this section will discuss in detail. First the bearings used in the handle mechanism will be analyzed to determine if they are capable of withstanding the applied loads. Second, the linkages in the handle mechanism will be analyzed to ensure that they are sized appropriately.

6.3.1 Forces

To begin this analysis the forces applied to the handle mechanism were determined. The handle was analyzed to determine the magnitude and direction of the forces applied to each link. Figure 6-12 illustrates a free body diagram of the handle mechanism. This model assumes that the patient is forcing the robot against a locked motor. Therefore, the point at which the handle attaches to the transmission is assumed to be fixed. The forces indicated on the free body diagram represent forces due to adduction/abduction and flexion/extension.

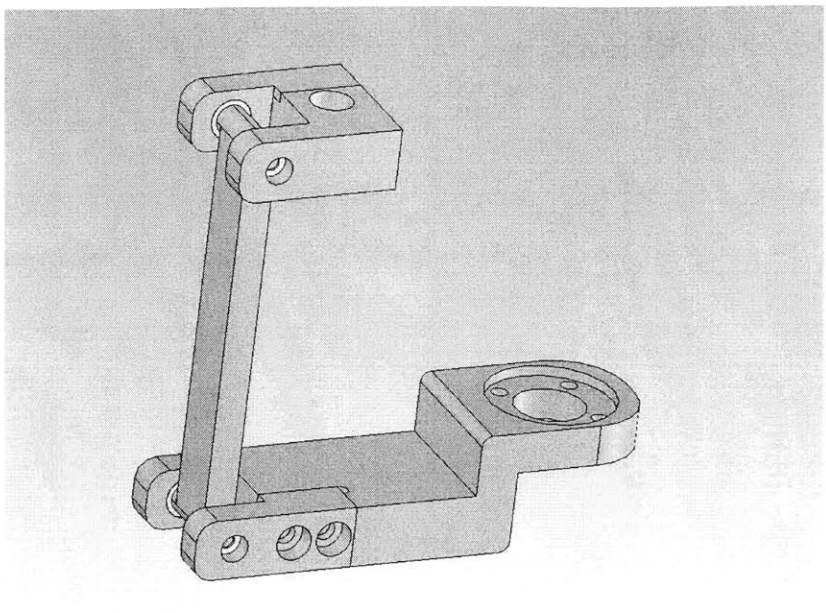

Figure 6-11: Solid model of the handle mechanism

The magnitude of these forces is equal to the torque a patient applies to the system, 1.2 Nm, divided by the distance from the wrist to the handle, which is 3 inches. Thus, the magnitude of all forces in the free body diagram is 16 N.

6.3.2 Bearings

The bearings used in the handle mechanism will be discussed in this section. The bearings must be capable of withstanding the loads applied to the system. Two bearings were used at the interface between each linkage. These are all deep groove ball bearings purchased from KMS Bearings. The model selected was AR3-G, which have plastic raceways and glass balls.

In the worst case scenario, each bearing will experience an axial load of 16 N and a radial load of 8 N. Because there is a combination of radial and axial loads, Equation 6.16 must be used to determine the equivalent bearing load. Based on the textbook design chart X was found to be 0.56 and Y was found to be 1.1[30]. Therefore, the equivalent load is equal to 22 N. Plugging this result into the bearing life equation, Equation 6.3, it was discovered that the life of these bearings is approximately 3500 hours.

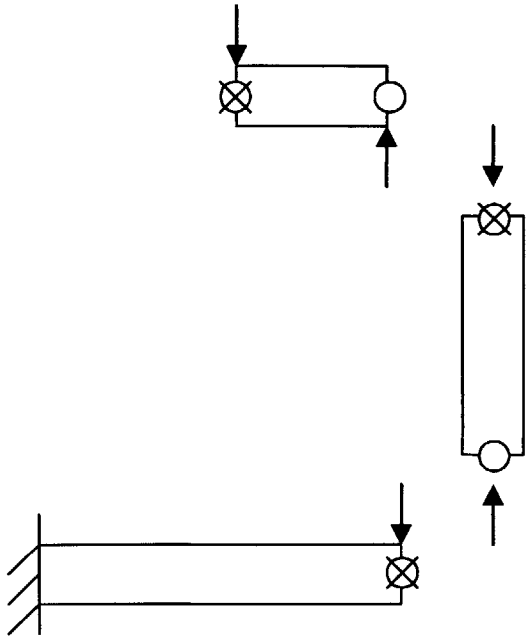

Figure 6-12: Free body diagram of the handle mechanism

Although the life of the bearings in the handle mechanism is not as high as that of other bearings in this design, the life should be appropriate for the application. Small bearings are desirable due to the size constraints of the robot. If, however, the life of the bearings proves to be a problem two possible solutions exist. First, the bearings can be replaced after a particular time has elapsed. This is a reasonable solution considering that the bearings are rather inexpensive. An alternative solution would be to use larger bearings. This would require minor alterations in the design of some of the components. Primarily, the size of the linkages in the handle mechanism would have to change, which would lead to a larger, heavier mechanism.

6.3.3 Linkages

The linkages were analyzed to determine that their dimensions are appropriate to withstand the applied loads. The linkages are undergoing forces in two directions. Therefore, the forces in one direction impact the thickness in the other direction and vice versa. As a result, it is not

Component	Direction	b (in)	l (in)	*h (in)*
Arm 1	x	1.75	4.25	*0.04*
Arm 1	z	0.50	4.25	*0.07*
Arm 2	x	0.75	4.78	*0.06*
Arm 2	z	0.375	4.78	*0.09*
Arm 3	x	1.75	1.5	*0.02*
Arm 3	z	0.75	1.5	*0.04*

Table 6.4: Summary of linkage size analysis

easy to set one dimension and solve for a second dimension. The design approach used here was to first design the linkages around the size of the bearings and gear that will be attached to the handle mechanism. The next step was to check the linkage dimensions to ensure that they are strong enough to withstand the required loads.

The beam bending equations, Equation 6.9 and Equation 6.8, that were used in previous sections will be employed again here. The results of the analysis are summarized in Table 6.4. The direction refers to Figure 6-12, where forces on the page are in the x direction and forces into the page are in the z direction. The objective of this analysis is to ensure that any arm thickness, h, for the analysis of a particular linkage in the x direction does not exceed the width of the linkage, b, used in the z direction analysis. For example, when Arm 1 is analyzed in the x direction the thickness of the arm must not exceed 0.04 inches. This thickness was set at 0.50 inches, and used as the width of Arm 1 analyzed in the z direction. If the results are compared in a similar fashion for each arm in both directions, it is discovered that the linkage dimensions easily meet the strength requirements.

6.4 Hydraulic Vane Motor

The hydraulic vane motor was designed in a similar fashion to the initial prototype. However, small alterations were made based on the information gained in testing the initial prototype. A solid model of the hydraulic motor design can be seen in Figure 6-13, Figure 6-14, and Figure 6-15. Each component in the motor and any accompanying design analysis will be discussed in this section. The components in the hydraulic vane motor include the shaft, motor housing, motor lids, vane, cap, bearings, and seals.

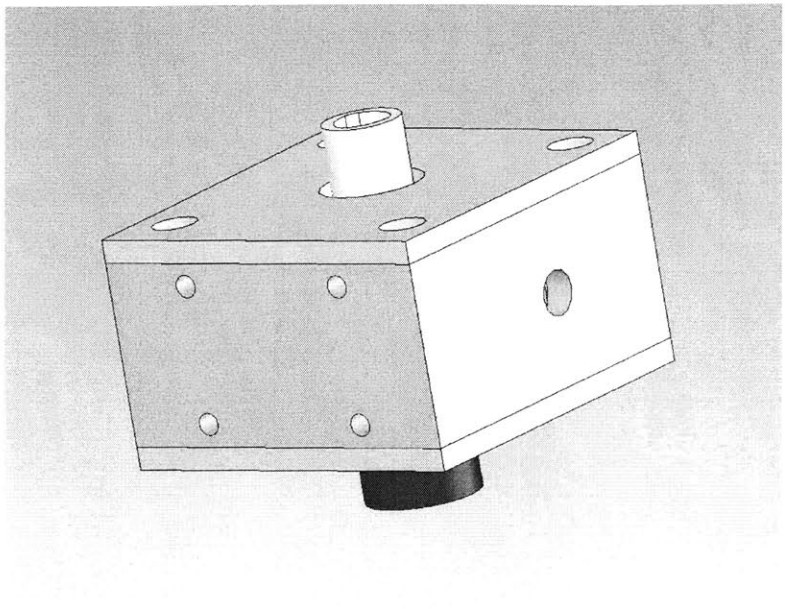

Figure 6-13: Solid model of the hydraulic vane motor

6.4.1 Shaft

The shaft in the hydraulic vane motor will be analyzed in this section. The shaft must be capable of withstanding the loads applied to the motor. In addition, the shaft must be used to transfer torque between the motor and various other components in the system. For example, the hydraulic motor shaft must be used to attach the hydraulic motor to the electric motor and to attach the hydraulic motor to the transmission shaft. These two connections require slightly different designs. The ends of the shaft, therefore, have two alternatives depending on the type of connection that is required. These two alternative shafts are illustrated in Figure 6-16.

The shaft analysis performed here is similar to that done for the shafts in the transmission designs. The shaft in the hydraulic motor is only anticipated to undergo a torsional force. Therefore, Equation 6.5 was used to find the minimum shaft diameter. The torsion on the motor shaft will either be 4.7 Nm, for the hydraulic motor that will attach to the electrical motor, or 1.2 Nm, for the hydraulic motor that will attach to the robot transmission. It is desired that the same shaft dimensions be used in both situations, to facilitate the design. The

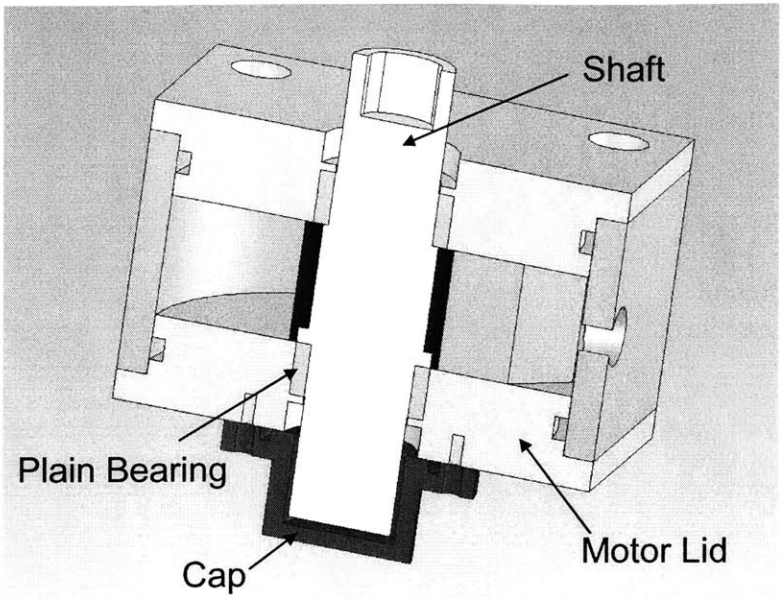

Figure 6-14: Section view of the hydraulic vane motor

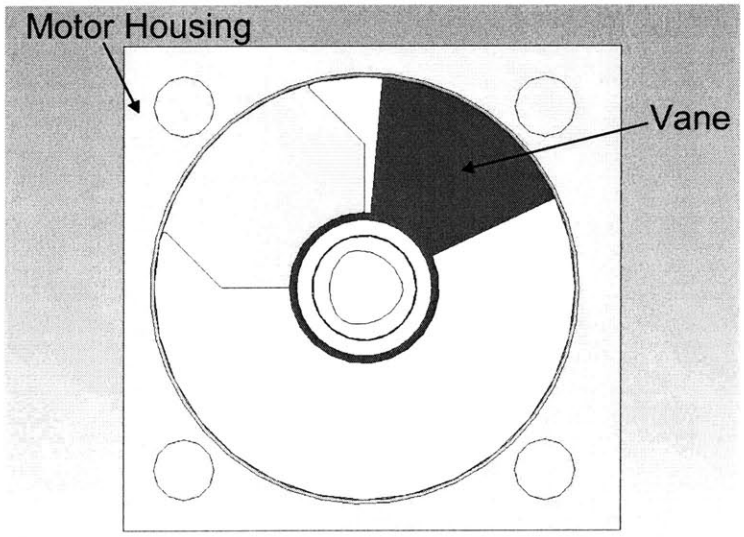

Figure 6-15: Top view of the hydraulic vane motor

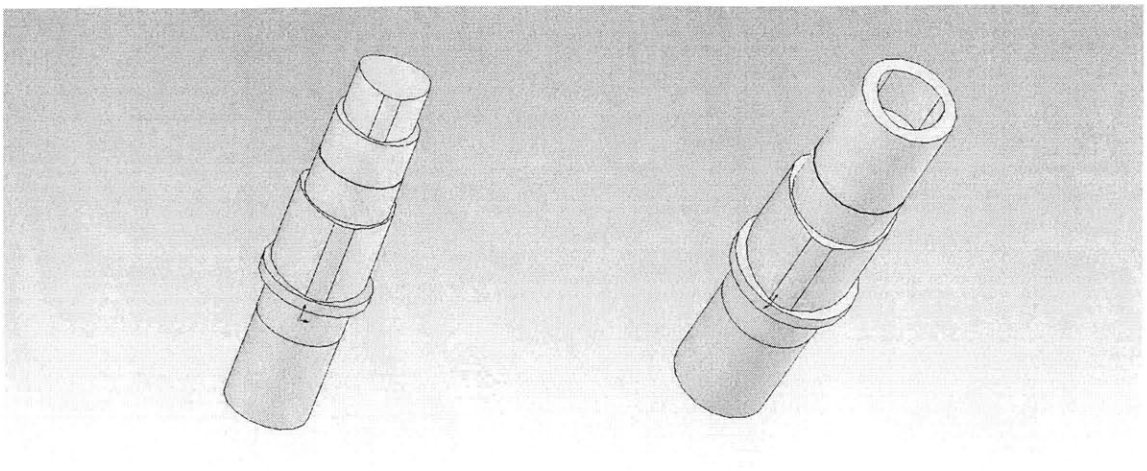

Figure 6-16: Two variations on the hydraulic motor shaft

Torque (Nm)	Diameter (in)
1.2	0.12
4.7	0.18

Table 6.5: Summary of hydraulic motor shaft diameter anaylsis

diameter of the shaft was determined for both torque loadings. The results of this analysis are summarized in Table 6.5. The results indicate that the motor shaft must be at least 0.18 inches. In fact, the shaft diameter was made a diameter of 0.86 inches, which was required to accommodate connections to other components in the system. The shaft of the motor is certainly strong enough to withstand the applied forces.

6.4.2 Motor Housing

The design details regarding the motor housing are discussed in this section. The motor housing is to be constructed on the wire EDM machine out of copper. This will ensure careful control of the space between the motor housing and the vane. The importance of the gap sizes inside the hydraulic vane motor was discussed in Section 3.3. There are two aspects of the motor housing that will be discussed here. First, geometrical changes were made to the initial prototype of the hydraulic vane motor. Second, a structural analysis was performed on the motor housing to ensure the component's strength.

	Thickness (in)
Hoop stress	8.9×10^{-6}
Longitudinal stress	4.4×10^{-6}

Table 6.6: Motor housing thickness based on internal pressure

The geometric changes that were made to the motor are primarily for design simplicity and convenience. The outside profile of the motor housing was made to be square. This facilitates mounting the motor to the robot and mounting the motor lids to the motor housing. In addition, the square design allows the fittings to be placed on the side of the motor rather than the top. The fittings will not interfere with the shaft and will allow a more direct flow path toward the vane inside the motor.

The second geometric change in the motor housing is the size of the stop. The stop was increased such that it eliminates 90 degrees of rotation of the hydraulic motor. This was done because of the limited rotation required from the motor. The idea here was to reduce the amount of unnecessary fluid. During testing of the initial prototype, it was noticed that a large mass of fluid was difficult to accelerate. Therefore, increased stop size is an effort to decrease the volume of moving fluid.

The next step in the motor housing design was to ensure that the material was capable of withstanding the fluid pressure that will be contained inside. The same analysis was performed for the initial prototype of the vane motor. Equation 3.28 was used to determine the hoop stress in the motor housing and Equation 3.29 was used to calculate the longitudinal stress in the motor housing. The internal pressure in the hydraulic vane motor is expected to be 1.4 kPa. This is a low pressure that is not anticipated to cause significant stress in the system. Nonetheless, the results from these equations give the required thickness of the motor housing, which are summarized in Table 6.6. As expected, the required thickness is significantly smaller than the 0.25 inch minimum thickness used in the motor housing design.

6.4.3 Vane

The vane in the hydraulic motor is the component responsible for converting the fluid flow into torque. Most of the vane design is based on experience gained while testing the initial prototype of the hydraulic motor. Therefore, this section will discuss the basis for the design

decisions made regarding the vane.

Although the motor vane is a simple construction, great care must be taken in the manufacturing of the part. This is to ensure that the gaps around the vane are tightly controlled. As was shown in Section 3.3, the function of the motor is highly dependent on the accuracy of the vane. Therefore, the vane was constructed out of copper and machined via wire EDM, which is an extremely accurate manufacturing technique.

The cross sectional area of the vane has an affect on the function of the motor. A small area means a higher pressure is required to produce the necessary torque. High internal pressure will increase the rate of fluid leakage through the gaps. A larger area increases the volume of fluid in the motor, leading to higher inertia. Additionally, the aspect ratio of the vane will affect the motor properties. A tall, thin vane profile will have low inertia but requires a higher pressure to achieve the required torque. A short, wide vane profile has the opposite characteristics of higher inertia and lower pressure. The vane shape thus requires a complicated trade off.

The area and shape of the vane in this design is primarily based on qualitative observations made during testing of the initial hydraulic motor prototype. The vane in the initial prototype was tall and thin, with a length to width ratio of approximately 2:1. During troubleshooting and testing, it was observed that the motor was more successful when a spacer was used to reduce the aspect ratio to 1:1. Therefore, the vane in the redesigned hydraulic motor was set to have a length approximately equal to its width.

The final alteration that was made during the redesign of the vane was the arc length of the component. The arc length of the vane affects the fluid loss from one chamber of the hydraulic motor to another. Equation 3.35 was used to explore the change in pressure acting on the vane as a result of gap width. This same equation can be used to explore effects of the arc length of the vane on pressure. Equation 3.35 shows that the pressure acting on the vane is proportional to the length of the gap. Therefore, a vane with a longer arc length will preserve more pressure and thus provide more torque. In the first prototype of the vane motor the arc length of the vane was only 0.25 inches. This is a very small value that can certainly be improved upon in the motor redesign. Therefore, the vane in this design has a 60 degree arc, which corresponds to a 1.83 inch arc length. This simple change should reduce the pressure loss in the motor by a factor of seven.

6.4.4 Motor Lids

This section will discuss the design of the hydraulic motor lids. The hydraulic vane motor contains two lids, a top lid and a bottom lid. The top and bottom lids are identical except for one feature. The bottom lid has attachment points for the cap. The primary function of the motor lids is to contain the fluid within the motor housing. However, to accomplish this task the motor lid must be capable of housing the required seals.

The motor lids are designed to accommodate two seals. The first seal is a static o-ring seal placed on the hub of the motor lid. This seal was placed in the same location used in the first hydraulic motor prototype due to its success. The location of the o-ring does not interfere with the motor lid being tightened against the rigid surface of the motor housing. The second seal housed in the motor lid is the PTFE dynamic shaft seal. This seal must be contained in a groove that does not require the seal to be stretched for assembly. Therefore, the motor lid has a slot rather than a groove for the shaft seal to occupy.

The motor lid does undergo a small amount of stress due to the internal pressure of the hydraulic motor. However, the internal pressure is only 1.4 kPa, which is tiny compared to the 275 MPa yield strength of the copper, the material from which the motor lids will be constructed. The thickness of the motor lids is not required for strength, it is merely necessary to accommodate the seals and bearings into the design.

6.4.5 Cap

The cap in the hydraulic motor is a new component from the initial hydraulic motor prototype. The necessity of the cap is due to a change in the motor shaft. In this design of the hydraulic vane motor, the shaft is extruding from the motor housing at both ends. This change was made to accommodate the addition of a sensor in the future. At this time the robot is not designed to have any sensors attached to the hydraulic motors. However, at a later date MRI compatible sensors may be added to the design or sensors might be required in testing. Therefore, the shaft was designed in anticipation of the use of sensors.

The drawback to having a through shaft is there are now two locations in which the shaft exits the motor housing. This means two dynamic rotary seals must be used. The addition of seals, however, increases the friction in the system. This added friction is undesirable and

should be avoided if possible. Therefore, the idea in this design is to employ the cap when no sensors are needed and thus a through shaft is unnecessary. The extra seal can then be removed and the cap will still contain the fluid inside the motor housing. When a through shaft is required, the cap can be removed and the second seal can be replaced. The cap allows the added friction from the seal to only be added when absolutely necessary.

The cap was designed to retain the fluid inside the motor housing without leaks. This was done by the use of a static o-ring placed on the face of the cap. The cap is then bolted to the bottom motor lid. The design of this component is a simple addition that will be helpful for future work on this MRI compatible robot.

6.4.6 Bearings

The bearings used in the hydraulic motor are discussed in this section. The bearings in the hydraulic motor are not anticipated to support any loads, rather they are designed to reduce the friction in the design. The bearings help locate the motor shaft and give it a smooth surface on which to rotate. The bearings in the hydraulic motor will come into contact with the hydraulic fluid, thus they must be capable of withstanding this type of contamination. Therefore, plain bearings were used in the design of the hydraulic vane motor. These bearings are composed of Rulon J, a low friction plastic material. The same bearings were used in the initial prototype with great success.

6.5 Stand

The stand for this design performs a number of functions. First, it is needed to mount the robot mechanisms and actuators. Additionally, the stand is used to provide a sort of table on which the robot can be placed and that will fit within the MRI machine. Finally, the stand provides an interface between the robot and the patient. The final design for the stand assembly is pictured in Figure 6-17 and Figure 6-18. The design decisions regarding the stand assembly will be presented in this section.

The stand is designed such that the patient will lie inside the opening of the table. The weight of the patient's body will secure the table to the MRI machine. The robot is thus

simple to insert and remove from the MRI machine. The table opening is 18 inches wide and 8 inches tall. This amount of space will accommodate the hip width of the 50 percentile male patient. However, the abdomen thickness of the 50 percentile male patient is 10.1 inches. The table size was reduced slightly so that the robot could fit inside the MRI machine. This may limit the number of patients that can use the MRI compatible wrist robot.

Once the patient and the robot inside the MRI machine, the patient will then place his or her lower arm on the arm rest. The patient will need to be secured to the arm rest and it is anticipated that the upper arm will have to be supported as well. The details regarding patient attachment and support have been left for future work after the robot is built and assembled. At that time the design can be tested with a human to assess where support is required and where attachment will be most comfortable.

The transmission and hydraulic motors are mounted to the mounting plate. Notice that all of the mounting locations have a recess that will accept the components. This will help locate the components and aid in their alignment. The mounting plate is then attached to the table, also with the use of a recess. In fact, there are two ways to mount the robot to the table. These different mounting locations depend on which arm is being exercised by the robot.

Notice that the robot is mounted with two different angles, one relative to vertical and the other relative to horizontal. There are several reasons for the different mounting angles. First, it was desired to keep the robot as square to the horizontal axis as possible. This is due to the computer interface that prompts the patient during therapy. The relative motion between the robot and the computer prompt must make logical sense to the patient. This is best achieved by keeping the robot square to horizontal. In fact, the horizontal angle of rotation is 10 degrees.

The second reason for adjusting the mounting angles of the robot was for comfort. Through qualitative testing it was determined that some mounting positions would be extremely uncomfortable for a patient while he or she is lying down. For example, the square mounting used for the original wrist robot would require a patient to place the lower arm parallel and approximately 5 inches above their torso if it was used for the MRI compatible wrist robot. This is nearly impossible to do based on the construction of the human body. It was determined that an angle 45 degrees from vertical was a comfortable and achievable position.

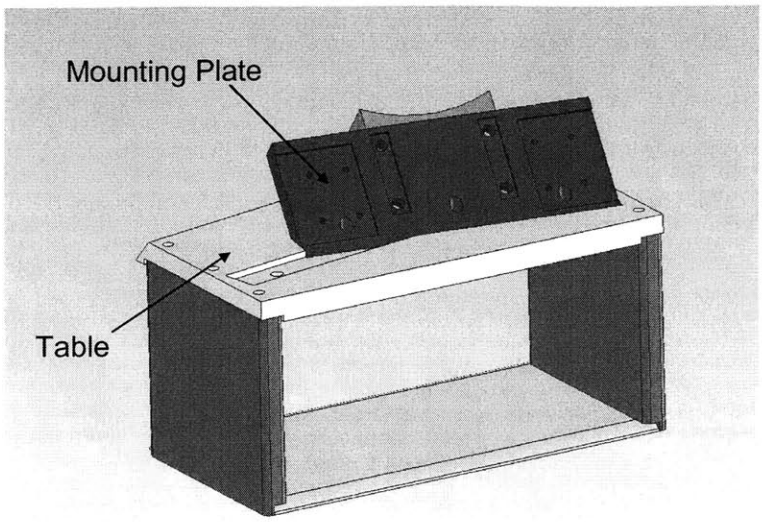

Figure 6-17: Solid model of the stand assembly

The final justification for the mounting angles is the space constraint set by the MRI machine. Remember that this robot must be able to fit inside the MRI machine with a patient. This is not an easy task and limits a number of otherwise desirable mounting positions. For example, it would be more comfortable for a patient to manipulate a robot placed on the outside of the body where the arm naturally lies. However, the patient width does not leave room to insert a robot. This could be a constraint that is eliminated if a closed bore MRI machine is not used. In which case, the mounting position of the robot may be adjusted to be more comfortable for the patient.

6.6 Non-MRI Compatible Subassembly

The non-MRI compatible subassembly consists of the components of the robot that are placed outside the MRI machine. These components are used to remotely drive the MRI compatible robot. The non-MRI compatible subassembly is composed of three parts: hydraulic motor, electric motor, and mounting structure. The hydraulic motor and electric motor have been discussed in previous sections. Therefore, this section will focus of the mounting structure design, which is shown in Figure 6-19.

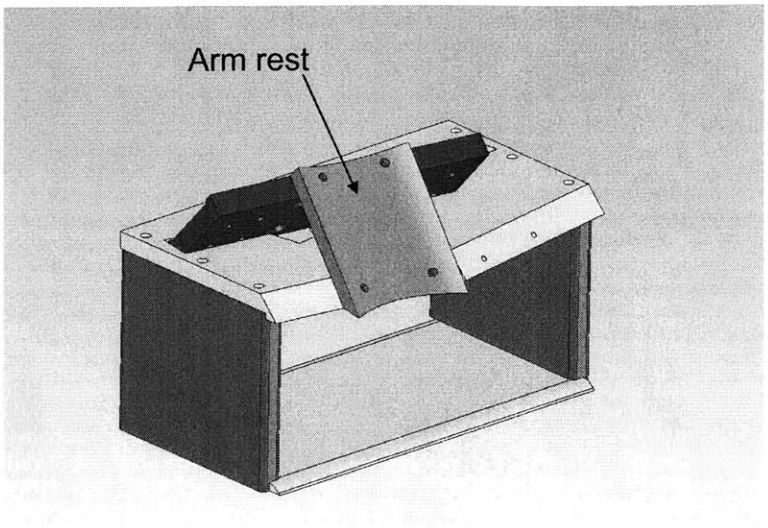

Figure 6-18: Alternative view of the stand assembly

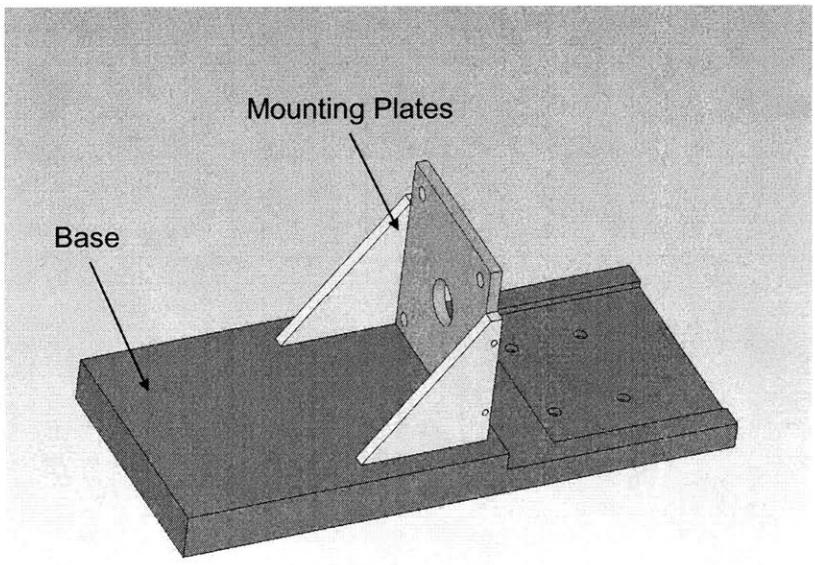

Figure 6-19: Non-MRI compatible mounting structure

The mounting structure serves a simple purpose in this design. It is used to align and fix the electric motor to the hydraulic motor. The mounting structure is machined out of aluminum because it is not inside the MR room and therefore does not need to comply with MRI compatibility requirements. The mounting structure uses recesses for the hydraulic motor and mounting plates to help in accurately locating and aligning the components. The base of the mounting structure may be attached to a cart or permanent assembly when it is used in the MRI facility. For initial testing of the MRI compatible robot this is not necessary. However, the base of the mounting structure provides room for such attachments to be added at a later date.

6.7 Polygon

The polygon method was used to connect elements to a shaft or link two shafts together. A polygon is a profile machined onto the shaft that allows the torque to be transmitted. There are several options for polygon profiles as shown in Figure 6-20. It is recommended to use the P3 profile with a taper if the design needs to be backlash free and separated regularly[44]. Both of these characteristics are important in this design. However, it was decided not to use the taper because it would require flexibility in the spacing of the components. It is important for most of the components in this design to be accurately spaced from each other. Therefore, the P3 profile was chosen but a taper was not included.

Several calculations must be done to determine that the proper sized profile is used. There is a minimum wall thickness for all female parts. This thickness is determined by the following equation

$$S = 1.44\sqrt{\frac{M_t}{\sigma_b}} \tag{6.18}$$

where S is the minimum thickness, M_t is the torsional moment, and σ_b is the maximum allowable tensile stress of the material. Most of the polygon profiles will experience a torsional moment of 1.2 Nm. In this case the minimum thickness is 0.035 in. However, there is a polygon profile used to connect the electric motor to the hydraulic motor. In this case, the torsional moment is higher because the electric motor must apply a higher torque to accommodate for

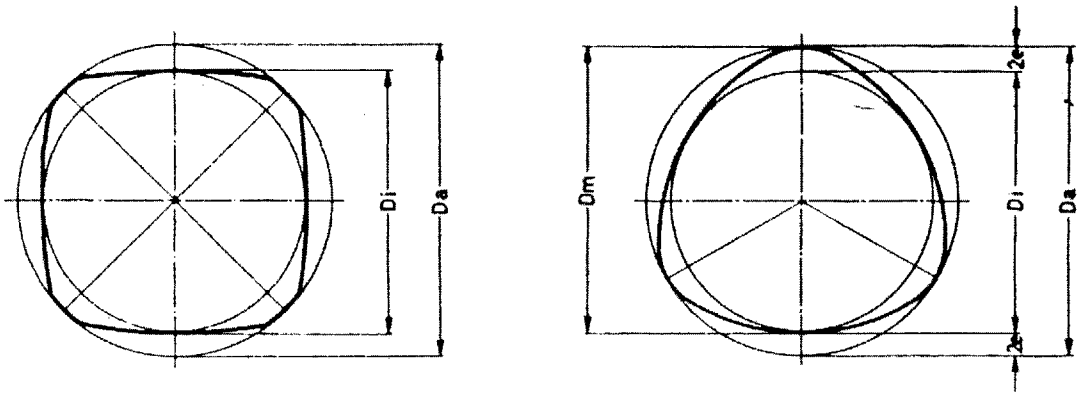

Figure 6-20: P4 and P3 polygon profiles[44]

frictional losses in the system. The torsional moment applied by the electric motor is 4.7 Nm. Therefore, the minimum thickness of the female polygon connecting the electric motor to the hydraulic motor is 0.070 in.

Another important consideration for the polygon is the maximum torsion, $M_{t_{\max}}$, and maximum bending, $M_{b_{\max}}$, that the profile can withstand. The following equations are used to determine the torsion a particularly sized polygon profile can withstand

$$M_{t_{\max}} = \tau w_p \tag{6.19}$$

$$w_p = \frac{\pi D_m^4}{16 D_a} \tag{6.20}$$

where τ is the allowable shear stress, D_m is the average diameter of the polygon, and D_a is the maximum diameter of the polygon, as illustrated in Figure 6-20. This design uses three different sized polygons. The dimensions of each polygon were plugged into the above equations to determine the maximum torsion that can be applied to the shaft. The results of these calculations are summarized in Table 6.7. Clearly the maximum torsion is much higher than the torsional forces expected in the robot, which are 1.2 Nm at the end point, and 4.7 Nm at the electrical motor.

There are no significant bending moments expected in this robot. Only the weight of the

	P3-3/4	P3-7/8	P3-1
Maximum torsion (N-m)	167	266	390
Maximum bending (N-m)	154	245	359

Table 6.7: Maximum allowable torsion for polygon profiles

robot handle creates a small bending moment of 0.03 Nm. Misalignment of parts can create an unexpected bending moment as well. Neither of these situations is expected to create the polygon to fail. However, for safety the maximum bending moment the polygon profile can withstand was verified. The equations for calculating the maximum bending in a polygon are as follows.

$$M_{b_{\max}} = \sigma_b w_x \tag{6.21}$$

$$w_x = \frac{\pi D_m^4}{32 D_a} \tag{6.22}$$

The results for the three polygon sizes used in this design are summarized in Figure 6.7. Again these values are much higher than the expected forces. As a result, there is little risk of polygon failure in this design.

6.8 Design Conclusions

This section has been thorough in describing each subassembly in the MRI compatible wrist robot. The design decisions for each component in the robot were discussed. Any analysis required to determine the strength, life, or reliability of the design was performed. The robot was deemed capable of withstanding the applied loads with a significant safety factor and long life.

The design was successful in fitting inside the MRI machine, as pictured in Figure 6-21. However, the space allotted for the thickness of the patient's abdomen was reduced. This may limit the number of patients that can use the MRI compatible wrist robot. It should be noted that if the robot is not used in a closed bore MRI machine the stand can be redesigned to accommodate a greater number of patients.

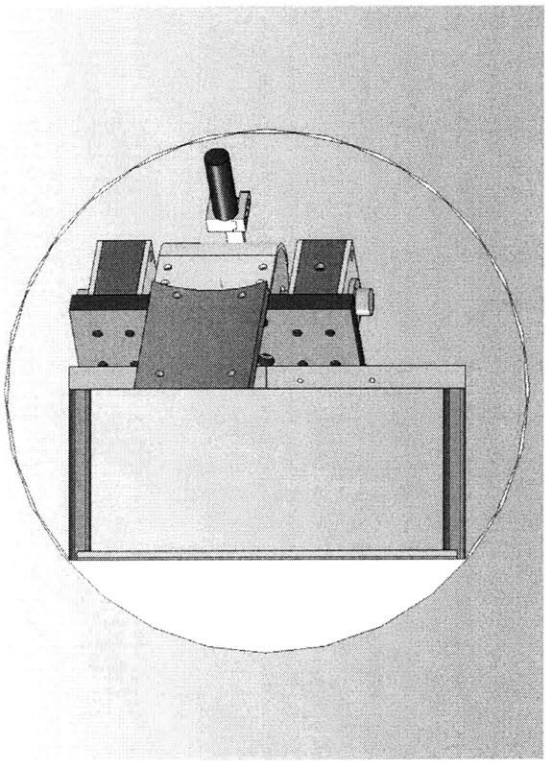

Figure 6-21: Model of the MRI compatible robot inside the MRI machine

Chapter 7

Assembly and Debugging

This section discusses the assembly and debugging process for the MRI compatible wrist robot. The problems that were encountered during assembly and initial operation are outlined. Alterations that were made to correct various problems are explained. Suggestions are offered for problems that remain to be fixed and improvements that could be made to the existing design. The completed design can be seen in Figure 7-1 and Figure 7-2.

7.1 Hydraulic Vane Motor

A great deal of work was required to assemble and debug the hydraulic vane motor. The hydraulic vane motor was designed with a very close tolerance between the vane and the motor housing. The gap between the vane and motor housing was held to 0.004 inches or less. However, the vane was not permitted to touch the motor housing. The hydraulic vane motor was initially assembled at the machine shop so that any problem that was encountered could be fixed immediately.

After assembly it was clear that the vane was touching the wall of the motor housing. To correct this mistake, small amounts of material were removed from the vane, primarily through sanding. The size of the vane was adjusted until it fit properly inside the motor housing while one motor cap was removed. However, whenever the motor cap was added so that the hydraulic motor was completely assembled the vane would not rotate properly. Usually the vane would get stuck in an isolated section of the vane's travel. Any sticking that occurred

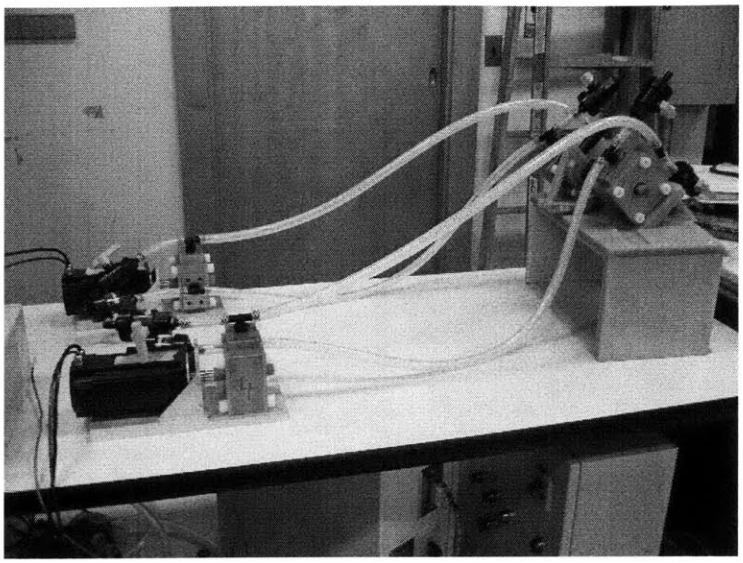

Figure 7-1: Assembled prototype of the MRI compatible wrist robot

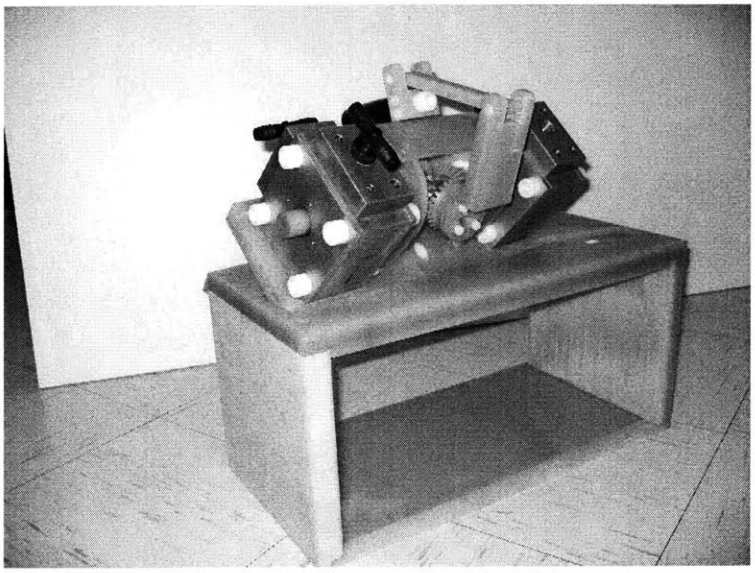

Figure 7-2: MRI compatible portion of the completed robot

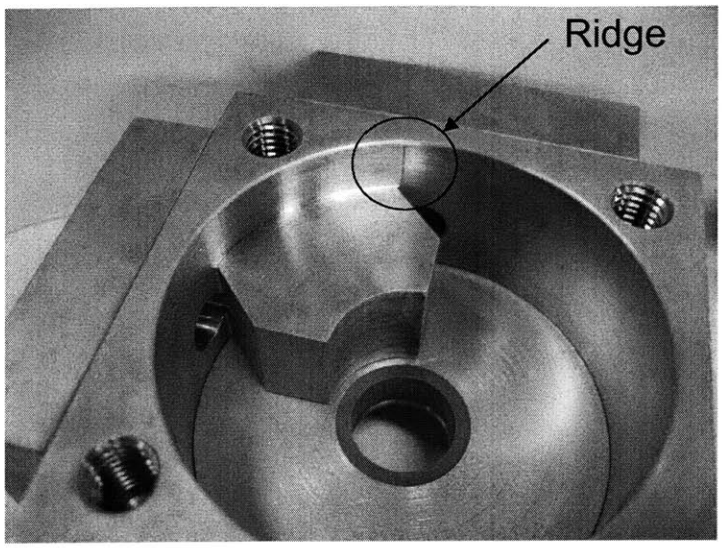

Figure 7-3: The ridge inside the motor housing that was due to a manufacturing inaccuracy

was particularly problematic because it produced chips of copper that would act as an abrasive and further compound the problem. Before assembly all marred surfaces were smoothed and all parts were cleaned thoroughly to remove dirt and metal chips. Although these steps were helpful in the debugging process they did not eliminate the problem.

The hydraulic vane motor was finally assembled properly after an error in the manufacturing of the motor housing was noticed. The profile inside the motor housing was manufactured via wire EDM. However, there was a section of material inside the motor housing that was removed above and below the barrier separating the inlet and outlet ports of the motor. The wire EDM was not capable of removing this material; therefore, it was machined on a mill. Unfortunately, the milling process did not make the diameter of the motor housing equal to the diameter that was cut using wire EDM. As a result, a tiny ridge remained on the wall of the motor housing as shown in Figure 7-3. The ridge was enough to move the center of the motor caps away from the center of the motor housing. This caused the assembled motor to be misaligned, thus making the vane touch the motor housing. To eliminate the problem the ridge inside the motor housing was removed on the mill.

Several alterations could be made to the design of the hydraulic vane motor to make the

assembly process easier. Alignment of the parts inside the hydraulic vane motor was critical to achieving a tight tolerance between the vane and motor housing. One way to improve the alignment of the motor is to drill the hole for the shaft after the motor has been assembled. This would ensure that both end caps are aligned and the shaft will be straight. Additionally, the problem encountered with the chips of copper could be eliminated by making the vane out of a plastic material. Plastic will be softer than the copper motor housing so that if the two parts touch metal particles will not be created.

7.2 Seals and Leakage

The seals that were purchased for this design were PTFE o-rings. However, these seals proved to be undesirable. They were extremely rigid which made it difficult to insert them into the o-ring groove for which they were designed. Because of the tight fit the seals added an undesirable amount of friction. Possible alternatives include a custom designed lip seal. This may be costly however the performance should be greatly improved. An additional option would be the use of a spring seal if an MRI compatible spring could be substituted for typical steel spring. A spring seal was used in the initial prototype with great success.

The hydraulic motor was run with no seal, thus relying on close tolerances to contain the fluid. Unfortunately the fluid leakage was excessive. The leakage was occurring where the shaft exists the motor housing. Curiously the hydraulic motors connected to the electrical motors had significantly more fluid loss than the hydraulic motors connected to the robot endpoint. There was no leakage observed in any of the static seals. The barb fittings used to connect the hoses were also successful in preventing leakage.

7.3 Weight

The hydraulic vane motors are constructed almost entirely of copper, which makes them quite heavy. This does not affect the function of the motor; however, it may affect the robot's ease of use. For example, the robot has two orientations based on which wrist is being exercised. To change from the right wrist to the left wrist a set of screws is removed and the mounting plate is moved to a new location on the table. This requires moving two hydraulic vane motors,

the transmission, and the handle mechanism. Due to the weight of the hydraulic motors this is a cumbersome procedure.

There are several options that could improve the weight of the device. First, the materials in the hydraulic vane motor can be altered. The only part that must be composed of copper is the motor housing because it is machined by wire EDM. The remaining copper parts could be made out of plastic, which is a lighter material. Plastic will tend to deform more than metal during assembly which can make alignment of the hydraulic motor difficult. Certainly the cap and fitting plates on the hydraulic motor can be made of plastic without effecting the performance or assembly of the hydraulic motor.

A second option for reducing the weight of the hydraulic motor is to decrease the thickness of the components. According to the design calculations the thickness of the motor housing and motor lids are significantly oversized. This was done to accommodate seals, bearings, and fasteners. Some weight can be removed from the design if non-functional material is removed or the size of the seals, bearings, and fasteners is reduced. For example, it would be simple to use a smaller size bolt for attaching the motor lids to the motor housing.

7.4 Patient-Robot Interface

Two aspects of the patient-robot interface were considered for this prototype. First, the space allotted for the patient should be appropriate. Second, the patient should feel comfortable in the robot. These two design objectives were qualitatively examined with the completed prototype.

The space allotted for the patient will only accommodate slender individuals, as shown in Figure 7-4.

There was sufficient room in the design to allow for a patient with a larger hip width. However, the space allotted for the depth of the abdomen would not allow for a patient with much larger stature. One observation was made that could improve the space available for the abdomen. It was expected that the base of the table would lie below the arch of the back. However, when the patient was comfortably inside the robot the base of the table was below the hips. This does not take advantage of the gap between the lower back and the floor that

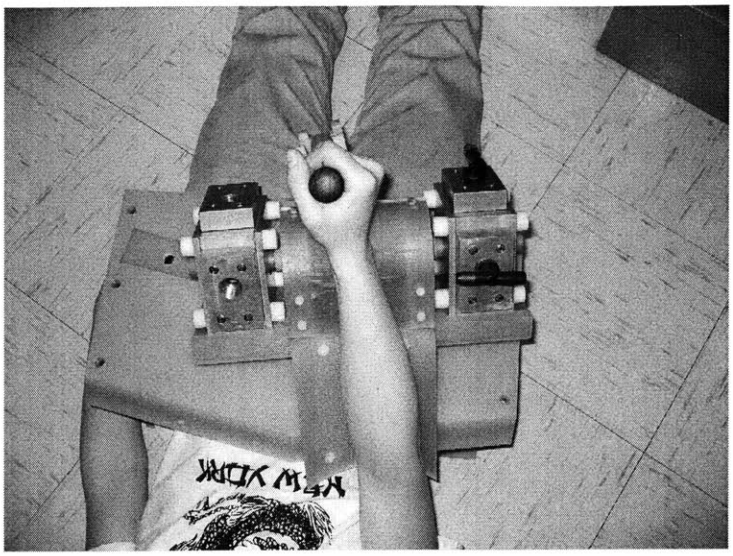

Figure 7-4: A patient inside the MRI compatible wrist robot

is present when one lies down. The table could be redesigned to move the base of the table to beneath the lower back. This could give the patient additional room to accommodate the depth of the abdomen; thus allowing a broader range of patient to be capable of using the MRI compatible wrist robot.

The comfort of the robot depends on the position of the arm when the patient is using the robot. The patient's arm was inclined at a 45 degree angle and locked at the elbow. This position allowed the handle of the robot to be reached easily. The position was comfortable for short periods of time, but became tiresome after extended periods of time. The comfort could be improved once the patient attachment features are included in the design.

7.5 Gears versus Friction drive

The robot functioned well with the gear transmission employed. A small amount of backlash could be observed; however, it was unclear whether the source was from the mechanism or from air in the hydraulic system. The system was easily backdrivable, which was a key functional requirement for this design. Overall, the differential gear transmission was quite successful and no obvious improvements were necessary.

The friction drive did not function well. There was a lot of friction in the system making the handle difficult to backdrive. Most likely the additional friction came from the large ball bearings supporting the transmission. When the preload force was applied to the friction drive a significant thrust force was applied to the bearings. The ball bearings are not the best variety for handling axial forces. One solution to this problem is to change the variety of ball bearing that is used. Deep groove ball bearings, for instance, are more suited for axial loading. Additionally, a plain thrust bearing with no rotating elements may improve the problem.

7.6 Filling Procedure

A different procedure was used to fill the system with fluid than was utilized during testing of the prototype hydraulic vane motor. Each port entering and exiting the hydraulic vane motors was equipped with a T-joint. One prong of the joint was connected to the system and the second was connected to a ball valve. In total there were four isolated sections in the hydraulic system, assuming there is minimal leakage across the hydraulic motor vane. Therefore, each section was filled separately.

One particular section was chosen and the ball valves at each end of that section were opened. All of the remaining valves in the setup remained closed. One end of the section was connected to a pump. The other end was led to drain into a bucket. The pump was turned on until the drainage into the bucket contained only fluid and no air. The pump was then turned off and both valves were closed. This process was then repeated for the three remaining sections of the system.

This filling procedure was very efficient, because it was fast and simple. Little air was visible in the hoses after the filling procedure was performed. The only drawback of the procedure was the addition of ball valves. The valves that were purchased for this prototype were quite large and could interfere with the robot or patient. A smaller ball valve design might be more appropriate.

7.7 Assembly and Debugging Conclusion

Overall, the design of the MRI compatible wrist robot was a great success. Most of the problems that were encountered during assembly and debugging were easily fixable. The major remaining difficulty at this time is reducing the fluid leakage from the hydraulic vane motor. This can hopefully be solved by purchasing new seals for the rotating shafts. All other suggested improvements do not affect the operation of the robot.

Chapter 8

Conclusion

This thesis has presented the design of an MRI compatible robot for wrist rehabilitation. The required background for design in the MR environment was discussed. The design process was outlined. A proof of concept prototype and testing was done to examine the effectiveness of a novel MRI compatible hydraulic actuator. The detailed design of the robot was then introduced and the necessary design analysis was presented. Finally, the assembly process and debugging of the completed MRI compatible robot was described. The success of this project and suggestions for future work will be discussed in this conclusion.

8.1 Project Evaluation

The goal of this project was to design a robot for wrist rehabilitation that can be safely and effectively used inside an MRI machine. To this date the following tasks toward the goal have been accomplished. First, a clear understanding was established regarding the requirements for designing an MRI compatible rehabilitation robot. For example, topics such as size limitations, MRI compatibility, and human anatomy were explored in detail. This background was essential to understand how to design a robot for use in an MRI machine.

The next contribution made in this project was the design and testing of a hydraulic actuator that is low friction and MRI compatible. The concept of the hydraulic motor was proven to be feasible through testing. However, modifications were required to the initial design to improve the performance of the motor. A second pass at the hydraulic motor design was performed.

The tolerances between the vane and the motor housing were carefully controlled. The second prototype functioned extremely well.

An additional contribution of this project was the design and analysis of the transmission, bearings, handle, and structure of the MRI compatible wrist robot. This task required altering the materials of the original wrist robot to be MRI compatible. Additionally, a great deal of analysis was performed to resize the components of the wrist robot and ensure that the use of MRI compatible materials would not affect the life or strength of the robot.

Finally, the prototype MRI compatible wrist robot was assembled and qualitatively tested. A variety of problems were fixed based on observations made during assembly and debugging. Additionally, suggestions were made for improvements that could be made to the robot design. Overall, the MRI compatible wrist robot was functional and successful.

8.2 Future Work

There are several suggestions that can be made for future work in this project. First, thorough testing in the laboratory is required to determine if the robot has met the functional requirements. If necessary, adjustments can be made to the design based on test results to improve the performance of the robot. After testing in the laboratory is complete a second set of testing inside the MRI machine is required. This is to ensure that the robot is in fact MRI compatible and that the machine will function properly in the MR environment. Again, design changes can be made as a result of testing in the MRI machine to improve the performance or compatibility of the robot.

The next step in the development of the MRI compatible wrist robot is to develop a control system. The control system will allow the therapy protocol to be introduced to the robot. Additionally, a properly designed control system can improve the performance of the robot. This process will require the testing of various control algorithms to determine the most appropriate for this application.

Clinical testing with human subjects can occur once the mechanical and electrical components of the robot are complete. First, it would be recommended to make design changes that facilitate clinical testing. For example, the details of the patient attachment and support need

to be designed. It is anticipated that an upper arm constraint and lower arm support will be required. However, other patient attachment components may prove to be necessary after testing on the robot is performed. Second, a permanent mounting structure might be designed for the components of the robot that are located outside the MRI machine. This will facilitate the setup of the robot in the MR facility and provide a neatly organized system. Finally, rigid pipes might be required to span a portion of the long distance between the MRI machine and outside the MR room. This would help reduce the compliance in the piping system and improve performance of the robot. Other design changes may become obvious after some amount of testing has been performed.

The final suggestion for future work is the development of MRI compatible sensors. Sensors were not pursued in this thesis; however, they may prove to be necessary once some testing has been performed. Several MRI compatible sensors have been designed, although none are available commercially. Optical sensing seems to be the most promising method because the light can be transferred to and from the MRI machine through fiber optics. This allows the electrical components to be placed outside the MR room. For example, one MRI compatible force sensor was developed that uses a light source, transmitted via optical fibers, attached to a frame with a known elasticity[45]. The frame is deflected under an applied load which causes a change in the position of the light source, which is captured with a photo sensor. The force is then related to the stiffness of the frame. This force sensor was capable of measuring the applied force within 0.3 N of the actual value.

Clearly there is still much work that can be performed on this MRI compatible wrist robot before it is complete. However, once this project is complete a valuable clinical tool will be available. This robot will provide valuable insight into the workings of the human brain and stroke recovery. In addition, an MRI compatible wrist robot can help improve the future design of rehabilitation robotics and therapy protocols. Overall, the design of the robot is a tremendous step toward the successful completion of this project.

Appendix A

Purchased Parts

A list of the purchased parts is included here along with the relevant data sheets.

Part Description	Manufacturer/Supplier	Part Number	Quantity
Motor	Kollmorgen	AKM43E-ANMNEH-00	2
Large ball bearings	KMS Bearings	AR16-G	2
Small ball bearings	KMS Bearings	AR3-G	8
Gears	QTC	PM2-25	4
Plain bearings	McMaster-Carr	10 - 6377K43	8
Thrust bearings	McMaster-Carr	6377K13	2
Large o-rings	McMaster-Carr	9452K165	8
Small o-rings	McMaster-Carr	9452K38	2
Shaft seal	McMaster-Carr	9559K33	4
Backup o-ring	McMaster-Carr	9560K63	4

Table A.1: List of purchased parts

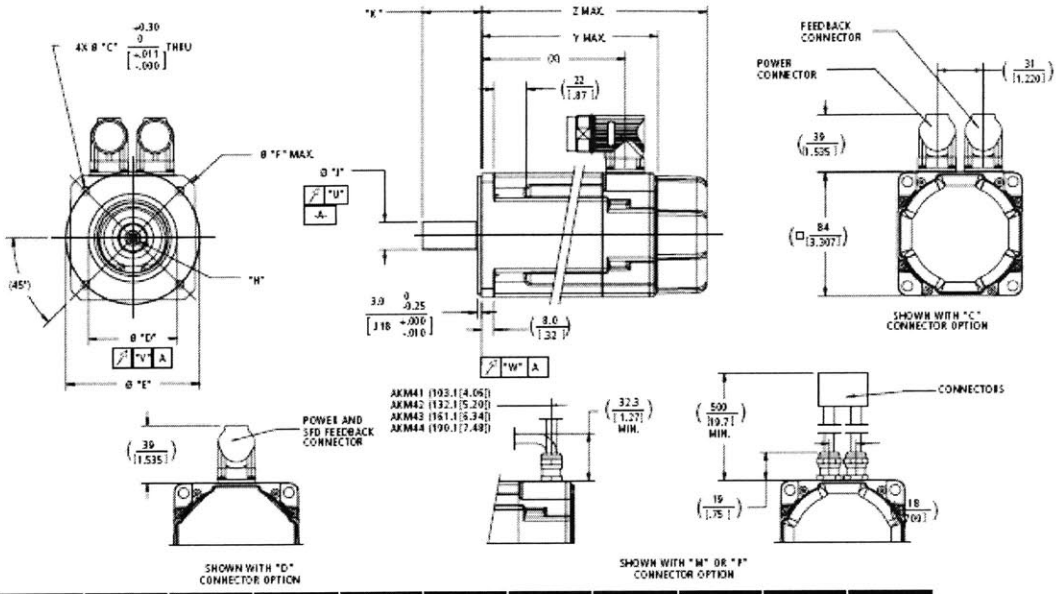

MOUNTING CODE	"C"	"D"	"E"	"F"	"H"	"J"	"K"	"L"	"M"	"N"
AC	7 [.276]	80 +.012 +.004 [3.1496 +.0004 +.0003] JS	100 [3.937]	–	D M6 DIN 332	19 +.013 +.000 [.7480 +.0005 +.0001] K6	40.0 [1.57]	–	–	–
AN	7 [.276]	80 +.012 +.004 [3.1496 +.0004 +.0003] JS	100 [3.937]	–	D M6 DIN 332	19 +.013 +.000 [.7480 +.0005 +.0001] K6	40.0 [1.57]	–	–	–
BK	5.54 [.218]	73.025 -.051 -.076 [2.8750 -.0020 -.0030]	98.43 [3.875]	–	–	15.875 -.013 -.026 [.6250 -.0005 -.0010]	52.40 ± 0.79 [2.063 ± .031]	17.02 0 -.43 [.670 0 -.017]	4.762 +.051 +.025 [.1875 +.0020 +.0010]	34.03 ± 0.25 [1.375 ± .010]
CC	5.54 [.218]	60 +.013 +.000 [2.3622 +.0005 +.0000] JS	90 [3.543]	109 [4.291]	D M6 DIN 332	19 +.013 +.000 [.7480 +.0005 +.0001] K6	40.0 [1.57]	–	–	–
CN	5.54 [.218]	60 +.013 +.000 [2.3622 +.0005 +.0000] JS	90 [3.543]	109 [4.291]	D M6 DIN 332	19 +.013 +.000 [.7480 +.0005 +.0001] K6	40.0 [1.57]	–	–	–
EK	5.54 [.218]	73.025 -.051 -.076 [2.8750 -.0020 -.0030]	98.43 [3.875]	–	–	12.700 0 -.013 [.5000 0 -.0005]	31.75 ± 0.25 [1.250 ± .010]	14.09 0 -.43 [.555 0 -.017]	3.175 +.051 +.025 [.1250 +.0020 +.0010]	19.05 ± 0.25 [.750 ± .010]

MOUNTING CODE	"P"	"R"	"S"	"T"	"U"	"V"	"W"
AC	21.5 -.013 -.026 [.846 -.0005 -.0010]	6 +.22 +.07 [.236 +.009 +.003] N9	4.00 [1.57]	32 0 -.25 [1.260 0 -.010]	0.040 [.0015]	0.080 [.0031]	0.080 [.0031]
AN	–	–	–	–	0.040 [.0015]	0.080 [.0031]	0.080 [.0031]
BK	–	–	–	–	0.051 [.0020]	0.10 [.004]	0.10 [.004]
CC	21.5 -.013 -.026 [.846 -.0005 -.0010]	6 +.22 +.07 [.236 +.009 +.003] N9	4.00 [1.57]	32 0 -.25 [1.260 0 -.010]	0.040 [.0015]	0.080 [.0031]	0.080 [.0031]
CN	–	–	–	–	0.040 [.0015]	0.080 [.0031]	0.080 [.0031]
EK	–	–	–	–	0.051 [.0020]	0.10 [.004]	0.10 [.004]

(X)	Y MAX.	Z MAX. (W/ BRAKE)	MODEL
96.4 [3.80]	118.8 [4.68]	152.3 [6.00]	AKM41
125.4 [4.94]	147.8 [5.82]	181.3 [7.14]	AKM42
154.4 [6.08]	176.8 [6.96]	210.3 [8.28]	AKM43
183.4 [7.22]	205.8 [8.10]	239.3 [9.42]	AKM44

Dimensions are in mm [inches].
Product designed in metric.
English conversions provided for reference only.

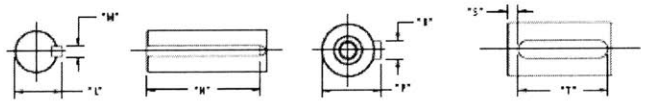

AKM4x - Up to 640 VDC

See system data beginning on page 8 for typical torque/speed performance.

	PARAMETER	Ref	SYMBOL	UNITS	AKM41 C	AKM41 E	AKM41 H	AKM42 C	AKM42 E	AKM42 G	AKM42 J	AKM43 E	AKM43 G	AKM43 K	AKM44 E	AKM44 G	AKM44 J
	Max Rated DC Bus Voltage•	Max	V_{bus}	Vdc	640	640	320	640	640	640	320	640	640	320	640	640	640
	Continuous Torque (Stall) for ΔT winding = 100°C ① ② ⑦ ⑨	Nom	T_{cs}	N-m	1.95	2.02	2.06	3.35	3.42	3.53	3.56	4.70	4.80	4.90	5.76	5.88	6.00
				lb-in	17.3	17.9	18.2	29.6	30.3	31.2	31.5	41.6	42.5	43.4	51.0	52.0	53.1
	Continuous Current (Stall) for ΔT winding = 100°C ① ② ⑦ ⑨	Nom	I_{cs}	A_{rms}	1.46	2.85	5.60	1.40	2.74	4.80	8.40	2.76	4.87	9.60	2.9	5.0	8.8
	Continuous Torque (Stall) for ΔT winding = 60°C ②	Nom	T_{cs}	N-m	1.56	1.62	1.65	2.68	2.74	2.82	2.85	3.76	3.84	3.92	4.61	4.70	4.80
				lb-in	13.8	14.3	14.6	23.7	24.2	25.0	25.2	33.3	34.0	34.7	40.8	41.6	42.5
	Max Mechanical Speed ⑤	Nom	N_{max}	rpm	6000	6000	6000	6000	6000	6000	6000	6000	6000	6000	6000	6000	6000
	Peak Torque ⑩	Nom	T_p	N-m	6.12	6.28	6.36	11.1	11.3	11.5	11.6	15.9	16.1	16.3	19.9	20.2	20.4
				lb-in	54.2	55.6	56.3	98.8	99.7	102	103	141	142	144	176	179	181
	Peak Current	Nom	I_p	A_{rms}	5.8	11.4	22.4	5.61	11.0	19.2	33.7	11.0	19.5	38.3	11.4	20.0	35.2
75VDC	Rated Torque (speed) ① ② ⑦ ⑨ ⑨		T_{rtd}	N-m	-	-	1.99	-	-	-	-	-	-	-	-	-	-
				lb-in	-	-	17.6	-	-	-	-	-	-	-	-	-	-
	Rated Speed		N_{rtd}	rpm	-	-	1000	-	-	-	-	-	-	-	-	-	-
	Rated Power (speed) ① ② ⑦ ⑨		P_{rtd}	kW	-	-	0.21	-	-	-	-	-	-	-	-	-	-
				Hp	-	-	0.28	-	-	-	-	-	-	-	-	-	-
160VDC	Rated Torque (speed) ① ② ⑦ ⑨ ⑨		T_{rtd}	N-m	-	1.94	1.86	-	-	-	3.03	-	-	4.08	-	-	-
				lb-in	-	17.2	16.5	-	-	-	26.8	-	-	36.1	-	-	-
	Rated Speed		N_{rtd}	rpm	-	1200	3000	-	-	-	3000	-	-	2500	-	-	-
	Rated Power (speed) ① ② ⑦ ⑨		P_{rtd}	kW	-	0.24	0.58	-	-	-	0.95	-	-	1.07	-	-	-
				Hp	-	0.33	0.78	-	-	-	1.28	-	-	1.43	-	-	-
320VDC	Rated Torque (speed) ① ② ⑦ ⑨ ⑨		T_{rtd}	N-m	1.88	1.82	1.62	-	3.12	2.90	2.38	4.24	4.00	2.62	5.22	4.90	3.84
				lb-in	16.6	16.1	14.3	-	27.6	25.7	21.1	37.5	35.4	23.2	46.2	43.4	34.0
	Rated Speed		N_{rtd}	rpm	1200	3000	6000	-	1800	3500	6000	1500	2500	6000	1200	2000	4000
	Rated Power (speed) ① ② ⑦ ⑨		P_{rtd}	kW	0.24	0.57	1.02	-	0.59	1.06	1.50	0.67	1.05	1.65	0.66	1.03	1.61
				Hp	0.32	0.77	1.36	-	0.79	1.42	2.00	0.89	1.40	2.21	0.88	1.38	2.16
560VDC	Rated Torque (speed) ① ② ⑦ ⑨ ⑨		T_{rtd}	N-m	1.77	1.58	-	3.10	2.81	2.35	-	3.92	3.01	-	4.80	3.76	2.75
				lb-in	15.7	14.0	-	27.4	24.9	20.8	-	34.7	26.6	-	42.5	33.3	24.3
	Rated Speed		N_{rtd}	rpm	3000	6000	-	1500	3500	6000	-	2500	5000	-	2000	4000	6000
	Rated Power (speed) ① ② ⑦ ⑨		P_{rtd}	kW	0.56	0.99	-	0.49	1.03	1.48	-	1.03	1.58	-	1.01	1.57	1.73
				Hp	0.75	1.33	-	0.65	1.38	1.98	-	1.38	2.11	-	1.35	2.11	2.32
640VDC	Rated Torque (speed) ① ② ⑦ ⑨ ⑨		T_{rtd}	N-m	1.74	1.58	-	3.02	2.72	2.35	-	3.76	2.57	-	4.56	3.19	2.75
				lb-in	15.4	14.0	-	26.7	24.1	20.8	-	33.3	22.7	-	40.4	28.2	24.3
	Rated Speed		N_{rtd}	rpm	3500	6000	-	2000	4000	6000	-	3000	6000	-	2500	5000	6000
	Rated Power (speed) ① ② ⑦ ⑨		P_{rtd}	kW	0.64	0.99	-	0.63	1.14	1.48	-	1.18	1.61	-	1.19	1.67	1.73
				Hp	0.85	1.33	-	0.85	1.53	1.98	-	1.58	2.16	-	1.60	2.24	2.32
	Torque Constant ①	±10%	K_t	N-m/A_{rms}	1.34	0.71	0.37	2.40	1.26	0.74	0.43	1.72	0.99	0.52	2.04	1.19	0.69
				lb-in/A_{rms}	11.9	6.3	3.3	21.2	11.2	6.5	3.8	15.2	8.8	4.6	18.1	10.5	6.1
	Back EMF constant ③	±10%	K_e	V_{pk}/krpm	86.3	45.6	23.7	154	80.9	47.5	27.5	111	63.9	33.2	132	76.6	44.2
	Resistance (line-line) ③	±10%	R_m		21.7	5.7	1.51	27.52	7.22	2.38	0.80	8.04	2.81	0.70	8.64	2.65	0.88
	Inductance (line-line		L	mH	66.1	18.4	5.0	97.4	26.8	9.2	3.1	32.6	10.8	2.9	33.9	11.5	3.8
	Inertia		J_m	kg-cm^2	0.81			1.5				2.1			2.7		
	(Includes Resolver Feedback) ③			lb-in-s^2	7.2E-04			1.3E-03				1.8E-03			2.4E-03		
	Optional Brake Inertia		J_m	kg-cm^2	0.068			0.068				0.068			0.068		
	(additional)			lb-in-s^2	6.0E-05			6.0E-05				6.0E-05			6.0E-05		
	Weight		W	kg	2.44			3.39				4.35			5.3		
				lb	5.4			7.5				9.6			11.7		
	Static Friction ⑧⑨		T_f	N-m	0.014			0.026				0.038			0.05		
				lb-in	0.12			0.23				0.34			0.44		
	Viscous Damping ⑨		K_{dv}	N-m/krpm	0.009			0.013				0.017			0.021		
				lb-in/krpm	0.08			0.12				0.15			0.19		
	Thermal Time Constant		TCT	minutes	13			17				20			24		
	Thermal Resistance		$R_{th\ c-a}$	°C/W	1.04			0.89				0.78			71		
	Pole Pairs				5			5				5			5		
	Heatsink Size				10"x10"x½" Aluminum Plate			10"x10"x½" Aluminum Plate				10"x10"x½" Aluminum Plate			10"x10"x½" Aluminum Plate		

Notes:
1. Motor winding temperature rise, ΔT=100°C, at 40°C ambient.
2. All data referenced to sinusoidal commutation.
3. Add parking brake if applicable for total inertia.
4. Motor with standard heatsink.
5. May be limited at some values of Vbus.
6. Measured at 25°C.
7. Brake motor option reduces continuous torque ratings by 0.12 N-m.
8. Commutating encoder/SFD options reduces continuous ratings by:
   AKM41 = 0.1 N-m AKM42 = 0.1 N-m
   AKM43 = 0.2 N-m AKM44 = 0.3 N-m
9. Brake plus commutating encoder/SFD motor option reduces continuous torque ratings by:
   AKM41 = 0.22 N-m AKM42 = 0.36 N-m
   AKM43 = 0.55 N-m AKM44 = 0.76 N-m
10. For motors with optional shaft seal, reduce torque shown by 0.021 N-m (0.038 lb-in), and increase T_f by the same amount.

AKM Series Brushless Servomotors

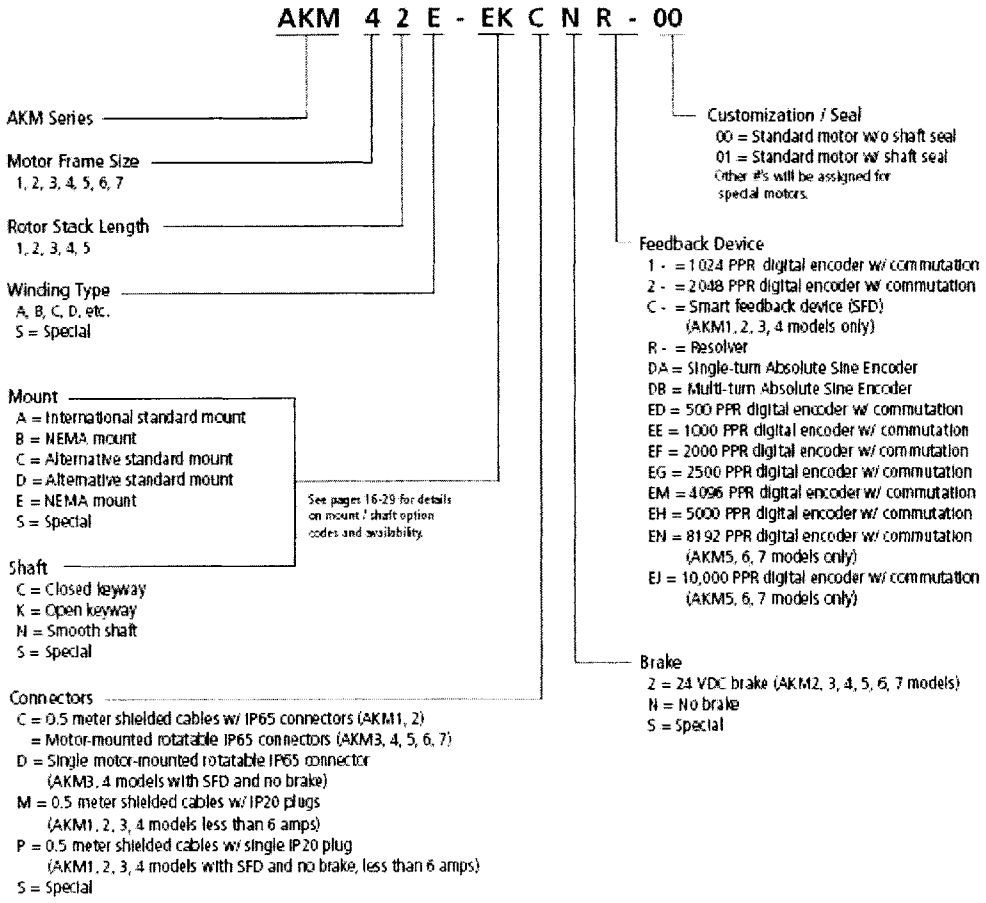

Plastic Miter Gears

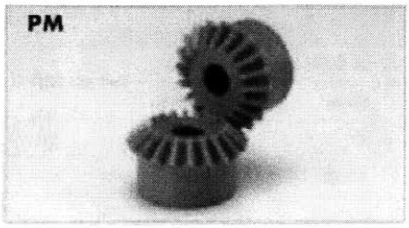

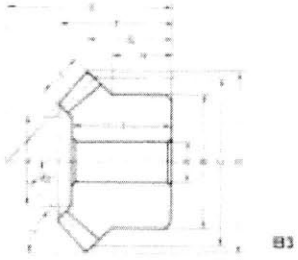

■20 Miter Module 1～4

Catalog No.	Module	No. of teeth	Bore	Hub dia.	Pitch dia.	Outside dia.	Mounting distance	Turret length	Crown to back length	Hub width	Length of bore	Face width	Holding surface dia.	Face angle
	m	z	A	B	C	D	E	F	G	H	I	J	K	L
PM1 -20	1	20	6	16	20	21.41	20	13.95	10.71	8	12	5	9.86	49 48
PM1.25-20	1.25	20	8	22	25	26.77	23	15.27	11.38	9	13	6	13.03	49 48
PM1.5 -20	1.5	20	8	26	30	32.12	30	21.24	16.06	13	19	8	15.37	49 48
PM2 -20	2	20	10	34	40	42.83	37	24.89	18.41	14	22	10	21.72	49 48
PM2.5 -20	2.5	20	12	42	50	53.54	48	32.54	24.77	19	29	12	28.06	49 48
PM3 -20	3	20	14	50	60	64.24	58	39.84	30.12	23	35	15	31.57	49 48
PM3.5 -20	3.5	20	20	60	70	74.95	65	44.13	32.47	25	40	18	39.09	49 48
PM4 -20	4	20	20	64	80	85.66	75	50.78	37.83	27	45	20	43.43	49 48

■25 Miter Module 1～3

PM1 -25	1	25	6	20	25	26.41	23	15.16	11.21	8	14	6	15.03	48 51
PM1.25-25	1.25	25	8	25	31.25	33.02	28	17.88	13.26	9.25	16	7	18.7	48 51
PM1.5 -25	1.5	25	8	30	37.5	39.62	34	22.25	16.31	11.5	19	9	19.54	48 51
PM2 -25	2	25	10	40	50	52.83	40	24.33	16.41	10	20	12	26.06	48 51
PM2.5 -25	2.5	25	14	50	62.5	66.04	50	30.41	20.52	12.5	26	15	34.57	48 51
PM3 -25	3	25	15	60	75	79.24	60	37.81	24.62	15	32	20	37.43	48 51

CAUTION Dimensions of the outside diameter, the overall length and crown to back length are all theoretical values, and some differences will occur due to the corner chamfering of the gear tips.

Injection Molded Miter Gears

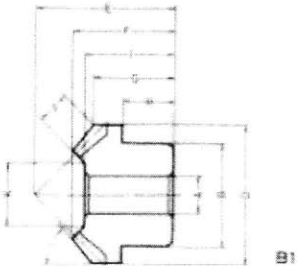

■20 Miter Module 0.5～1.5

Catalog No.	Module	No. of teeth	Bore	Hub dia.	Pitch dia.	Outside dia.	Mounting distance	Turret length	Crown to back length	Hub width	Length of bore	Face width	Holding surface dia.	Face angle
	m	z	A	B	C	D	E	F	G	H	I	J	K	L
DM0.5-20	0.5	20	3	8	10	10.71	11	7.97	6.35	4	7	2.5	4.93	49 48
DM0.8-20	0.8	20	5	12	16	17.13	16	10.83	8.56	5	10	3.5	10.1	49 48
DM1 -20	1	20	6	16	20	21.41	21	14.62	11.71	7	13	4.5	11.27	49 48
DM1.5-20	1.5	20	8	20	30	32.12	30	20.59	16.06	10	19	7	18.2	49 48

CAUTION The bore tolerance is generally -0.05 to -0.1 but may be + values at the central portion of the hole.
CAUTION Remachining the bore is not recommended since it may expose voids.

Module 1～4

Specifications			
Precision grade	JIS B 1704 grade 4	Core hardness	HRB115～120
Gear tooth	Gleason	Surface hardness	
Pressure angle	20°	Surface treatment	—
Material	MC901	Surface finish	Cut
Heat treatment	—	Datum reference surface for tooth cutting	Bore

Shape	Allowable torque (kgf·m) Bending strength	Surface durability	Allowable torque (N·m) Bending strength	Surface durability	Backlash (mm)	Weight (gf)	Catalog No.
B3	0.0183	—	0.1795	—	0.08～0.18	0.01	PM1 -20
B3	0.0354	—	0.3472	—	0.09～0.19	0.01	PM1.25-20
B3	0.0626	—	0.6139	—	0.1 ～0.2	0.01	PM1.5 -20
B3	0.1465	—	1.437	—	0.11～0.21	0.02	PM2 -20
B3	0.283	—	2.775	—	0.12～0.22	0.04	PM2.5 -20
B3	0.4943	—	4.847	—	0.13～0.23	0.07	PM3 -20
B3	0.7899	—	7.746	—	0.15～0.25	0.12	PM3.5 -20
B3	1.172	—	11.49	—	0.17～0.27	0.16	PM4 -20

Pitch Angle 45°

B3	0.0301	—	0.2952	—	0.08～0.18	0.01	PM1 -25
B3	0.0575	—	0.5639	—	0.09～0.19	0.01	PM1.25-25
B3	0.1015	—	0.9954	—	0.1 ～0.2	0.02	PM1.5 -25
B3	0.2406	—	2.359	—	0.11～0.21	0.03	PM2 -25
B3	0.47	—	4.609	—	0.12～0.22	0.06	PM2.5 -25
B3	0.8315	—	8.154	—	0.13～0.23	0.1	PM3 -25

NOTE: The allowable torques shown in the table are calculated from the Lewis formula.

Pitch Angle 45°

Module 0.5～1.5

Specifications			
Precision grade	JIS B 1704 grade 8	Core hardness	HRB110～120
Gear tooth	Gleason	Surface hardness	
Pressure angle	20°	Surface treatment	—
Material	Duracon(M90-44)	Surface finish	Injection molded
Heat treatment	—	Datum reference surface for tooth	Bore

Shape	Allowable torque (kgf·m) Bending strength	Surface durability	Allowable torque (N·m) Bending strength	Surface durability	Backlash (mm)	Weight (kgf)	Catalog No.
B1	0.0102	—	0.1	—	0.04～0.14	1	DMO.5-20
B1	0.0356	—	0.3491	—	0.06～0.16	2	DMO.8-20
B1	0.0614	—	0.6021	—	0.08～0.18	4	DM1 -20
B1	0.1078	—	1.057	—	0.1 ～0.2	13	DM1.5-20

NOTE: The allowable torques shown in the table are calculated from the Lewis formula.

Pitch Angle 45°

6 PMDM

Bibliography

[1] R. Thirumala, et al. "Motor recovery after stroke: Lessons form functional brain imaging". *Neurological Research*, 2002, Vol. 24, July, pp 453-458.

[2] M.L. Aisen, et al. "The Effect of Robot-Assisted Therapy and Rehabilitative Training of Motor Recovery Following Stroke". Archives of Neurology, 54:443-446, 1997.

[3] D. Williams, *A Robot for Wrist Rehabilitation.* MSME Thesis, Massachusetts Institute of Technology, June 2001.

[4] A.R. Tilley, *The Measure of Man and Woman.* Henry Dreyfuss Associates, 1993.

[5] S. Pheasant, *Bodyspace.* 2nd ed., Taylor and Francis Inc, 1996.

[6] J. Celestino, *Characterization and Control of a Robot for Wrist Rehabilitation.* MSME Thesis, Massachusetts Institute of Technology, June 2003.

[7] J.P. Hornak PhD, *The Basics of MRI.* Copyright 1996-2004. Available HTTP: http://www.cis.rit.edu/htbooks/mri/index.html

[8] M.A. Brown, PhD and R.C. Semelka. MD, *MRI: Basic Principles and Applications.* 2nd ed., Wiley-Liss Inc, 1999.

[9] J.F. Schenck. "The role of magnetic susceptibility in magnetic resonance imaging: MRI magnetic compatibility of the first and second kinds". *Medical Physics*, vol. 23, no. 6, June, pp. 815-850, 1996.

[10] Howstuffworks, "How strong are the magnets in an MRI machine?", Available HTTP: http://science.howstuffworks.com/question698.htm

[11] W. Patola RTMR and B. Coulter RTMR, "MRI Artifacts", Available HTTP: http://wwwrad.pulmonary.ubc.ca/stpaulsstuff/MRartifacts.html

[12] B.T. Larson, et al. "A Robotic Device for Minimally Invasive Breast Interventions With Real-Time MRI Guidance", IEEE Computer Society, 2003.

[13] K. Yoshihiko, et al. "Endoscope Manipulator for Trans-nasal Neurosurgery, Optimized for and Compatible to Vertical Field Open MRI", Splinger Verlag, Lecture Notes on Computer Science, MICCAI 2002.

[14] R. Moser, et al. "An MR Compatible Robot Technology". 2003 IEEE International Conference of Robotics and Automation.

[15] G. Ganesh, et al. "Dynamics and Control of an MRI Compatible Master-Slave System with Hydrostatic Transmission". 2004 IEEE International Conference on Robotics and Automation.

[16] Hogan et al. *System and Method for Medical Imaging Utilizing a Robotic Device, and Robotic Device for use in Medical Imaging.* United States Patent 5,794,621. Aug. 18, 1998.

[17] Greeley X-Ray Group. Available HTTP: http://www.greeleyxray.com/open-mri-11-03-1-3Ta.cfm

[18] Siemens Allegra MRI, Available HTTP: http://smuc.siemens.se/info/produkter

[19] Siemens C! MRI, Available HTTP: http://www.smmr-siemens.com/english/Production

[20] Nanomotion HR8 ultrasonic motor user manual. Available HTTP: http://www.nanomotion.com/data/docs/HR8.pdf

[21] Atlas Copco Airmotor, Available HTTP: http://www.atlascopco-airmotors.com/

[22] Dynatork Airmotor, Available HTTP: http://www.dynatork.co.uk

[23] Beco Manufacturing Co. air cylinder, Available HTTP: http://www.becomfg.com/products/aircylinder.html

[24] Airpot Piston/Cylinder set, Available HTTP: http://www.airpot.com

[25] Rineer hydraulic vane motor, Available HTTP: http://www.rineer.com

[26] Viking Pump gerotor, Available HTTP: http://www.vikingpump.com

[27] J. Verdirame, *Characterization of a Hydraulic Actuator for a Functional Magnetic Resonance Imaging Robot.* BSME Thesis, Massachusetts Institute of Technology, June 2000.

[28] S. J. Buerger, *Stable, High-Force, Low-Impedance Robotic Actuators for Human-Interactive Machines.* PhD Thesis, Massachusetts Institute of Technology, June 2005.

[29] F.M. White, *Fluid Mechanics.* 4th ed., McGraw-Hill, 1999.

[30] J.E. Shigley and C.R. Mischke, *Mechanical Engineering Design.* Sixth ed., McGraw-Hill, 2001.

[31] Gurley Precision Instruments model R119 datasheet, Available HTTP: http://www.gpi-encoders.com/PDF/R119.pdf

[32] ATI Industrial Automation force transducer catalog available HTTP: http://www.ati-ia.com/library/documents/ATI_FT_Sensor_Catalog_2005.pdf

[33] Stock Drive Products/Sterling Instruments Online Catalog, Available HTTP: https://sdp-si.com/eStore

[34] Sensable Technologies Phantom, Available HTTP: http://www.sensable.com

[35] Parker Daedal Division, Available HTTP: http://www.daedalpositioning.com

[36] Florida Institute of Technology Robotics and Spatial Systems Laboratory, Available HTTP: http://my.fit.edu/~pierrel/research.html

[37] Howstuffworks, "How Bearings Work", Available HTTP: http://science.howstuffworks.com/bearing3.htm

[38] United States Plastic Corp. online catalog. http://www.usplastic.com/catalog/default.asp

[39] Parker online catalog, Available HTTP: http://www.parker.com

[40] R. Armstrong, "Feedback for Servos". Available HTTP: http://www.machinedesign.com

[41] Quality Transmission Componets. *Handbook of Metric Gears: Product Guide and Technical Data, Catalog Q410*, 1999.

[42] A.H. Slocum, *Precision Machine Design.* Society of Manufacturing Engineers, 1992.

[43] S.H. Loewenthal and E.V. Zaretsky, "Design of Traction Drives", NASA Reference Publication 1154, 1985.

[44] Stoffel Polygon Systems. *Polygon Systems Catalog.*

[45] M. Tada, S. Sasaki, and T. Ogasawara. "67.4: Development of an Optical 2-axis Force Sensor Usable in MRI environments". IEEE Sensors 2002.